

RECEIVED

NOV 22 1995

OSTI

IS-T 1744

Connection Between NMR and Electrical Conductivity in Glassy
Chalcogenide Fast Ionic Conductors

by

Kim, Kyung-Han

PHD Thesis submitted to Iowa State University

Ames Laboratory, U.S. DOE

Iowa State University

Ames, Iowa 50011

Date Transmitted: July 7, 1995

PREPARED FOR THE U.S. DEPARTMENT OF ENERGY

UNDER CONTRACT NO. W-7405-Eng-82.

MASTER

DISTRIBUTION OF THIS DOCUMENT IS UNLIMITED

pt

DISCLAIMER

This report was prepared as an account of work sponsored by an agency of the United States Government. Neither the United States Government nor any agency thereof, nor any of their employees, makes any warranty, express or implied, or assumes any legal liability or responsibility for the accuracy, completeness or usefulness of any information, apparatus, product, or process disclosed, or represents that its use would not infringe privately owned rights. Reference herein to any specific commercial product, process, or service by trade name, trademark, manufacturer, or otherwise, does not necessarily constitute or imply its endorsement, recommendation, or favoring by the United States Government or any agency thereof. The views and opinions of authors expressed herein do not necessarily state or reflect those of the United States Government or any agency thereof.

DISCLAIMER

Portions of this document may be illegible in electronic image products. Images are produced from the best available original document.

Connection between NMR and electrical conductivity in glassy
chalcogenide fast ionic conductors

Kyung-Han Kim

Major Professor: Dr. F. Borsa
Iowa State University

Pulsed Nuclear Magnetic Resonance measurements and electric conductivity measurements have been performed in glassy fast ionic conductors, lithium thiogermanates ($x\text{Li}_2\text{S} + (1-x)\text{GeS}_2$) and lithium thioborates ($x\text{Li}_2\text{S} + (1-x)\text{B}_2\text{S}_3$) in order to investigate the microscopic mechanism of ion dynamics. Both ^7Li - nuclear spin lattice relaxation rate (NSLR) versus temperature at several resonance frequencies (4 MHz to 135 MHz) and conductivity, $\sigma(\omega)$ versus temperature, in the frequency range from 1 Hz to 4 MHz have been measured. The ^7Li NSLR show BPP - type behavior with strong asymmetry of the bell shaped curve on the two sides of the maximum. A sizable dependence of the NSLR on the type and composition of the glass is found. The results have been analyzed in terms of both a phenomenological model using a stretched exponential correlation function and a model based on a distribution of activation energies. The model based on a simple hopping of the free ions over the barriers of a given distribution gave a good fit of the NSLR data. By using the distribution obtained from NMR we could also account for the value and the temperature dependence of the dc. conductivity. In the framework of this model we can explain the different correlation times obtained

from NMR and conductivity as a consequence of percolation effects in the conductivity. It is shown that the distribution of barriers should lead to small but detectable deviations from Arrhenius behavior of dc conductivity. This deviation has been indeed observed in lithium thioborate glasses which have lower activation energy. The phenomenological model based on the stretched exponential was compared with the experiments in the light of the interpretation of the "coupling model" and found in partial disagreement with our data. In thioborate glasses it was found that the ^7Li NSLR has two maxima as a function of temperature. The ^{11}B NSLR on the other hand displays two relaxation rates associated with trigonal and tetragonal structural groups respectively. It is shown that the NSLR of the mobile (^7Li) ion and immobile (^{11}B) ion are indirectly related to each other and from this one can deduce information about energy barriers associated to each structure for the mobile ion and immobile ion.

Connection between NMR and electrical conductivity in glassy
chalcogenide fast ionic conductors

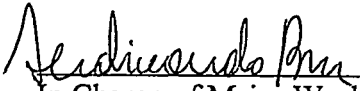
by

Kyung-Han Kim

A Dissertation Submitted to the
Graduate Faculty in Partial Fulfillment of the
Requirements for the Degree of
DOCTOR OF PHILOSOPHY

Department: Physics and Astronomy
Major: Condensed Matter Physics

Approved:


In Charge of Major Work

For the Major Department

For the Graduate College

Iowa State University
Ames, Iowa

1994

TABLE OF CONTENTS

CHAPTER I.	INTRODUCTION	1
1.1	Preview	1
1.2	Fast Ionic Conduction in Glasses	1
1.2.1	Literature Review	1
1.2.2	General Features of Fast Ionic Conduction in Glass	4
1.2.3	General Features of ac Conductivity	8
1.3	NMR and Impedance Spectroscopy Measurements of Ionic Conductivity in Glass	12
1.3.1	Probes for the Study of Fast Ionic Conductors (FIC)	12
1.3.2	NMR and Impedance Spectroscopy	14
1.4	Summary of Measurements to Date and the Objectives of the Thesis	17
1.4.1	Summary of Measurements to Date	17
1.4.2	The Objectives of the Thesis	24
CHAPTER II.	BACKGROUND	27
2.1	Structural Properties of Chalcogenide Fast Ionic Conducting Glass	27
2.1.1	Glass Formation in Chalcogenide Systems	27
2.1.2	Fast Ionic Conducting Chalcogenide Glasses	28
2.1.2.1	Structure of Boron Based Glasses	30
2.1.2.2	Structure of Silicon and Germanium Based Glasses	31
2.1.2.3	Structural Trends and Ionic Conductivity	33
2.1.2.4	Structural Trends of Boron and Silicon Based Glasses Studied by NMR	34
2.1.2.5	Structural Trends Studied by the other Techniques	36
2.1.2.6	Structure of Thiogermanate Glasses	37
2.2	Nuclear Magnetic Resonance Theory	39
2.2.1	Hamiltonian and Nuclear Spin Lattice Interactions	41
2.2.1.1	Nuclear Zeeman Interaction	41
2.2.1.2	Dipolar Interaction	43
2.2.1.3	Quadrupolar Interaction	44
2.2.1.4	Hyperfine Interaction	46
2.2.1.5	Indirect Interaction	47
2.2.2	NMR Spectrum and Nuclear Spin Lattice Relaxation	48
2.2.2.1	Classical Description	48
2.2.2.2	NMR Spectrum	50
2.2.2.3	Nuclear Spin Lattice Relaxation	59

2.2.3	BPP and Beyond	69
2.2.3.1	Beyond BPP	70
2.2.3.2	NSLR in Glass	71
2.3	Model for Ionic Conduction	77
2.3.1	Free Ion Type Model	77
2.3.2	Hopping Model	79
2.3.2.1	Hopping Models in Disordered System	79
2.3.2.2	Simple Hopping Model	81
2.3.2.3	Hopping Model with Distribution of Hopping Frequencies and Percolation Scheme	83
2.3.2.4	Other Hopping Models; The Coupling Model	85
CHAPTER III. EXPERIMENTAL DETAIL		87
3.1	Sample Preparation	87
3.1.1	Lithium Thiogermanate Glasses	87
3.1.2	Lithium Thioborate Glasses	88
3.2	Conductivity Measurement by Impedance Spectroscopy	89
3.3	Measurement of Nuclear Spin Lattice Relaxation time	94
3.3.1	Inversion Recovery Method of Measuring T_1	94
3.3.2	NMR Pulse Spectrometer	95
3.3.2.1	Pulse Generation and Transmission	95
3.3.2.2	Pulse NMR Probe	98
3.3.2.3	Receiver	100
3.3.2.4	Magnet	100
3.3.3	Experimental Procedure and Data Processing	101
3.4	Methods for Data Analysis and Computer Program	103
3.4.1	KWW Stretched Exponential Model	103
3.4.2	Limiting Behavior of Stretched Exponential Correlation Function	106
3.4.3	Distribution of Activation Energies and Percolation Scheme	108
CHAPTER IV. RESULTS AND DISCUSSIONS		111
4.1	$x\text{Li}_2\text{S} + (1-x)\text{GeS}_2$	112
4.1.1	^7Li Nuclear Spin Lattice Relaxation Measurements	112
4.1.2	Conductivity Measurements	
4.1.3	Direct Comparison of Correlation Times from NMR and Conductivity	116
4.1.4	Analysis of Data with the Phenomenological KWW Correlation Function and the Coupling Model	119
4.1.5	Analysis of the Data with a Distribution of Activation Energies and the Percolation Model	131

4.2	$x\text{Li}_2\text{S}+(1-x)\text{B}_2\text{S}_3$	142
4.2.1	^7Li Nuclear Spin Lattice Relaxation Measurements	144
4.2.2	Conductivity Measurements	144
4.2.3	Interpretation of the Anomalous ^7Li NSLR Curves	144
4.2.4	Analysis of the Data with a Distribution of Activation Energies and the Percolation Model	150
4.2.5	Measurements of ^{11}B NSLR	157
CHAPTER V. CONCLUSIONS		165
REFERENCES		167
ACKNOWLEDGMENTS		179
APPENDIX		180

CHAPTER I. INTRODUCTION

1.1 Preview

The work documented in this thesis follows the traditional order. In this chapter a general discussion of ionic conduction and of glassy materials are followed by a brief outline of the experimental techniques for the investigation of fast ionic conduction in glassy materials, including NMR and impedance spectroscopy techniques. A summary of the previous and present studies is presented in the last section of this introductory chapter.

The details of the background theory and models are found in the Chapter II, followed by the description of the experimental details in Chapter III. Chapter IV of the thesis describes the experimental results and the analysis of the experimental observations followed by the conclusions in chapter V.

1.2 Fast Ionic Conduction in Glasses

1.2.1 Literature Review

Fast ionic conduction in solids, especially in glassy materials, has stimulated interest both in the scientific and technical communities [1]. The scientific community is interested in the microscopic mechanism of mass and ionic charge transport through glassy or crystalline hosts [2]. Due to the high concentration of mobile ions, the hopping motion of ionic charges is strongly affected by mutual interactions whereby collective effects become very relevant [3-6]. From the technical point of view, solid

state ionic conductors are good candidates for high energy density solid state batteries [7-9], as well as numerous electrochemical applications [10].

The study of electrical properties of glasses began as early as 1748 with the observation of high dielectric absorption in Ben Franklin's study of residual charges on Leyden jars [11]. The ionic conduction in glass was found by Warburg in 1884 [12]. In 1966, Otto [13] discovered fast ionic conducting oxide glasses. With the discovery of RbAg_4I_5 and β -Alumina in 1967, the field began to grow with the possibility of applications of fast ionic conductors (FIC). The introduction of glassy FIC offers a wide variety of materials which are both easy and cheap to prepare and can be modified to yield improved performance [14].

A variety of chemical compounds have been studied to optimize ionic conduction for use as a solid electrolytes in solid state batteries and high capacitance capacitors. Thermally activated hopping is always assumed to be the mechanism of ionic transport and is analogous to electronic hopping in disordered system with the important exception of impurity conduction and Mott's [15,16] variable range hopping model. The attempt to optimize conduction properties was done on the basis of simple free ion type models and using the techniques of synthesis developed in glass-chemistry. The effort was concentrated on investigating the dc ionic conductivity for various fast ionic conductors, both in crystalline [7,9] and glass [18-21] phases. Referring to the dc conductivity, ionic conductors may be defined as SIC (super ionic conductor) when the dc conductivity at room temperature exceeds $10^{-3}(\Omega \text{ cm})^{-1}$, and as FIC (fast ionic conductor) when dc conductivity at room temperature less than $10^{-3}(\Omega \text{ cm})^{-1}$ [21]. Hunter and Ingram[19] classify glassy FIC materials which show dc conductivity at the glass transition temperature, T_g , exceeding $10^{-2}(\Omega \text{ cm})^{-1}$.

The study of the frequency dependent ionic conductivity began around 1930 [23]. Historically, one can distinguish two schools of thought depending on the method chosen for presenting data. The "dielectric school" uses the complex dielectric function,

$$\varepsilon(\omega) = \varepsilon'(\omega) - i\varepsilon''(\omega) \quad (1.1)$$

while the "semi conductor school" prefers the complex conductivity,

$$\sigma(\omega) = \sigma'(\omega) + i\sigma''(\omega) \quad (1.2)$$

The interest in the dielectric losses of materials was strong in the 50's and it was stimulated by the use of these materials as insulating components in electronic devices. The interest in both crystalline and amorphous semiconductor boomed in the 60's and thereafter.

Experimental work within the semi-conductor school started in 1961 when Pollak and Geballe [25] measured the ac properties of n-type doped crystalline silicon at very low temperature. They observed an approximate power law for the ac electric conductivity,

$$\sigma(\omega) \sim \omega^s, \quad \text{where } s \cong 0.8 \quad (1.3)$$

The same kind of behavior was observed in the ionic conductivity of glassy-FIC and in a wide variety of non-metallic disordered solids[24]. This frequency dependence suggests an origin which could be found in the disorder of the structure.

The interest in solid state electrolytes remains strong both for the technical aspects where applications have been demonstrated and for the scientific aspects. Nevertheless, it is not yet economically viable and the understanding of the basic physics of the microscopic mechanism for the ionic conductivity is far from complete.

1.2.2 General Features of Fast Ionic Conduction in Glass

Solid ionic conductors may be classified into three different groups; crystalline ionic materials or defect types such as NaCl, CaF₂, AgI, etc.; traditional super ionic conductors or so called molten sub lattice types [9] such as RbAgI₅, β-Al₂O₃, etc.; and materials with low structural organization e.g. inorganic glasses and polymers. The last group is further classified into sub-T_g materials (glasses) and super-T_g materials (polymer) [18].

In this work, the main focus is on glassy-FIC, especially lithium sulfide glasses which belong to the class of chalcogenide glasses. The choice is motivated by their superior conductivity and by the access to the microscopic study of ion-dynamics by means of ⁷Li NMR.

Glass characteristics, such as isotropic and flexible structure [26], absence of grain boundaries, wide composition ranges, and easy fabrication, are attractive features for the development and applications of glassy-FIC. A glass is generally regarded as a frozen liquid of high viscosity obtained from the melt by quenching. A fluid becomes a rigid glass when the time required for structural change is much longer than the time of observation. The material then appears solid, when in fact it may flow on a long time scale. Glass properties are known to be closely related to the glass

composition. In the case of ionic conductivity, the glass composition and its glass forming range are of paramount importance.

Glass forming elements in the periodic table are in groups V and VI; for example, phosphorus, sulfur, and selenium. Binary glasses are mostly artificial ones, of practical value; oxide, halide, and chalcogenide glass [27]. According to the Zachariasen rule[27], one can predict the formation of glassy materials by combining two of the above glass forming elements. The binary glasses so obtained will have some ionic character in the bonding and are known as network formers (NWF). Other compounds such as alkaline oxide, alkaline earth oxide, and some transition metal oxide (and their sulfide) dissolve in NWF and react due to the high charge density of glass former cations. Thus those compounds which alter the glass properties of the NWF, are called as network modifiers (NWM). The structure of covalent glasses (group V and VI) is described by the continuous random network model [28]. However, in the covalent glass one finds short range order, which indicates that the glass structure is not completely random.

The oxygen atoms in the NWM of oxide glasses (or sulfur atoms in sulfide glasses) enter NWF by depolymerizing or by bonding to glass forming cations. Bonding occurs when a glass forming cation has the ability to increase its coordination number, and actually increase the dimension of the network. These two mechanisms are shown in Fig. 1.1 (A) and (B) respectively. The important consequence of the NWM reaction with NWF is the creation of modifier cations weakly bound to the NWF, and the creation of non bridging oxygen (NBO). From the figure we notice that silicate are more apt to have NBO. Since the modifier cation is being weakly bound, it attempts to escape from its shallow potential energy wells and hop to the nearest vacancy site. The defect formation mechanism was illustrated by M. D. Ingram [19].

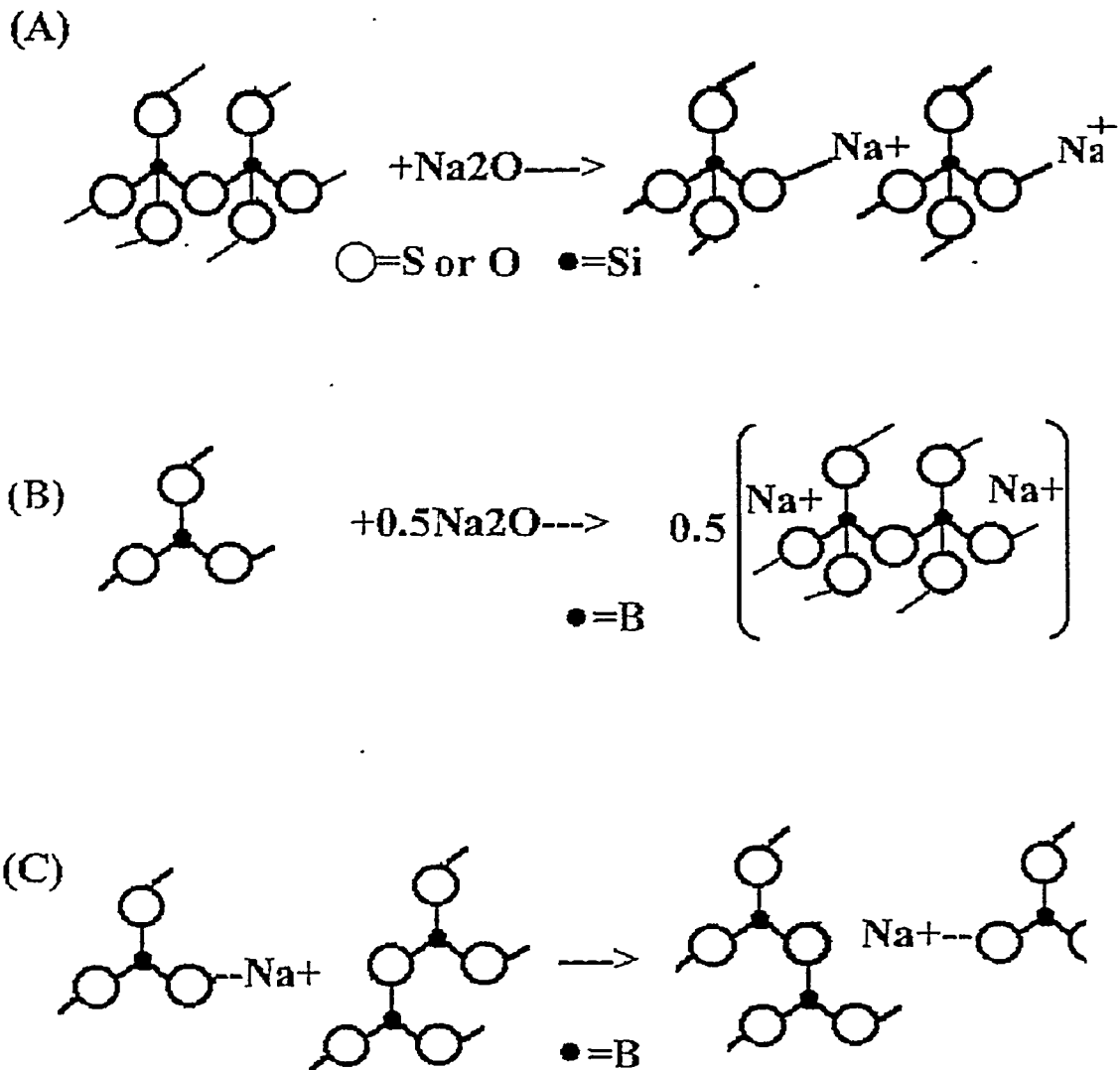


Fig. 1.1 Schematic diagram of the reaction of NWM to NWF by (A) depolymerizing, (B) Bonding of oxygen (or sulfur) to the cation of NWF. Actual increase of dimension takes place which can be monitored by ^{11}B -NMR [119-122] and (C) The illustration of the possible ion jump mechanism for conducting ions, especially in the low alkali limit.

Under the influence of an electric field, the hopping of ions become biased in the direction of the field leading to the observation of ionic conduction. Although the ionic conduction described above is neither a conduction process in an extended state of charge carrier nor their motion is not free, free ion-type model (or Drude-type analogy) approach has been used extensively with appropriate interpretation of the activation energy [184] for thermally activated hopping of ionic charge carriers.

A simple expression for the dc conductivity can be obtained by using viscous flow of ions and Nernst - Einstein relation;

$$\sigma_{d.c.} = \frac{n(Ze)^2}{k_B T} a \lambda^2 v_0 \exp(-Ea / k_B T) \quad (1.4)$$

where, n is a number density of the charge carriers,
 a is a geometrical factor for random hopping,
 λ is the jump distance of the charge carriers,
 v_0 is a primitive attempt frequency, and
 Ea is the activation energy of the hopping ion.
 k_B is a Boltzman factor

Whereby the detailed discussion of equation (1.4) will be presented in the section 2.3.1 of Chapter II. The simple expression (1.4) has been able to account for the main conduction properties of the sulfide glasses, which are investigated in the present work with more extended models.

1.2.3. General Features of ac Conductivity

One of the most characteristic features of ionic conductivity of glass material is the frequency dependence of the conductivity which appears to have a universal behavior i.e. $\sigma \sim \omega^s$, with $0 \leq s \leq 1$ (see section 1.2.1). A frequency dependence of the conductivity is an indication of non - Debye relaxation behavior for the mobile ions. This feature has been observed in many complex systems by various methods of observation [29-31]. Good fits to the experimental data have been obtained with a functional form for the polarization correlation function termed as the Kohlraush - William - Watts (KWW) function [29], after R. Kohlraush [32] and G. Williams and DC Watts [33].

$$\varphi_{\beta}(t) = \exp [-(t/\tau^*)^{\beta}], \quad 0 < \beta < 1 \quad (1.5)$$

where, τ^* is a characteristic decay time which is related to the hopping time of the mobile ions in the lattice and β is an exponent which measures the deviation from the simple Debye like single exponential relaxation function.

In glass-systems, the dielectric function which is related to the conductivity shows KWW-behavior. In order to show the connection between the frequency dependence of the conductivity (equation 1.3) and the non Debye-like relaxation (equation 1.5), we might start from Maxwell equation of electromagnetic field,

$$\mathbf{J}_{\text{total}} - \mathbf{J}_{\text{free}} = d\mathbf{D}/dt \quad (1.6)$$

where J refers to the electric current density and D refers to the electric displacement. The conductivity and dielectric property of the system can be related as,

$$\sigma(\omega) - \sigma(0) = i\omega\epsilon_0\epsilon(\omega) \quad (1.7)$$

where, $\epsilon_0 = 8.854 \times 10^{-12}$ farad/meter, is a permittivity of free space. Since we are dealing with a conducting dielectric, we expect that the ac conductivity is driven in part by the same microscopic mechanisms which drive the dc conductivity namely the hopping ions. Therefore the low frequency limit of the ac conductivity should yield the dc conductivity. We will write in general:

$$\sigma'(\omega) - \sigma(0) = \omega\epsilon_0\epsilon'' \quad (1.8)$$

However it should be pointed out that at high frequencies other dissipation mechanisms may be present besides the motion of mobile ions. In the frequency domain, the complex dielectric function $\epsilon^*(\omega)$ can be written as [35],

$$1/\epsilon^*(\omega) = 1/\epsilon_\infty \left[1 - \int_0^\infty dt \exp(-i\omega t) [-d\phi(t)/dt] \right] \quad (1.9)$$

where, ϵ_∞ is the relative permittivity of glass at high enough frequency, i.e. in the optical region. Integrating by parts one has,

$$1/\epsilon^*(\omega) = 1/\epsilon_\infty \left\{ 1 - [\exp(-i\omega t)\phi(t)]_0^\infty + i\omega \int_0^\infty dt \exp(-i\omega t) \phi(t) \right\} \quad (1.10)$$

Using the equation (1.5) for the correlation function one has; $\phi(0) = 1$ and $\phi(\tau) \rightarrow 0$ as $t \rightarrow \infty$, then equation (1.10) reduces to,

$$1/\varepsilon^*(\omega) = 1/\varepsilon_\infty \int_0^\infty dt \exp(-i\omega t) \varphi(t) \quad (1.11)$$

Therefore, we have a relation between conductivity $\sigma(\omega)$ (or dielectric function, $\varepsilon(\omega)$) and the correlation function for the decay of the macroscopic electric field \mathbf{E} . The reciprocal of the complex dielectric constant in equation (1.11) is referred as the electric modulus :

$$1/\varepsilon^*(\omega) = M^*(\omega) \quad (1.12)$$

and was formulated by C. T. Moynihan [36], V. Provenzano [37], and P. B. Macedo [38] in analogy to the mechanical relaxation (shear stress relaxation [39,40]). In this way the dielectric relaxation function is expressed in terms of the decay of the electric field (or electric stress),

$$\mathbf{E}(t) = \mathbf{E}_0 \varphi(t) \quad (1.13)$$

The stretched exponential form for the correlation function (see equation 1.5) is equivalent to a distribution of correlation times. Indicating $g(\tau)$ as the normalized distribution of correlation times, one can write

$$\varphi(t) = \exp[-(t/\tau^*)^\beta] = \int_0^\infty dt g(\tau) \exp(-t/\tau) \quad (1.14)$$

From equation (1.11-14) one has

$$\begin{aligned} 1/\varepsilon^*(\omega) &= (1/\varepsilon_\infty) i\omega \int_0^\infty dt \exp(-i\omega t) \int_0^\infty d\tau g(\tau) \exp(-t/\tau) \\ &= (1/\varepsilon_\infty) i\omega \int_0^\infty d\tau g(\tau) \tau/(1+i\omega\tau) \end{aligned} \quad (1.15)$$

Here, we should keep in mind that equation (1.13) and (1.14) are purely phenomenological and convey little information about the microscopic origin of the non-exponential decay of the correlation function. In fact equation (1.14) has been used without reference to the physical basis of how it originated, although it describes the observed data quite well.

It has been quite popular to express the results of dielectric measurements in terms of the electric modulus although some doubts have been raised about the correct interpretation of the data in terms of dielectric relaxation [44-46]. The electric modulus formalism is based on the analogy to the mechanical relaxation. Provenzano et al. [37] termed the relaxation in FICs as 'Conductivity Relaxation' rather than 'Electrical Relaxation'. He also recognized the usefulness of the Stevels [41] and Taylor [42] model. In this model, the low frequency dispersion in $\sigma(\omega)$ and $\varepsilon(\omega)$, and the non exponential decay of electric field (or frequency dependent conductivity) were attributed to the lack of translational invariance of the potential energy barrier. The potential barrier impedes ion-diffusion in the vitreous quasi-lattice.

It also has been argued [3, 51, 52, 62, 63, 75, 104] that the frequency dependence of the conductivity (see equation 1.3) is a direct consequence of the non-

exponential decay of the electric field (equation 1.13), whereby the two coefficients β and s are simply related :

$$\beta = (1-s) \tag{1.16}$$

The main scope of this work is to characterize more fully the ionic conduction process in glassy-FIC on a microscopic level by employing NMR techniques in an effort to relate the above described macroscopic ionic conductivity to the microscopic ion-dynamics. Although we still have a poor picture of how the conductivity is related to the thermally activated hopping rates of individual ions, the importance of developing the physics of relaxation in complex systems was recently pointed out in a workshop on "Relaxation in Disordered Systems" [43], whereby the multiple role of relaxation in many branches of science, technology and engineering is also recognized.

1.3 NMR and Impedance Spectroscopy Measurements of Ionic Conductivity in Glass

1.3.1 Probes for the Study of Fast Ionic Conductors (FIC)

A glassy-FIC provides two challenging problems in the field of the study of the relaxation in complex systems. One is the structure relaxation [59] of glassy-matrix and the other is the conductivity relaxation of the diffusing ions in the glassy or liquid state. The phenomenology of conductivity relaxation seen in many ionic glasses is similar to the one seen in molten salts [60], in electrolyte solutions [61] and Na β -Al₂O₃ [58, 62, 63]. These similarities require that a theory or model may be structure independent, as was pointed out by C. T. Moynihan [58]. Furthermore, as was

mentioned above, some analogy of conducting ionic glasses [3,4, 30, 71-80] such as the power law dependence of ac conductivity is also observed in amorphous semiconductors pointing toward a rather general origin for the observations.[64- 70].

Experimental techniques which have been used to investigate glassy-FIC are conductivity, X - ray, EPR, NMR, IR and Raman spectroscopy, neutron and electron scattering and electrochemical techniques [12]. When the long range structure is of concern, elastic scattering of X-rays, neutrons and electrons are employed. Electrochemical study has some advantage, since the ionic conductor acts as a probe for chemical potentials, partial pressures, energies of formation, atomic disorder, stoichiometric deviations, phase equilibria, partial conductivity, diffusion coefficients, mobility and reaction rate constants with high precision [81]. In particular diffusion coefficient measurement are important in connection with our work on ionic conductivity. In principle one could use noble gas diffusion techniques or radioactive tracer [82] but in many cases such as lithium glasses the NMR method remains the most widely applicable.[83].

For the study of ionic motion in FIC, mechanical and electrical methods are widely used at frequencies below the far infrared (FIR) range. Above the FIR range and below optical range (typically 10^{12} - 10^{14} Hz) Raman scattering, Brillouin scattering, and Infrared absorption techniques are widely used. Overall, energies below the range of an electron volt are of interests, where we observe the low frequency fluctuation and dissipation phenomena [62,63]. IR absorption measurements are used in the range from 1.5×10^{12} Hz to 6×10^{13} Hz typically, where vibrational spectra of local structure and the spectra of vibrational motion of cations are observed [87-89]. A similar range is covered by Raman scattering and Brillouin scattering [90,91].

Mechanical methods measure the mechanical stress relaxation of glass, where Rheovibron [84] and ultrasonic techniques [85,86] covers frequency range between 10^2 Hz and 10^8 Hz, respectively. Electrical methods measure the impedance as a function of frequency (so called Impedance Spectroscopy, IS), where low frequency bridge methods are used up to 10^6 Hz typically, and high frequency bridge method are used up to 1×10^9 Hz at the present time at Iowa State University [46]. There is an experimental gap in measurement frequency between 10^9 Hz and 10^{12} Hz, although a decades above 10^7 Hz might be covered by time domain reflectometry [91]. The coverage of each technique in the frequency domain is depicted in Fig. 2.2. The importance of crystallographic studies using Bragg scattering of X-rays and neutrons is obvious and another broad open area for the study of disordered systems. The techniques employ tunable X-ray source (synchrotron) and pulsed neutron sources (Spallation) [1]. These techniques are not considered in this work, where we are mainly interested in the dynamic aspects of glassy systems.

The experimental measurements performed in the present work are NMR measurements in the range 4 to 135 MHz and Impedance spectroscopy (IS) measurements in the frequency range 0 to 4 MHz. A comparison of the two techniques is presented in the next section.

1.3.2 NMR and Impedance Spectroscopy

As was seen in the previous section, many spectroscopic techniques can be employed for the study of glasses, which rely both on scattering and resonance phenomena. The two techniques most widely used are NMR and conductivity measurements. The NMR spin lattice relaxation rate (NSLR) is related to the

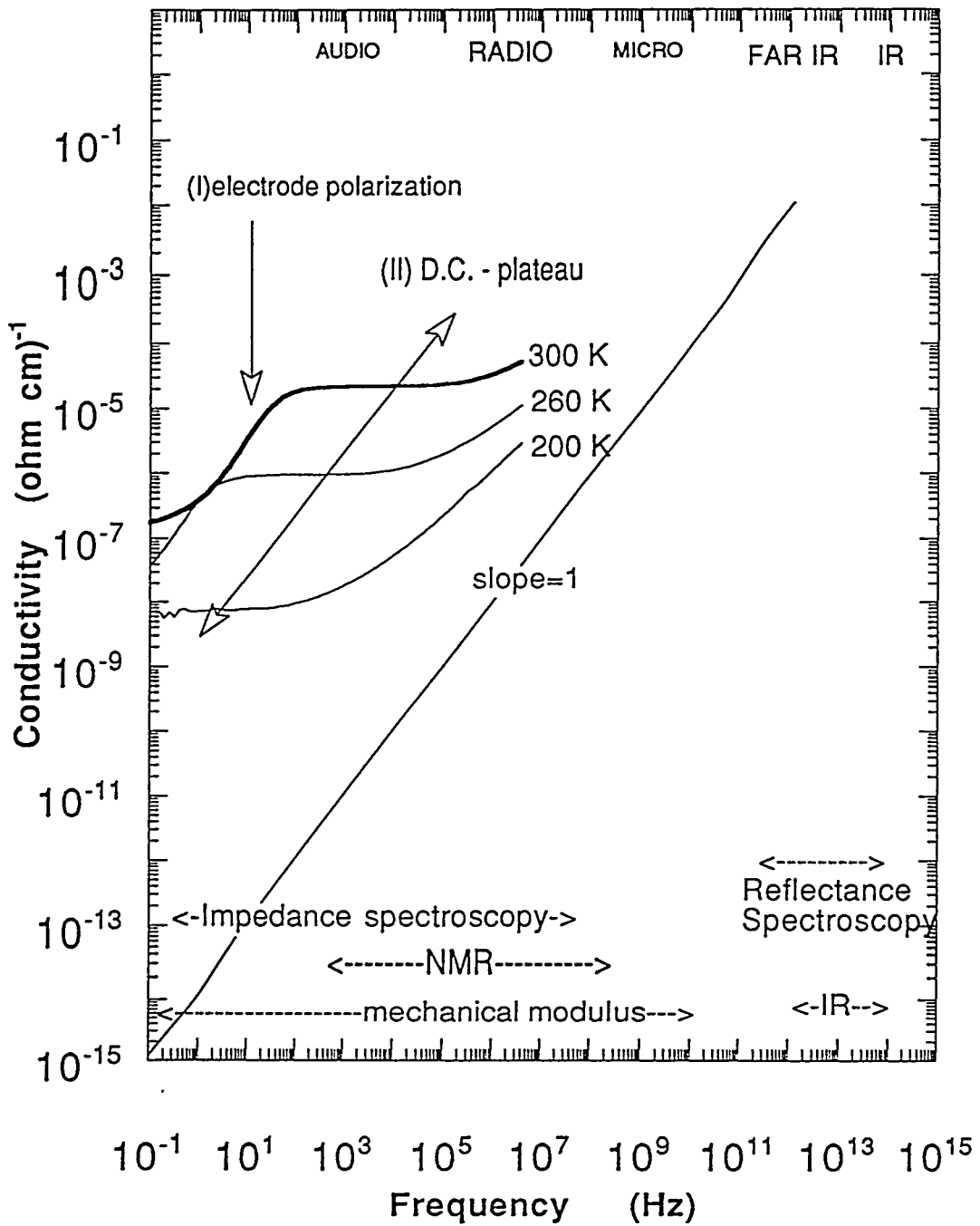


Fig. 1.2 The experimental frequency range of the most widely utilized experimental techniques in the study of the Fast Ionic Conductors

spectral density of the position-position correlation function and thus probes the local charge - density fluctuations. The frequency dependent conductivity, on the other hand, measures the macroscopic relaxation properties of the electric field and thus probes the dissipation due to the long range diffusion of the charges [51,52].

The correct comparison of the results obtained by the two techniques is of paramount importance for the understanding of the ionic transport dynamics from a microscopic point of view. The comparison of measured parameters, such as the activation energies, obtained from limited ranges of temperature and/or frequency has often led to discrepancies and ambiguous conclusions [97].

The frequency dependence of the conductivity [92,97], and the deviation from ω^{-2} frequency dependence of the NSLR [97] are both a consequence of the non exponential behavior of the relevant correlation functions. Non exponential behavior in the correlation function has been the observation for nearly all fast ion conducting glasses and is most often interpreted as a result of correlation between the ions during diffusive motion. Only in the limit of nearly zero (ppm) ion concentration does exponential relaxation result. Non exponential behavior is often described by a time dependence of the form of equation (1.5), which often called as KWW function. The physical significance of the KWW function is an important, but debated, question: It could be simply the indication of inhomogeneous relaxation, i.e., a distribution of correlation times [97,106] or it could represent the more fundamental effect of the slowing down of the relaxation at long times due to cooperative effects [104].

The combined study of ac conductivity and NSLR for the same FIC system over a wide range of frequency and temperature are rare [54,55], as well as the tests of theories or model with all known experimental data. Previous work of lithium thio-silicate is well described both by KWW correlation function [54] and by distribution of

activation energies [56,57], indicating that the two approaches are equivalent although they may describe different physical mechanisms.

The issue here is what are the microscopic physical phenomena which lead to the phenomenology described above. To do this, one has to relate the phenomenological parameters to microscopic quantities and test the validity of the theoretical predictions. This was done for both the description in terms of a KWW correlation function [104] and for the distribution of activation energies [56,57], but in either case the test was limited to only a few systems. In this work, the test will be extended to several glassy-FIC where the concentration of cations is changed systematically within the same NWF .

1.4 Summary of Measurements to Date and the Objectives of the Thesis

1.4.1 Summary of Measurements to Date

Previous studies of conductivity in glasses are numerous, but until recently the research was mainly directed towards the optimization of the dc-conductivity and very few studies were concerned with the understanding of the conduction process. The procedure for enhancing the dc conductivity has been done by varying the network former (NWF) and/or the network modifier (NWM) and/or the concentration of dopants systematically, as shown graphically in Fig. 1.3 as is the result of intensive study in glass chemists. The interests in the conduction mechanism was largely originated by the observation of the strong composition dependence and the frequency dependence of the conductivity. As mentioned in section 1.2.3., Macedo et al. [38] were the first ones to show that the dispersion of conductivity is a consequence of the

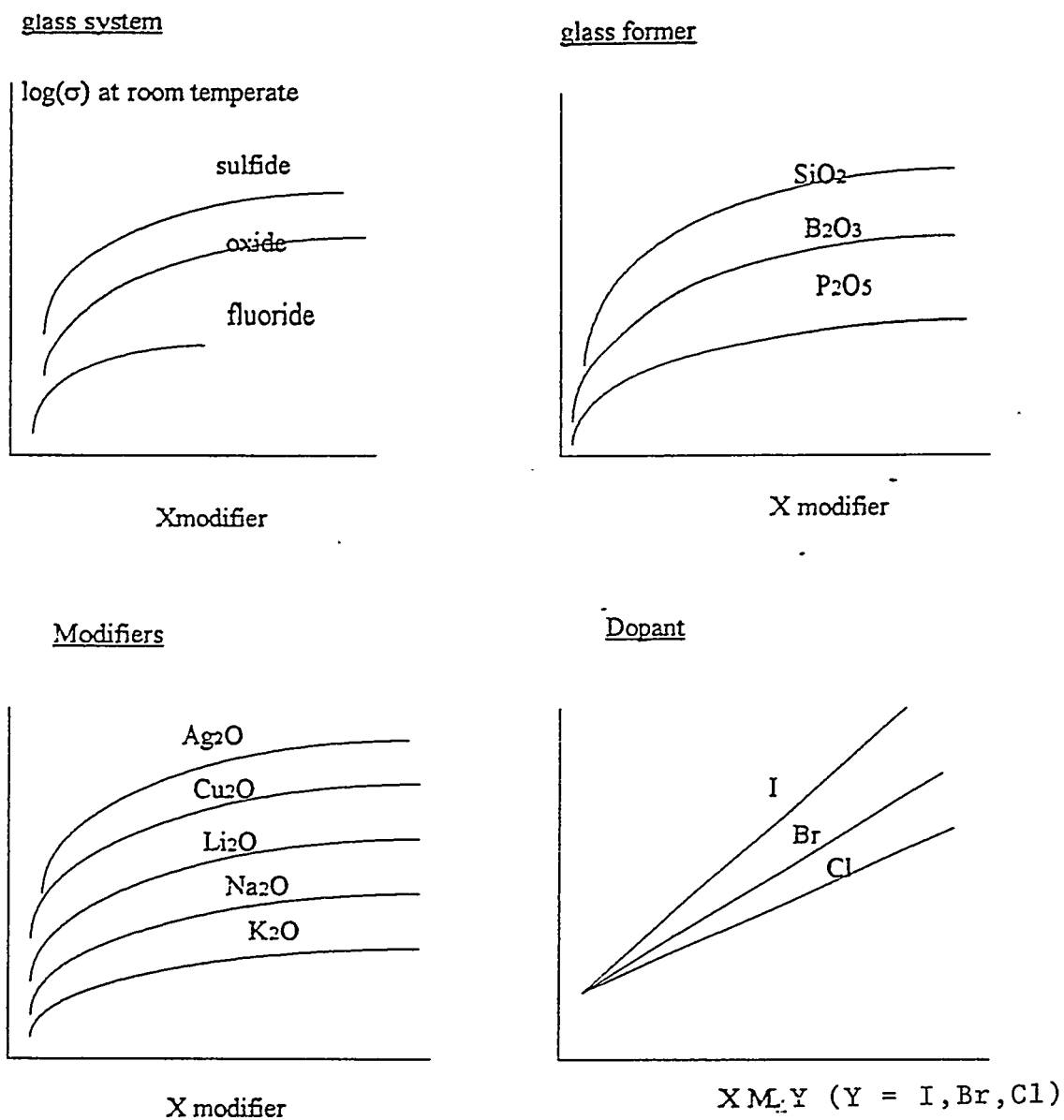


Fig. 1.3 The relative value of the room temperature dc conductivity in log scale due to the variation of the glass system, NWF, NWM, and salt dopant variations vs. the amount X of modifier or dopant. For real data see [196] and references in there.

non-exponential nature of relaxation in the time domain. Two main approaches were used to study this behavior. The first and most widely used approach refers to the electric modulus $M^*(\omega)$ defined in equation (1.12). The electric modulus was fitted using the relationship (1.11) and by modeling the correlation function with the KWW function (equation 1.5). A typical fit obtained by using the KWW-function is shown in Fig. 1.4. In general, the KWW-function does not reproduce the experimental data at high frequency. Recently, several authors have suggested that artifacts may be present in the electric modulus spectra [44 - 46]. These criticisms should be considered carefully, if one wants to use the electric modulus formalism to describe the conductivity. The other type of correlation functions such as Cole - Cole and Cole - Davidson functions have also been tried [105 - 107]. The 2nd. approach to the ac conductivity data analysis concentrates on the power-law dependence of conductivity [46 and references therein], and attempts were made to explain the physical meaning of exponent "s" in equation (1.3). This approach, however, is not considered in this work because it is purely macroscopic and phenomenological.

Regarding NMR, Bishop and Bray [96] appear to have been the first to have examined the effect of fast ion dynamics on the NMR response of an ionic conducting glass. They observed the narrowing of the mobile ion spectrum due to motional average [94] of interactions among nuclei. Göbel et al.[83] observed the asymmetry in the semi-log plot of the NSLR vs. $1000/T$, which is a salient feature of all NMR measurements in glassy FIC-systems. Typical results obtained from the NSLR as a function of temperature and resonance frequency are shown in Fig. 1.5.

S. W. Martin and C. A. Angell [97] related the observations in NMR to the observations in the conductivity data which shows the characteristic frequency dependence at high frequency and at low temperature as shown in Fig. 1.6.

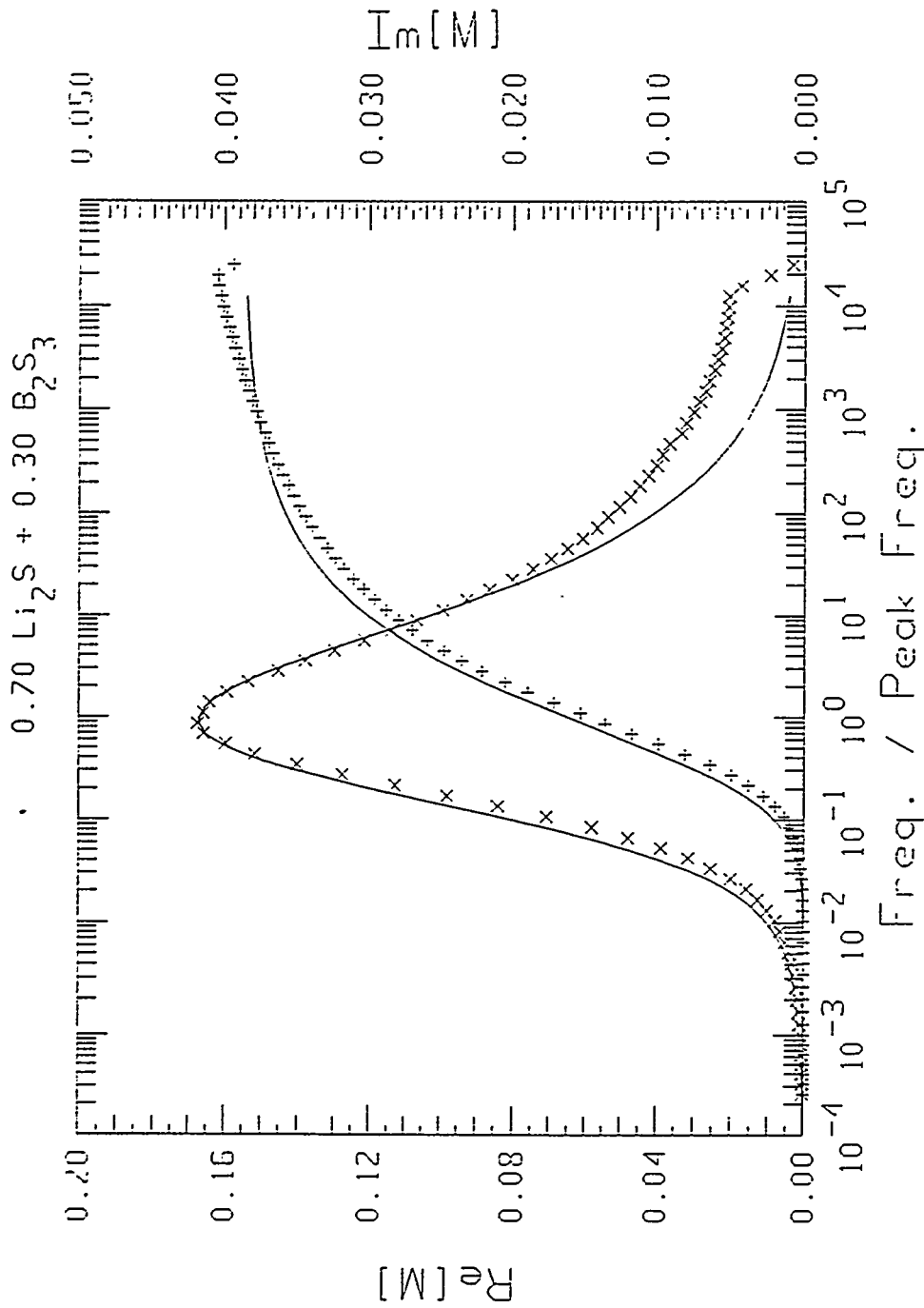


Fig. 1.4 Fitted electrical modulus of lithium thio borate with KWW correlation function. The fit using KWW model underestimate the high frequency electric modulus data.

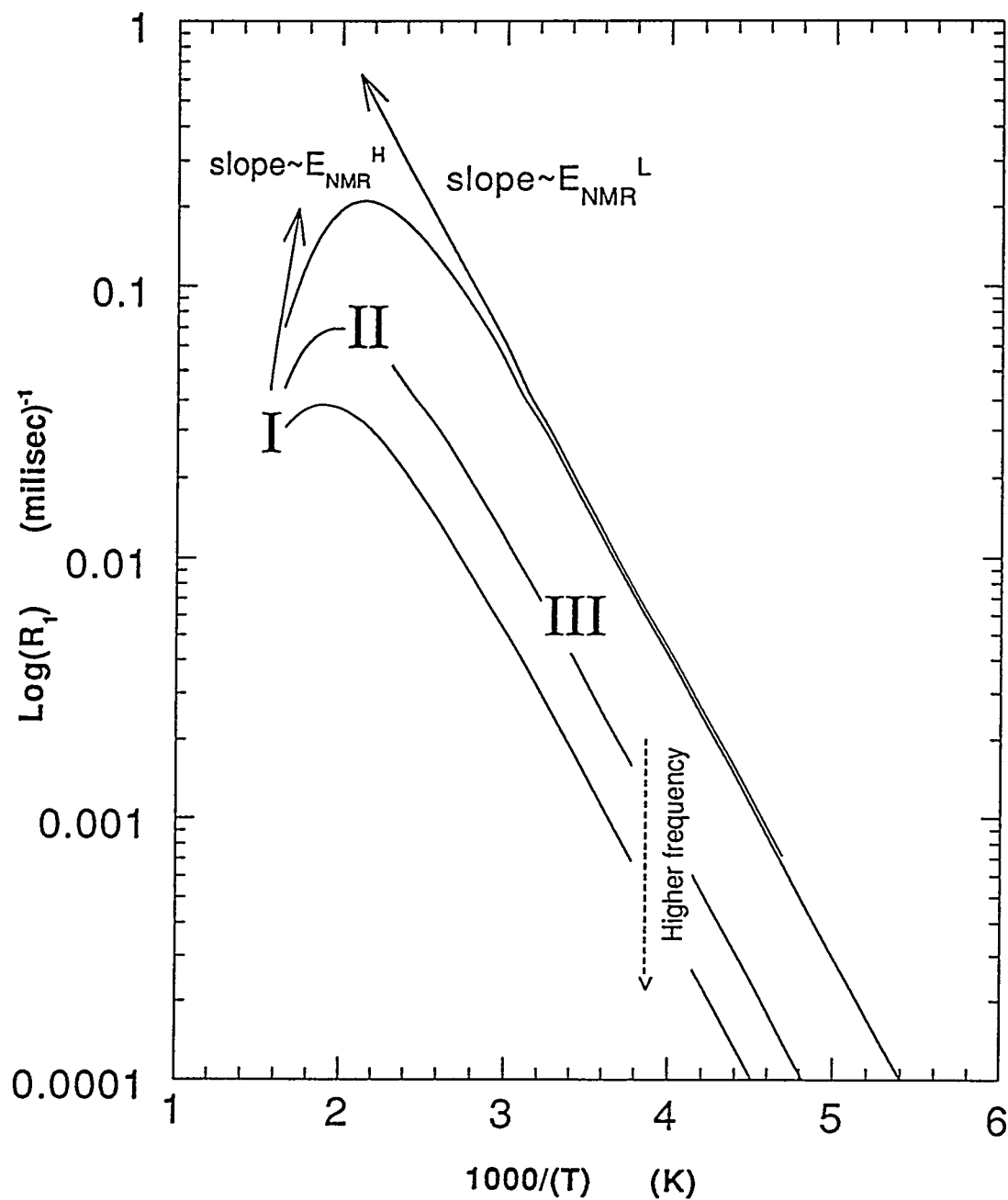


Fig. 1.5 A typical plot of $\text{Log } T_1^{-1}$ vs. $1000/T$. The shape of the curve is asymmetric about the peaks (T_1^{-1} maximum, where $\omega\tau \sim 1$), which is a landmark of non exponential behavior different from conventional BPP [94] behavior.

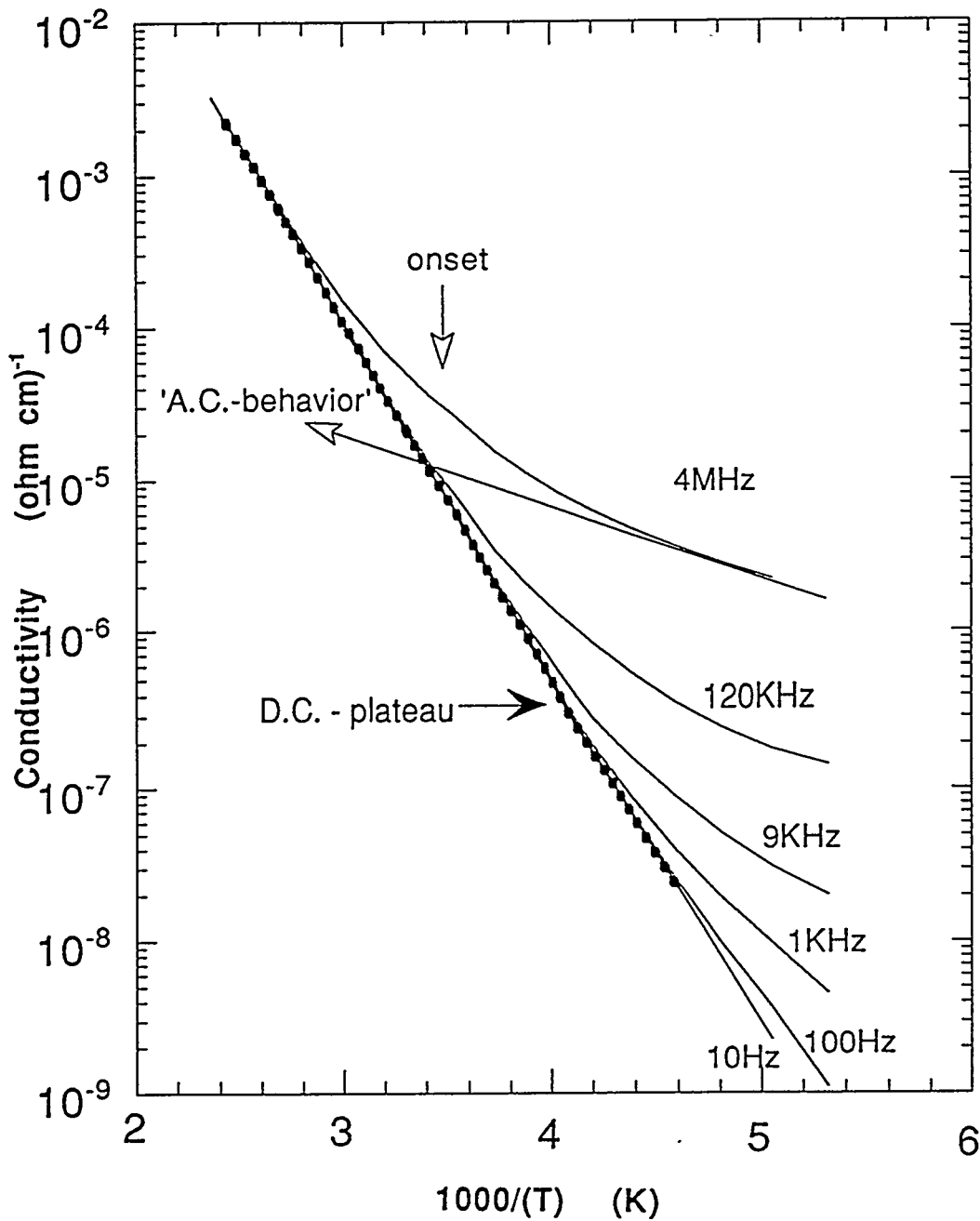


Fig. 1.6 A typical Arrhenius plot of conductivity data of glassy fast ionic conductor. The slope of the d.c. plateau gives E_{σ}^{dc} , and the slope of the line marked by arrow shows 'a.c.-behavior' which was interpreted as $E_{\sigma}^{\text{a.c.}}$. The solid curve calculated from KWW - correlation function gives E_{σ}^* .

Martin and Angel predicted also that FIC chalcogenide glass to be an ideal candidates for the combined study of NMR and conductivity. This is because one wants to exclude any effects due to glass transition, in other words the observation with NMR and conductivity should be done much below the glass transition temperature, T_g for the following reasons: (i) The deviation from dc plateau occurs around T_g , which might be an effect of structural relaxation of the glass host. If the ratio of structural relaxation time with respect to the conductivity relaxation time is large, then the above mentioned effect will be small. The ratio was defined as the 'de coupling index' by C.A. Angell [98]. (ii) The microscopic observation by NMR techniques demands enough data points on the high temperature side of NSLR which should not be affected by the glass transition. Therefore the choice of chalcogenide glass for the combined study of NMR and conductivity is important not only because the combined study is possible by the better conductive glasses, but also it has been found [54 - 57] that the two techniques seem to probe different aspects of ionic conduction and the accompanying relaxation phenomena which should be revisited and confirmed.

A brief summary of the observations and results in the study of FIC are as following: (i) Ionic conductivity, $\sigma(\omega)$, has a frequency dependence described approximately by a power law behavior, below infra-red range. Unlike electronic conductors, the power law behavior in glasses is believed to be only an approximation since the exponent seems to have a slight temperature dependence [93]. (ii) The corresponding relaxation behavior is observed to be non - Debye type and describable by a stretched exponential correlation function (or KWW - function). (iii) The frequency independent plateau observed for $\omega \rightarrow 0$ is interpreted as dc conductivity due to the thermally activated diffusion of individual ions (see the region II in Fig. 1.2). What is peculiar here is that one observes non-vanishing dc conductivity

coexisting with a broad dielectric loss peak [49]. (iv) Another general observation is the frequency-temperature superposition, where the experimental data for conductivity can be made to overlap in a master plot when proper scaling in the frequency is done. This superposition is known to hold true when the hypothetical distribution of activation energy is broad enough [45]. (v) Regarding the NMR the recurrent feature in glassy FIC is the asymmetry of the semi log plot of T_1^{-1} vs. $1000/T$ which is indicative of non exponential behavior of the position - position correlation function of the mobile ion or, equivalently, of a distribution of correlation times.

Since both conductivity and NSLR are controlled largely by the dynamics of the mobile ions it is believed that the comparison of parameters such as activation energies, correlation times etc., between the two techniques can shed light on the microscopic mechanism of ionic motion. In a number of recent publications [54-57, 100,188] it was pointed out that, contrary to previous beliefs, the correlation time deduced from NMR and the one deduced from conductivity are different. This point is illustrated in Fig. 1.7, where the correlation times obtained directly from three techniques are compared. This point is addressed in the present work in the attempt to learn more about the microscopic mechanisms of the mobile ion dynamics.

1.4.2 The Objectives of the Thesis

As was discussed in the previous section, the correct comparison of the results obtained by the two techniques (conductivity and NMR) is of paramount importance for the understanding of the ionic transport dynamics from a microscopic point of view. This is because the NMR spin lattice relaxation rate is related to the spectral

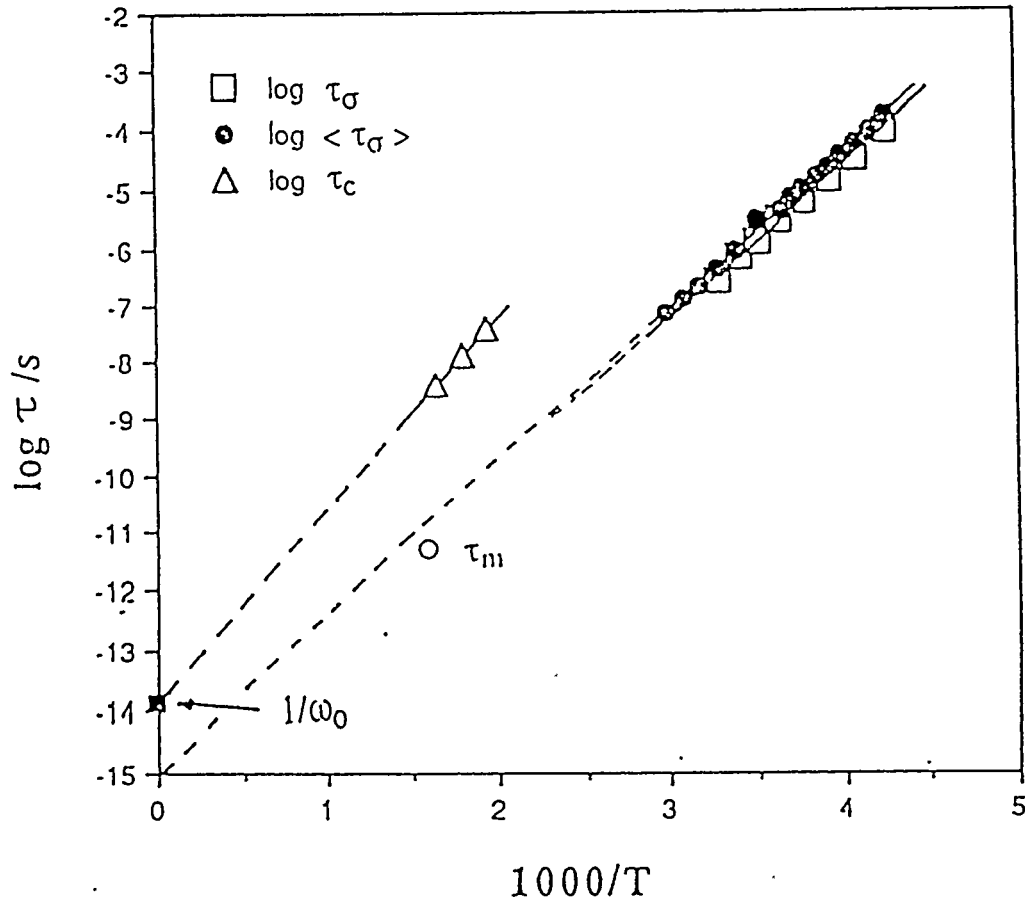


Fig. 1.7 Correlation times from NSLR(triangle)[55], mechanical modulus (open circle) [47], and electrical modulus (filled circles and rectangles) are compared. The point marked as $1/\omega_0$ is from the data of FIR spectrum [61]. The subscript c, σ , and m refers to NSLR, electrical conductivity and mechanical (Brillouin scattering) measurements respectively. Taken from M. Tatsumisago, C. A. Angell and S. W. Martin[100].

density of the position - position correlation function and thus probes the local charge - density fluctuations. The frequency dependent conductivity, on the other hand, measures the macroscopic relaxation properties of the electric field and thus probes the dissipation due to the long range diffusion of the charges.

In a previous work [56,57] the differences in the correlation times observed in lithium thio silicate glass were explained by a model based on a distribution of activation energies and percolation effects dominating the dc conduction. This assigns the dominant role to "disorder effects". A totally different approach based on the assumption of the dominant role of "correlation effect" on ionic motions was also applied to the observed differences in correlation times in lithium thio silicate glasses [56, 108]. *The main objectives* of the present work is a critical assessment of the two above models and their comparison with the experimental data. In order to achieve this goal it is important to perform measurements of both NMR and conductivity on the same samples in wide composition, frequency and temperature ranges. The systems investigated here were chosen carefully for the present purpose and for comparing with previous studies. Once the objectives of establishing which of the two models is more suitable to describe NMR and conductivity, we aimed extracting microscopic information about the hopping ion dynamics from the data.

CHAPTER II. BACKGROUND

2.1 Structural Properties of Chalcogenide Fast Ionic Conducting Glass

2.1.1 Glass Formation in Chalcogenide Systems

The chalcogenide glasses are based on elements from group VI, or combined with elements from group IV and group V, such as photo conductive a - Se and a - As_2Se_3 which is used in photocopiers [108] and a - $\text{Ge}_{33}\text{As}_{12}\text{Se}_{55}$ which is used in IR optical windows [27]. The attention to the chalcogenide glasses during the last two decades has been motivated originally by their relatively high infrared transparency [110],whereby the superior ionic conductivity of chalcogenide ionic conductive glasses were predicted by the weak electrolyte theory [103] and the Anderson - Stuart model[184] for dc ionic conductivity (see section 2.3.1).

The chalcogenide conductive glasses which were studied in this thesis are described in the frame work of continuous random network (CRN), although short range order (SRO) are present in the glass net work. The oxide glass analogy was used for the description of short range order (SRO), as well as the concepts of the network former (NWF) and the network modifier (NWM). The glass properties related to the structure (SRO) will be discussed in the section following for the chalcogenide conductive glasses of general formula, $x\text{M}_2\text{S} + (1-x)\text{FS}_2$ (sulfide glasses), where x is mole percents and $F = \text{Si}, \text{Ge}, \text{B}_{2/3}, \text{P}_{4/5}, \text{As}_{2/3}$ and $M = \text{Li}, \text{Na}, \text{K} \dots, \text{Rb}$ etc., as in the oxide glasses of formula, $x\text{M}_2\text{O} + (1-x)\text{FO}_2$. The comparison of ionic conductivity of the sulfide glasses to the one of oxide glasses are also discussed.

2.1.2 Fast Ion Conducting Chalcogenide Glasses

The first vitreous electrolyte studied were oxide glasses. They were the results of a reaction between NWF, and NWM which bring cations responsible for ionic conductivity. In general these glasses present low conductivity at room temperature ($< 10^{-8} (\Omega\text{cm})^{-1}$). It was essential to improve their conductivity before considering their use in any electrochemical devices.

The prefactor σ_0 ($= \frac{n(Ze)^2}{k_B T} a \lambda^2 v_0$) of dc conductivity in equation (1.4) was in the ranges from $10^2 (\Omega\text{cm})^{-1}$ to $10^3 (\Omega\text{cm})^{-1}$ for all oxides and sulfides. These more or less constant prefactor support the weak electrolyte model rather than the strong electrolyte model. In other words, the dc conductivity is mainly controlled by the variation of activation energies. Regarding the mobility of mobile ions, the Hall effect measurement on silver thio phosphate glass shows that the mobility of the Ag^+ ions remains constant in the whole composition range (mobility of $\text{Ag}^+ = 6 \times 10^{-4} \text{ cm}^2 \text{ v}^{-1} \text{ s}^{-1}$ was reported at room temperature [113]).

The overall trend of dc conductivity of the sulfide glasses are similar to the oxide system as summarized in the Fig. 1.3. The only exception is that the glass former effect is such that $\sigma_{\text{dc}}^{\text{B}} > \sigma_{\text{dc}}^{\text{Si}} > \sigma_{\text{dc}}^{\text{Ge}} > \sigma_{\text{dc}}^{\text{P}}$, therefore thio borate is superior to thio silicate in sulfide glasses. This inverted sequence in the NWF effect in dc conductivity in sulfide glasses makes exception to the first approximation of relating σ_{dc} to the bond strength between mobile ion (Li^+) and the anion of NWF (S^{-2} or O^{-2}). This bond strength will be weaker as S(or O) is tightly bound to the cation of NWF, and then the smaller the conductivity (e.g. $\sigma_{\text{dc}}^{\text{Si}} > \sigma_{\text{dc}}^{\text{B}} > \sigma_{\text{dc}}^{\text{Ge}} > \sigma_{\text{dc}}^{\text{P}}$) as seen in oxide glass. To go further in that course would imply an exact knowledge of

the glass structure. The detailed comparison of dc conductivity between oxide glasses and sulfide glasses can be seen in the review article of A. Pradel and M. Ribes [111] and J. H. Kennedy et al. [112], respectively.

The structure of disordered materials is generally modeled in a two distinct ways :(i) the one is 'disordered model' such as continuous random network model (CRN) of covalent glasses, random close packing model (RCP) of metallic glasses and random coil model of low dimensional glasses [108] and (ii) the other is the 'ordered model ' which postulates the existence of crystalline micro-domains as in the quasi crystal model [27, 111]. One finds few complete models which can describe the observed SRO and IRO (intermediate range order) in a collection of disordered materials. Though liquid is a good example of disorder, it does not support shear thus one can not call a liquid a glass, therefore liquid can not be used for modeling glasses.

In the chalcogenide glasses, the coordination is given by 8-n rule [108] in which one has the basic relation for the coordination :

$$\text{Number of Valence Electron} + \text{Number of Covalent Coordination} = 8$$

This relation is exemplified in Table 2.1.

If a glass forms a structure following 8-n rule in a completely random manner, there should be a *continuous distribution* of the bond angles and distances in the structure as is assumed in the continuous random network model for the covalent glasses. In reality, the short range orders observed in the glasses which does not fully support the complete disordered model.

Table 2.1 A part of the periodic table with elements exemplifying covalent bonding behavior

Number of Valence Electrons		
n = 4	n = 5	n = 6
Si	P	S
Ge	As	Se
Number of covalent coordination		
Z = 4	Z = 3	Z = 2

2.1.2.1 Structure of Boron Based Glasses

Regarding boron based glasses, the observed SRO's (structural groups in short range order) in thio borate glass (i.e., $a\text{-B}_2\text{S}_3$) are; ortho thio borate, trimer (six membered ring or boroxol or meta thio borate) and dimer (four-membered ring). Each structural units form covalent random network in the glass [115]. The borate glass (i.e., $a\text{-B}_2\text{O}_3$) does not have dimer (four-membered ring) which is found in thio borate. The study of SRO in $a\text{-B}_2\text{O}_3$ was reviewed by J. Krogh - Moe [116], and according to the extensive literature search by D. R. Bloyer, Jr. [118], the study of the sulfide glasses (e.g. thio borates) are far from complete till very recent time. The SRO of the thio borate glasses seems to be qualitatively similar to the borate glasses, although quite different quantitatively.

Intermediate range order (IRO) may be found both in the borate and thio borate systems in the form of chain-meta (thio) borate, cyclic-meta (thio) borate, pyro (thio) borate, and penta (thio) borate, as one adds up the amount of NWM to the NWF As

was shown in Fig. 1.1, there occurs a change in the coordination of boron (from three coordinate to four coordinate as one adds up the amount of the NWM to NWF) which complicates the SRO in the boron based glasses. The short range order and possible intermediate range order are illustrated in Fig. 2.1.

2.1.2.2 Structure of Silicon and Germanium Based Glasses

The structure of silicon based glasses is the simplest of all the glass structure, yet many of the details are not yet fully understood like the other glasses. The building block of silicate glasses is tetrahedral (SiO_4) similar to the low alkali borate or thio borate, and these SiO_4 units are linked by corner to form a glass network. The information about the connectivity of silica tetrahedra (SiO_4) obtained through ^{29}Si - MAS (magic angle spinning) NMR gives the information about corner sharing (or number of bridging oxygen's which give the magnitude of the chemical shift of ^{29}Si - NMR resonance line) of the tetrahedra, which is expressed as Q_n ($n = 0$ to 4): Q_0 represents all NBO's (or isolated SiO_4 tetrahedron) and Q_4 represents all bridging oxygen's (BO's). One may have impression of having more available sites for mobile ion hopping as one have more fraction of low Q's in the glass structure.

In the thio silicate glasses, differing from silicon oxide glasses, it appears that the NMR reveals not only sulfur connectivity (Q_n 's) but also differences between edge shared and corner shared silicon tetrahedra (Em 's, where m is the number of the shared edges of tetrahedra) [131]. The structure of the germanium and phosphorus based glasses are quite similar to the silicon based glasses in the sense that the basic structural units (SRO) are the germanium tetrahedra (GeS_4) or phosphorus tetrahedra, though their connectivity might be different from composition to composition.

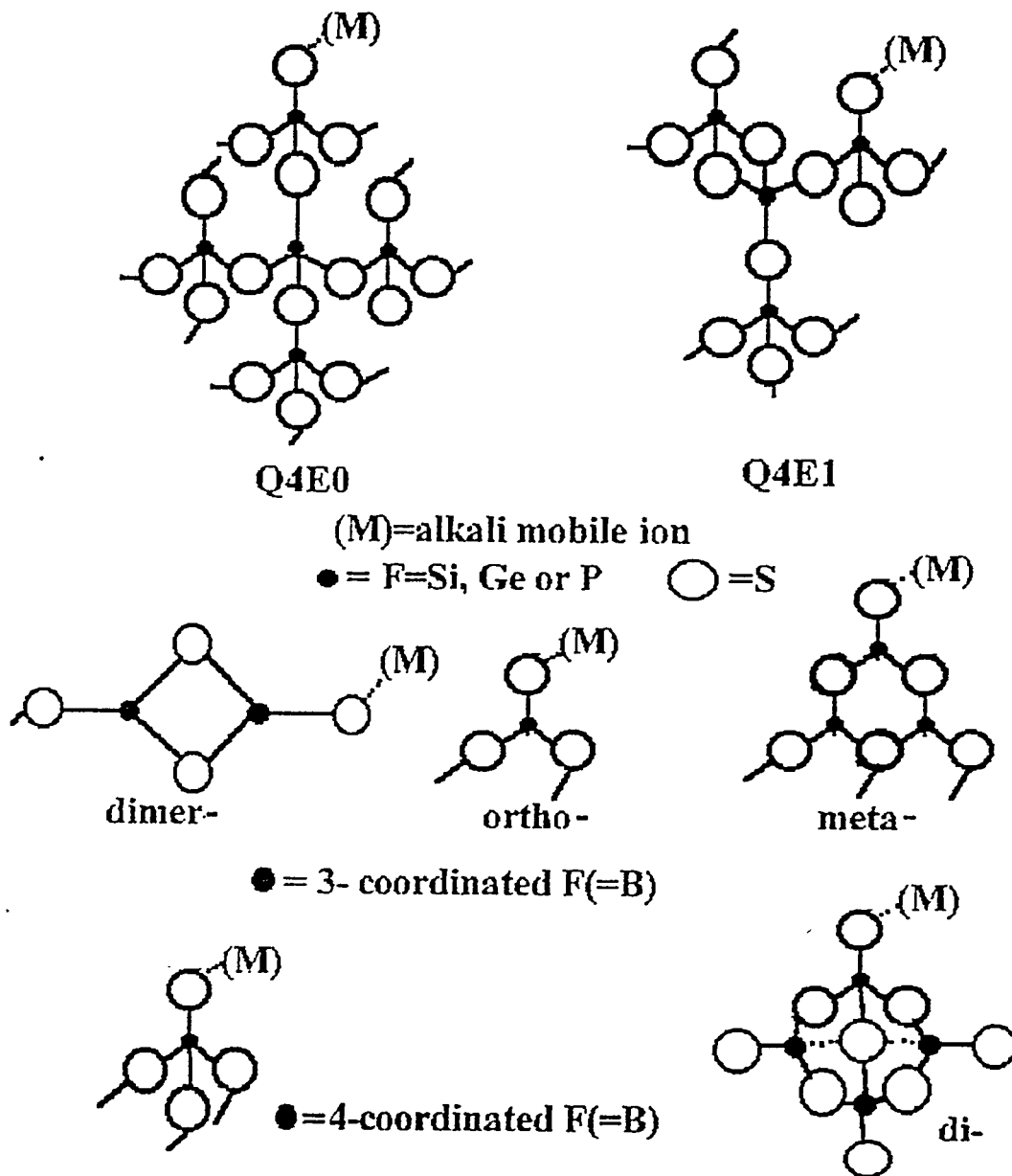


Fig. 2.1 The short range orders found in the sulfide glass of general formula $xM_2S+(1-x)F_2S_3$. For $F = Si, Ge$ or P corner sharing (Q_n) and edge sharing (E_m) of tetrahedron are seen in SRO which depend on composition x . For $F = B$, various 3- and 4-coordinated Borons are seen in SRO which depend on composition x .

The composition dependence of structure of alkali germanate glasses are as following: (i) $x = 0 \sim 0.18$, only Q4 groups are present (ii) $x = 0.18 \sim 0.33$ one NBO per octahedra are gradually formed (iii) $x = 0.33 \sim 0.5$ iso structure to silicate (only Q3 groups at 33% alkali and only Q2 groups at 50% alkali are present)

2.1.2.3 Structural Trends and Ionic Conductivity

A glass generally has more wide composition range than its crystalline partner, thus the glass shows wide variation of the structure and related glass properties including ionic conductivity. Sodium glasses $\{x\text{Na}_2\text{O}(\text{or S}) + (1-x)\text{FO}_2 (\text{or S}_2)\}$ exhibit the most wide composition range and thus studied the most extensively including the study of the ionic conductivity, where 'F' is the anion of the glass former (F = Si, Ge, B_{2/3}, P_{4/5}).

The ionic conductivity, which is structure related glass property, described in the free ion-type model does not have much connection to the microscopic structure and related glass properties such as the observed trends in the dc activation energy determined from the temperature dependent dc plateau, which decreases as one adds the amount of the NWM to the NWF. Therefore detailed study of structure does not give much help to the understanding of the mechanism of the ionic conductivity in the glass. On the other hand a microscopic model for ionic conductivity do requires detailed information of the structure of the glass fast ionic conductor.

Regarding the structural trends, SRO found in a pure NWF (e.g., FO₂ or FS₂) shows continuous structural variations upon adding the NWM to the NWF. The boron based glasses shows di (thio) borate, meta (thio) borate and ortho(thio) borate at about 33, 50 and 75 mole percent of NWM is added to NWF respectively. The Si or Ge

based glasses on the other hand shows change in the number of shared corner (Q_n 's) and/or number of shared edges (E_m 's) of the tetrahedra as one adds up the NWM to the NWF. The conversion ratio of the above structural units varies from one glass system to the other glass system.

The main interest of structural trends for the study of ionic conductivity is the amount of the non bridging oxygen (or sulfur) (NBO or NBS), which provides the sites for ionic hopping motion. Regarding glass system, silicon based glasses are more capable of having NBO (or NBS) than the boron based glasses as was seen in Fig. 1.1. This idea can be applied to the oxide glasses, although it can not be applied to the sulfide glasses where thio borate shows superior ionic conductivity than thio silicate glasses. Thio borate glasses shows rich and variable structural trends with the variation of compositions and of the anion of NWM.

2.1.2.4 Structural Trends of Boron and Silicon Based Glasses

Studied by NMR

The ^{11}B NMR is an excellent tools for probing the coordination of the boron in the borate and thio borate via quadrupole interaction between nuclei and the electric field gradient specific to the symmetry of the certain SRO. The ^{29}Si -MAS (magic angle spinning) NMR is an excellent tools for the structure study of silicate or thio silicate via chemical shielding effect (chemical shift of the resonance line) of the surrounding electron clouds specific to the nature of the chemical bonding.

The recent study of ^{11}B -NMR performed by J. A. Sills, S. W. Martin and D. R. Torgeson on alkali thio-borate revealed the ratio between 3-coordinated boron (N_3) and 4-coordinated boron (N_4) of the sodium sulfide glasses [119] and potassium

sulfide glasses [120]. J. A. Sills et al. found more rapid conversion rate of four coordinated boron's from the three coordinated boron's than the borate glasses at lower alkali region, which was attributed to the presence of the di thio borate structures which might have four coordinated sulfurs instead of two coordination. Though the structural hypothesis is still questionable, thio borate seems to have more rich SRO than the borate.

Regarding the silicon based glasses, thio silicate has more rich structures than silicate glasses. The simpler structural trends in silicate is as following. A statistical arguments for a *random model* would predict the presence of all Q_n the relative numbers of which are determined by x , the amount of NWF in the glasses. The *ordered model* on the other hand, predicts for certain stoichiometric compositions to specific Q_n units, for instance, Q_3 at 33% of alkali and Q_2 at 50% alkali. The experimentally determined Q_n distribution using MAS-NMR in lithium, sodium, and potassium silicate glasses as a function of mole % alkali oxide [130], shows the trends such that the almost Q_3 's at about 33% and Q_2 's at about 50%. It may be said that the occurrence of NBO's in the network are not entirely random.

Differing from oxide glasses, thio silicate glass, it appears that the NMR reveals not only sulfur connectivity (Q_n 's as in oxide glasses which structural units are all corner shared) but also differences between edge shared and corner shared silicon tetrahedra [131]. This idea was proposed by Terhover et al. [132] for pure SiS_2 glass which consists of only Q_4 species but showed three NMR peaks which are assigned to : (i) two edge shared tetrahedra E_2 , (ii) one edge shared tetrahedra E_1 and (3) all corner shared tetrahedra E_0 . Therefore edge sharing is expressed as E_m where m represents the number of shared edges of tetrahedron. The possibility of edge sharing in lithium thio silicate glasses was first suggested by Angell [133] from MD (molecular

dynamics) simulations and H. Eckert et al [131,136] provided the experimental support for this hypothesis.

The addition of Li_2S to SiS_2 decreases the amount of edge sharing dramatically, such that no E_2 units remain at $> 40\%$ Li_2S . In this region the E_1/E_0 ratio remains approximately constant, while Q values may be continuously changing. Thus, bonding concepts used to describe the local structures of oxide glasses can not be applied directly to the structural description of chalcogenide glasses, even when they are stoichiometric analogies.

2.1.2.5 Structural Trends Studied by the other Techniques

The IR absorption is sensitive to the corresponding normal mode of molecular vibration of particular SRO. Density measurement may reveal the free volume and possible packing structure. Glass transition temperature, T_g , may be sensitive to both SRO (e.g., coordination and bond type) and IRO (e.g., possible chains and/or cyclic structures).

The observed structural trends by ^{11}B -NMR are supported by IR-absorption, density measurement and glass transition temperature measurement. The appearance of BS_4 units and reappearance of BS_3 unit were observed, which corresponds to the absorption line at $800\text{-}600\text{ cm}^{-1}$ (at about 33% of NWM addition) and the line at $900\text{-}800\text{ cm}^{-1}$ (at about 75% of NWM addition) respectively. Therefore the increase of density at about 33% of NWM is thought to be due to the increase of BS_4 units. The smaller density of the sulfide comparing to the oxide is due to the larger volume of structural unit of thio borate glasses [126]. The supposed trends of increasing T_g with BO_4 conversion, is observed in borate. The opposite trends are observed in thio

borate. Unlike the borate's, the decreasing T_g is observed as NWM is added to the sulfide network former even in the presence of rapidly increasing BS_4 , which was attributed to the "over cross linking" effect of the sulfide ions. This is due to the high conversion rate of 4-coordinate boron's, which is suggested to result in the formation of local tightly-bounded molecular like structures that exhibit less long range network bonding than the borate glasses. As a result, T_g decreases with added alkali in thio borates rather than increase as in the borate glasses [119,120].

It is interesting to note that observed IR absorption line at around 200 cm^{-1} , which is thought to be the vibrational mode due to the mobile ion motion [87,124,125]. This may be important information for the estimation of attempt frequency of mobile ion hopping motion.

2.1.2.6 Structure of Thiogermanate Glasses

Glasses with, NWF based on Si, Ge, and P are known to have basic structure unit of tetrahedra FS_4 or FO_4 , where, $F = \text{Si, Ge, and P}$. Sulfide glass have similar structural trends to oxide glasses which are based on Si, Ge, and P when one adds up the alkali content, although the trends are qualitatively the sequence $\sigma_{dc}^{\text{Si}} > \sigma_{dc}^{\text{Ge}} > \sigma_{dc}^{\text{P}}$, holds for oxides and sulfides.

Germanates (even thio germanates) seemed to be considered as less interesting for FIC due to its low conductivity and less interesting due to very similar structure as silicate. Therefore it was studied less than silicate or borate glasses. Sodium glass usually has wide glass forming range, thus structure of sodium thio germanate glasses were studied and referred in this work for structural information of thio germanate glasses.

Seemingly the first work on the thio germanate glasses was done by M. Ribes et al.. In the structure study of sodium thio germanate glasses by B. Barrau et al. [138] the presence of the GeS_4 tetrahedra and different types of chains are suggested by Raman spectroscopy.

Unambiguous assignment of vibrations to the Raman spectrum was possible for crystalline di thio germanate ($\text{Na}_4\text{Ge}_4\text{S}_{10}$) and compared to a-di thio germanate. The assignment could be expanded to the whole glass forming range and gave similar trends as thio silicate glasses. By joining these units so that the tetrahedra are connected at the corners, and each germanium atom has two terminal sulfurs, space being left for the network-modifying ions, a particular model of meta-thio germanate glass can be constructed. It was also suggested that the glass may have a repetitive pattern in the chain of 2,3,4,...etc., tetrahedra, instead of two as in the chain of the crystallized compound, and the same reasoning was suggested for di thio germanate and pyro thio germanate glasses.

The information of structure of germanate, silicate, thio silicate and sodium thio germanate would be suffice to give a picture of the structure of lithium thio germanate glasses studied in this work such as: (i) for connectivity Q_n (corner sharing) , we may use the qualitative trends of alkali germanate glasses (ii) for connectivity E_m (edge sharing), we may use the qualitative trends of alkali silicate glasses (iii) and we may notice the suggested chain structure in sodium thio germanate glasses

2.2 Nuclear Magnetic Resonance Theory

Nuclear Magnetic Resonance (NMR) uses the phenomena of nuclei absorbing resonant radio frequency energy in a static magnetic field. This phenomena is always accompanied by nuclear relaxation [137]. The first observations of NMR were published in 1946 by Purcell, Pound, and Torrey at Havard and Bloch, Hansen, and Packard at Princeton following the successful Electron Paramagnetic Resonance (EPR) experiment reported by Zavoisky and by Cumberow and Halliday [138]. The Magnetic resonance absorption and induction were used at Havard and Princeton respectively.

Here are NMR - physicist list [139],

- static or rate process
- perfect or imperfect solids
- insulators, conductors, semiconductors, superconductors
- dia magnets, para magnets, ferro magnets, ferri magnets, anti ferro magnets
- single crystals, powders, amorphous solids
- simple solids, multi component solids, alloys, molecular solids, polymers, biological molecules
- phase transitions

In the study of FIC (fast ionic conductors), one might be interested in the rate process of non-magnetic, ionic conducting and amorphous powders.

In NMR experiments, the nuclei are to be used as probes for the matter under study, one must consider whether the properties are indeed intrinsic, when nuclei experience the interactions of an atomic environment. The intrinsic properties of isolated nuclei, such as the total angular moment (spin), parity, and electric or

magnetic multipole moment must be considered first. Intra nuclear interactions are exceedingly strong (of order of 10^6 eV) compared to electron-proton electrostatic interactions (of order of an eV), so that the latter interactions have entirely negligible effect on the nuclear states. Accordingly, only nuclear ground states will be of interest in NMR experiment.

The nuclear spin I is a constant of motion, because of the negligible mixing of nuclear states by atomic interactions. The nuclear magnetic moment is proportional to the spin and is conventionally written as,

$$\mu = \gamma \hbar I = g_n \mu_n I \quad (2.1)$$

where, g_n is nuclear g-factor, $\mu_n = e \hbar / 2m_p = 0.050\ 7806(17) \times 10^{-27}$ (Joule/Tesla), is the nuclear magneton, and γ is the nuclear gyro magnetic ratio. Due to the smallness of m_n , observation of ordering in nuclear magnetic moments should be below $\sim 10^{-7}K$, below which nuclear spin coupling is order of $k_B T$. Diamagnetic is also negligible. One left with nuclear para magnetism [140],

$$M = N \gamma^2 \hbar^2 I(I+1) H_0 / 3k_B T \quad (2.2)$$

when a static field H_0 is applied to N nuclei in a solid at constant uniform temperature T . Conventional magneto static method is not capable of observing this small ($10^{-6} \sim 10^{-8}$ of electronic paramagnetic susceptibility) nuclear magnetization. In NMR experiment , which is a branch of radio frequency spectroscopy, a negligible spontaneous emission and a usage of coherent radiation suffices to describe the usage of electromagnetic radiation as a classical quantity [140]. Much of the theory in this

section is drawn from the classic work of Abragam [140] with some help from the book by Slichter [142], Wolf [143], C. P. Poole [141], T. C. Farrar and E. D. Becker [144] and Fukushima [145].

2.2.1 Hamiltonian and Nuclear Spin Lattice Interactions

The Hamiltonian of the system under study might be written in order of energetic of each terms as,

$$H = (H_{\text{electronic}} + H_{\text{crystal field}} + H_{\text{L-S coupling}} + H_{\text{electron spin coupling}} + H_{\text{Zeeman electronic}} + H_{\text{hyperfine}} + H_{\text{nuclear spin coupling}} + H_{\text{nuclear quadrupole}} + H_{\text{Zeeman nuclear}}) + (H_0 + H_1) \quad (2.3)$$

where H_0 is static external magnetic field and H_1 is radio frequency perturbing field to excite the nuclear system in NMR experiment. In NMR the terms after the $H_{\text{hyperfine}}$ might be interested. Higher energy terms might be probed by electron spin resonance and optical spectroscopy, which techniques may be complimentary to NMR.

2.2.1.1 Nuclear Zeeman Interaction

Zeeman Hamiltonian of nucleus placed in a magnetic field \mathbf{H} is given by,

$$H_{Zn} = -\mu \cdot \mathbf{H} \quad (2.4)$$

For a static field H_0 in the Z-direction, the energy eigen values

$$E_m = -\gamma h H_0 m \quad m = I, I-1, \dots, -I \quad (2.5)$$

are separated by

$$\Delta E = h\omega_0 \quad (2.6)$$

where ω_0 is a Lamer frequency, $\omega_0 = \gamma H_0$, which is typically on the order of 10 MHz. Here one introduces rotating coordinate rotating at rf frequency, a smaller radio frequency field,

$$H_1 = 2H_1 \cos(\omega t) \mathbf{i} = H_R + H_L \quad (2.7)$$

is applied perpendicular to the Z-axis, where $H_R = H_1(\cos(\omega t)\mathbf{i} + \sin(\omega t)\mathbf{j})$, and $H_L = H_R(-\omega)$. The time dependence of the expectation value of the total magnetic moment of the nuclear spin system, $\langle M(t) \rangle$, is easily found by transforming to a rotating frame of angular velocity ω with respect to the laboratory frame. In the rotating frame,

$$d\langle M \rangle / dt = \langle M \rangle \times \gamma H_{\text{eff}} \quad (2.8)$$

where the effective field (in the rotating frame) is given by

$$H_{\text{eff}} = k'(H_0 + \omega/\gamma) + iH_1$$

If the perturbing field has frequency ω_0 , then H_{eff} has only x' - component in the rotating frame. The spins will precess about x' -axis with a frequency of γH_1 . NMR experiments can thus manipulate the spin system by varying the strength and time

duration of H_1 . Here $H_1 = H_R$ is used to emphasize the effect of the resonance, where $\omega = \omega_0$, without losing generality. That is because one may neglect the counter rotating component, H_L , near the resonance [142].

2.2.1.2 Dipolar Interaction

Zeeman Hamiltonian alone, the spin system would absorb energy at the Lamor frequency, and the NMR spectrum would be a delta function with minimum broadening due to the uncertainty principle. The most important interaction which alter Zeeman split energy level, is the dipolar interactions among nuclei, thus alter the shape of NMR spectra as well as transitions between Zeeman levels (therefore affect the relaxation times). The dipolar Hamiltonian is given by,

$$H_d = \sum_{j < k} \left[\frac{\vec{\mu}_j \cdot \vec{\mu}_k}{r_{jk}^3} + \frac{3(\vec{\mu}_j \cdot \vec{r}_{jk})(\vec{\mu}_k \cdot \vec{r}_{jk})}{r_{jk}^3} \right] \quad (2.10)$$

where the sum is over all nuclear moments with r_{jk} , the vector from m_j to m_k . The interaction between two spins I and S is more transparent in the form

$$H_d = (\gamma_I \gamma_S / r^3) h^2 (A + B + C + D + E + F) \quad (2.11)$$

with

$$A = I_z S_z (1 - 3 \cos^2 \theta)$$

$$B = -1/4 (I_+ S_- + I_- S_+) (1 - 3 \cos^2 \theta)$$

$$C = -3/2 (I_+ S_z + I_z S_+) (\sin \theta \cos \theta \exp(-i\phi))$$

$$D = C^* = -3/4 (I_- S_z + I_z S_-) (\sin \theta \cos \theta \exp(i\phi))$$

$$E = -3/4 I_+ S_+ \sin 2\theta \exp(-2i\phi)$$

$$F = E^* = 3/4 I_- S_- \sin 2\theta \exp(2i\phi)$$

Where, I and S are spin operators, and polar coordinate with H_0 along z-axis is used.

The secular terms A, B commute with H_Z . Term A corresponds to the energy of one dipole in the static field produced by the second dipole.

The term B represents simultaneous flips of interacting dipoles. The terms A and B correspond to the transitions $\Delta m = 0$, the terms C and D correspond to $\Delta m = \pm 1$, and the term E and F correspond to $\Delta m = \pm 2$.

2.2.1.3 Quadrupole Interaction

The electric field gradients, EFG existing in non-cubic sites interact with nuclear quadrupole moment of nuclei with non-spherical charge distributions. This interaction is electrical in nature in contrast to the magnetic dipole-dipole interaction.

The quadrupole Hamiltonian is given by,

$$H_Q = \sum_{m=-2}^2 Q_2^m E_2^{-m} \quad (2.12)$$

where the E^m are combinations of EFG terms,

$$V_{ij} = \frac{\partial^2 V}{\partial x_i \partial x_j} = \frac{\partial^2}{\partial x_i \partial x_j} \left(\int \frac{\rho(r') dr'}{|\vec{r} - \vec{r}'|} + \sum_i \frac{Z_i}{|\vec{r} - \vec{r}_i|} \right) \quad (2.13)$$

and are given by

$$\begin{aligned}
E_2^0 &= \frac{1}{2}V_{zz} \\
E_2^{\pm 1} &= -\frac{1}{\sqrt{6}}(V_{xz} \pm iV_{yz}) \\
E_2^{\pm 2} &= \frac{1}{2\sqrt{6}}(V_{xx} - V_{yy} \pm 2iV_{xy})
\end{aligned} \tag{2.14}$$

The Q_m describes the charge distribution of the nucleus in terms of the nuclear quadrupole moment,

$$Q = \langle I, m = 1 | \sum_p (3Z_p^2 - r_p^2) | I, m = 1 \rangle \tag{2.15}$$

where the sum is over all protons in the nucleus. They are

$$\begin{aligned}
Q_2^0 &= \frac{eQ}{2I(2I-1)}(3I_z^2 - I^2) \\
Q_2^{\pm 1} &= \frac{eQ}{2I(2I-1)} \frac{\sqrt{6}}{2} [I_z(I_x \pm iI_y) + (I_x \pm iI_y)I_z] \\
Q_2^{\pm 2} &= \frac{eQ\sqrt{6}}{4I(2I-1)}(I \pm iI)^2
\end{aligned} \tag{2.16}$$

In a principle axis frame of reference where $V_{ij} = V_{ij}\delta_{ij}$ and $|V_{zz}| \geq |V_{xx}| \geq |V_{yy}|$.

Then,

$$H_Q = \frac{h\nu_Q}{6} \left[3I_z^2 - I(I+1) + \frac{1}{2}\eta(I_+^2 + I_-^2) \right] \tag{2.17}$$

with, $e q = V_{zz}$ and the asymmetry parameter and ν_Q .

$$\eta = \frac{V_{xx} - V_{yy}}{V_{zz}} \quad (2.18)$$

$$\nu_Q = \frac{3e q e Q}{2I(2I - 1)}$$

The EFG terms V_{ij} are calculated at the nucleus. The electric field gradients may originate from charges external to the atoms, except there is an additional contribution to the quadrupole coupling that is due to the distortion of the spherical electronic shell of the atoms by external charges. The induced field gradient is given by,

$$V_{ij} = \gamma V_{ij}^c \quad (2.19)$$

and the total field gradient

$$V_{ik}^{\text{tot}} = [1 - \gamma(r)] V_{ik}^c \quad (2.20)$$

$\gamma(r)$ is called the “sternheimer anti shielding factor” and r is the distance from the external charge to the nucleus.

2.2.1.4 Hyperfine Interactions

The Hamiltonian for the magnetic interaction of an electron to the nucleus might be written as

$$H_{HF} = -gg_I\mu_I\mu_B \left\{ \frac{8\pi}{3} \delta(\vec{r})(S \cdot I) + \frac{(\vec{S} \cdot \vec{R}) \cdot (\vec{I} \cdot \vec{r})}{r^3} + 3 \frac{(\vec{S} \cdot \vec{R}) \cdot (\vec{I} \cdot \vec{r})}{r^5} \right\}$$

(2.21)

where μ_B is a Bohr magneton, μ_I is a nuclear magneton $\left(\frac{e\hbar}{2m_p} \right)$, g is a g-factor of electron, g_I is a g-factor of nucleus, and I and S are the spins of the nucleus and electron respectively. Each term represents Fermi contact, orbital, and dipolar interaction in order. Each term can be deduced from calculating interactions between magnetic field due to nuclei and electronic moment in a reference frame of electron ,

$$E_{hf} \sim -\vec{\mu}_s \cdot \vec{H}_j \quad (2.22)$$

The Fermi contact term is from the expectation value of nuclear magnetic field in a sphere which enclosing nucleus. Regarding the electronic moment or spin, one distinguish conduction electrons and core electrons.

2.2.1.5 Indirect Interactions

This type of interaction is smaller in nature and couples nuclei via electron. In a simple picture, as nucleus induced current in the electron cloud, which then coupled to the other nucleus. This coupling might be spin dependent . The example of the former case is RKKY [146] interactions, and the Fridel interaction [147] , which is due to the scattering of the conduction electron by point defects leading to local variations of the hyperfine interaction for the latter case.

2.2.2 NMR Spectrum and Nuclear Spin Lattice Relaxation

NMR spectrum of resonant NMR frequencies, is a finger print of the local electronic environment of the nucleus, but depends upon the external magnetic field, which is at the control of the experimenter. The nuclear spin lattice relaxation gives dynamic information of the interactions to the environments. The intensity or the shape of the spectrum depend on the nuclear spin lattice relaxation.

The NMR spectrum with only Zeeman splitting due to external field H_0 would be quite narrow. A further interactions alter and/or shift the nuclear energy level, then gives the characteristic spectrum of the system. The relaxation process could be described either quantum mechanically or semi classically, depending on the mechanism of the de-excitation of the nuclear spins by lattice. An appropriate approximation of the rate process might always be utilized.

For FIC systems, the inherent disorder makes the situation rather complex and even to be lack of theoretical formulation except some fortunate cases where we still may use the formalism based on the regular structural. One may study either mobile or immobile ions in FIC, thus one may apply different formulations for each cases.

2.2.2.1 Classical Description

The most visible description might be solving the classical equation of motion for nuclear magnetization vector in a static magnetic field (equivalently solving the *Bloch equation* [148], which give the macroscopic definition of the spin-spin and spin-lattice relaxation time.). The equation (2.8) is not complete to describe the

motion of the nuclear magnetization, since it does not account for the relaxation. Bloch et al. assumed that the spin-spin relaxation and spin-lattice relaxation would be treated as first order process with characteristic time T_2 and T_1 respectively, such that,

$$\begin{aligned} dM_z/dt &= (M_0 - M_z)/T_1 \\ dM_{x,y}/dt &= -M_{x,y}/T_2 \end{aligned} \quad (2.23)$$

In the rotating frame, by employing H_R as rotating radio frequency,

$$\begin{aligned} dM_z/dt &= -\gamma M_y H_1 + (M_0 - M_z)/T_1 \\ dM_x/dt &= \gamma M_y H_0 - M_x/T_2 \\ dM_y/dt &= \gamma (M_z H_1 - M_x h_0) - M_y/T_2 \end{aligned} \quad (2.24)$$

where $h_0 = H_0 + \omega/\gamma$.

Since M_x and M_y must vanish as $H_1 \rightarrow 0$, one sees that M_z differs from M_0 to the order H_1^2 in a steady state. Therefore one replaces M_z by M_0 and by introducing $M_+ = M_x + iM_y$. One finally has,

$$M_x(t) = (x' \cos(\omega t) + x'' \sin(\omega t)) H_{x0} \quad (2.25)$$

where

$$\begin{aligned} \chi' &= \frac{\chi_0}{2} \omega_0 T_2 \frac{(\omega_0 - \omega) T_2}{1 + (\omega - \omega_0)^2 T_2^2} \\ \chi'' &= \frac{\chi_0}{2} \omega_0 T_2 \frac{1}{1 + (\omega - \omega_0)^2 T_2^2} \end{aligned} \quad (2.26)$$

where $H_{x0} = 2H_1$, $\omega_0 = H_0$, and $X = X' - iX''$.

The absorption line, X'' , is a Lorentzian in shape typical to narrow NMR spectrum of liquid. This absorption line can be obtained by sweeping $\omega (= \gamma H)$ or H_0 as is typically done in a continuous-wave NMR experiment in frequency domain. On the other hand $M_x(t)$ can be acquired in a time domain after applying a short duration of the radio frequency pulse. Such an obtained transient (Free Induction Decay, or FID) would be Fourier transformed to have NMR spectrum in frequency domain, which was first demonstrated by Lowe and Norberg in 1957 [149]. The pulse NMR technique is described in section 3.3 of Chapter III.

2.2.2.2 NMR Spectrum

In solid state NMR, one is interested in both the line shape and position of NMR. In high resolution NMR, or MAS NMR (magic angle spinning NMR) [150], one may be mainly interested in the position of the narrow line. The position of line, thus a shift from Lamor frequency, is accessible through *spin Hamiltonian*,

$$H = \mathbf{I} \cdot \vec{A} \cdot \mathbf{S} \quad (2.27)$$

where, \vec{A} is coupling tensor of the 2nd. rank of interaction between nuclei and its environment. The S can be a spin of either a nuclei (like or unlike) or an electron. The diagonalization of the coupling tensor with respect to the eigen states, and the use of the selection rule for the nuclear transition will suffice to give a resonance frequencies. Since the equation (2.27) is dealing with the two body interactions, it is quite an approximation which could be applied only to the narrow enough lines. In a real systems, such as solids, which involves many body interactions, the line is usually broadened and shifted by interactions to the surroundings. The main key for the formulation of the above complex spectrum might be simplification, considering the nuclear spin, lattice symmetry and the electromagnetic properties of the interactions.

2.2.2.2.1 Dipolar Interaction

Even for the dipolar line shape can not be predicted exactly, and the most basic being the moment expansion derived by VanVleck [151]. The nth. moment are defined as,

$$M_n = \int_{-\infty}^{\infty} f(\omega)(\omega - \omega_0)^n d\omega \quad (2.28)$$

where $f(\omega)$ is the normalized line shape. Usually the 2nd. moment is considered and averaged over all angles for power samples, such that,

$$M_2'' = \frac{3}{5} \gamma_j^4 h^2 I(I+1) \sum_k \frac{1}{r_{jk}^6} \quad (2.29)$$

for like spins I and I , and for unlike spins,

$$M_2^{IS} = \frac{4}{15} \gamma_I^2 \gamma_S^2 h^2 S(S+1) \sum_k \frac{1}{r_{jk}^6} \quad (2.30)$$

The simplest approximation for the solid line shape assumes that $f(w)$ to be a Gaussian,

$$f(\omega) = \frac{1}{\sigma\sqrt{2\pi}} \exp\left(-\frac{(\omega - \omega_0)^2}{2\sigma^2}\right) \quad (2.31)$$

where $M_2 = \sigma^2$, and $1 \cdot 3 \cdot 5 \cdots (2n-1)\sigma^{2n} = M_{2n}$ for the n th. moment. Then the full width at half maximum intensity, FWHM is given as,

$$\text{FWHM} = 2\sqrt{M_2} \cdot \sqrt{2\log 2} \quad (\text{in radians per seconds}) \quad (2.32)$$

which is typically on the order of kHz. The dipolar broadening of the Zeeman level and the corresponding broadened line is shown in Fig. 2.2.

2.2.2.2.2 Quadrupolar Interaction

The quadrupole interaction described in equation (2.12) is described in the laboratory coordinate system. The EFG tensor which is the 2nd. rank symmetric, traceless tensor, may be diagonalized. In the EFG principle axis system, $V_{ij} = V_{ij} \delta_{ij}$, there are three components, and since the EFG tensor is traceless,

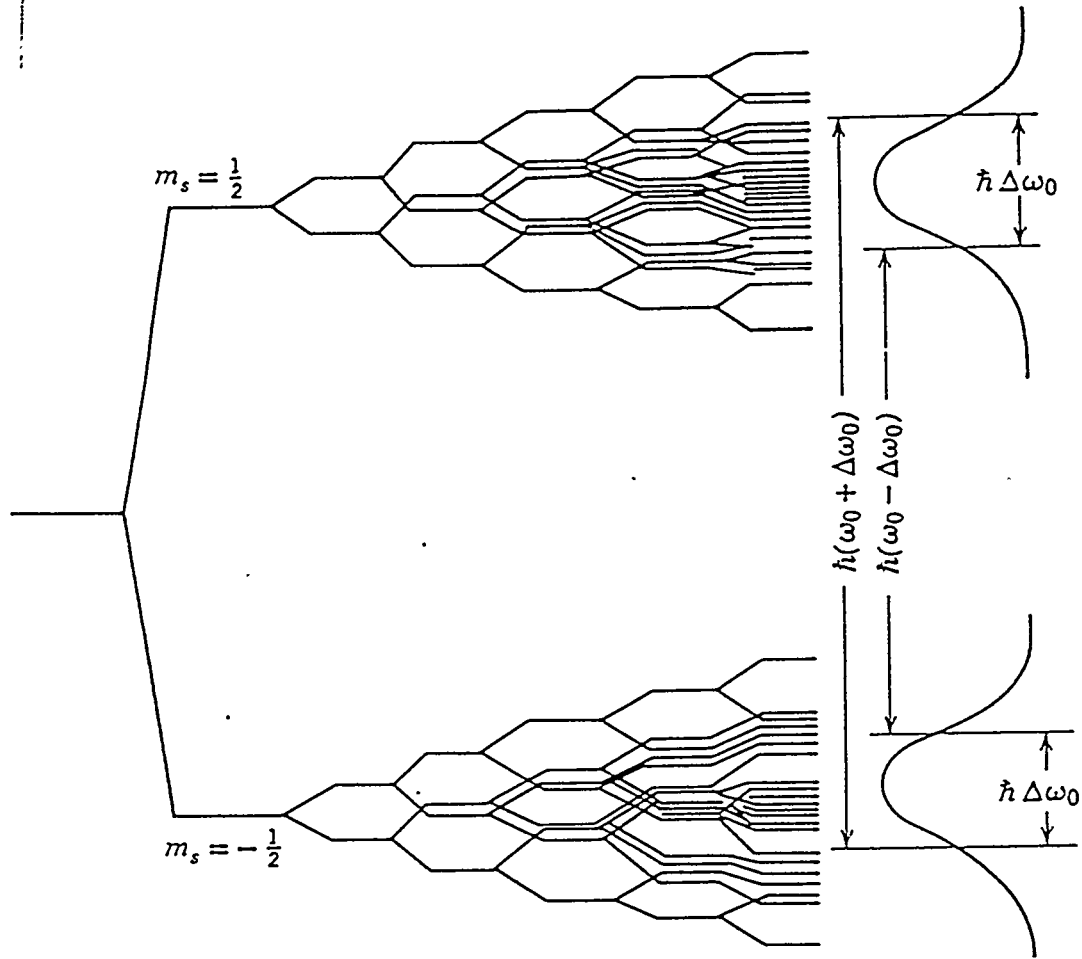


Fig. 2.2 Broadening of spin = 1/2 Zeeman energy levels by the successive applications of $I = 1/2$ dipolar interactions. The line shape of each level is shown at the right, where $\Delta\omega_0$ is the intrinsic half width of dipolar spectrum [141].

$$V_{xx} + V_{yy} + V_{zz} = \nabla^2 V = 0 \quad (2.33)$$

only two of these are independent. These are usually chosen as,

$$V_{zz} = eq \quad \text{and} \quad \eta = (V_{xx} - V_{yy})/V_{zz} \quad (2.34)$$

where η is called the asymmetry parameter and is a measure of the departure of the EFG from axial symmetry. The principle axis are usually chosen so that $|V_{zz}| \geq |V_{yy}| \geq |V_{xx}|$, then $0 \leq \eta \leq 1$. With these definitions the Hamiltonian becomes,

$$H_Q = \frac{e^2 q Q}{4I(2I-1)} [3I_z^2 - I^2 + \eta(I_x^2 - I_y^2)] = \frac{h\nu_Q}{6} [3I_z^2 - I^2 + \eta(I_x^2 - I_y^2)] \quad (2.35)$$

where $\nu_Q = \frac{3e^2 q Q}{2I(2I-1)h}$, which is the lowest pure quadrupolar energy when $\eta=0$.

When the quadrupolar energy is considerably weaker than the Zeeman energy, the first order perturbation treatment is adequate, such that,

$$E_m = -h\nu_0 m + \langle m | H_Q | m \rangle = -h\nu_0 m + \frac{h\nu_Q}{12} [3m^2 - I(I+1)] \Theta \quad (2.36)$$

where $\Theta = 3 \cos^2 \theta - 1 + \eta \cos 2\varphi (\cos^2 \theta - 1)$. The transitions for $I = 3/2$ is,

$$\begin{aligned}
\nu_{3/2 \leftrightarrow 1/2} &= \nu_0 - \frac{\nu_Q}{2} \Theta \\
\nu_{1/2 \leftrightarrow -1/2} &= \nu_0 \\
\nu_{-1/2 \leftrightarrow -3/2} &= \nu_0 + \frac{\nu_Q}{2} \Theta
\end{aligned} \tag{2.37}$$

Therefore the satellite peak are at $\nu_0 \pm \frac{\nu_Q}{2}$ and shoulder are at $\nu_0 \pm \nu_Q$ which is shown in Fig. 2.3 (A) and (B), with the dipolar broadened powder spectrum.

The 2nd. order quadrupole interaction, the single crystal energy levels for the axially symmetric case ($\eta=0$) are,

$$\begin{aligned}
E_m &= -h\nu_0 m + \frac{h\nu_Q}{12} [3m^2 - I(I+1)] [3\mu^2 - 1] \\
&\quad - \frac{h\nu_Q^2}{32\nu_0} m(1-\mu^2) \left\{ \mu^2 [18I(I+1) - 34m^2 - 5] - [2I(I+1) - 2m^2 - 1] \right\}
\end{aligned} \tag{2.38}$$

where $\mu = \cos\theta$. The transitions are

$$\begin{aligned}
\nu(m \leftrightarrow m-1) &= \nu_0 + \frac{\nu_Q}{2} (3\mu^2 - I) \left(m - \frac{1}{2} \right) \\
&\quad - \frac{h\nu_Q^2}{32\nu_0} (1-\mu^2) \left\{ \mu^2 [102m(m-1) - 18I(I+1) - 34m^2 - 5] \right. \\
&\quad \left. - [2I(I+1) - 2m^2 - 1] \right\}
\end{aligned} \tag{2.39}$$

The 2nd order term produces a splitting of the central transition, and the separation between two maximums are given by,

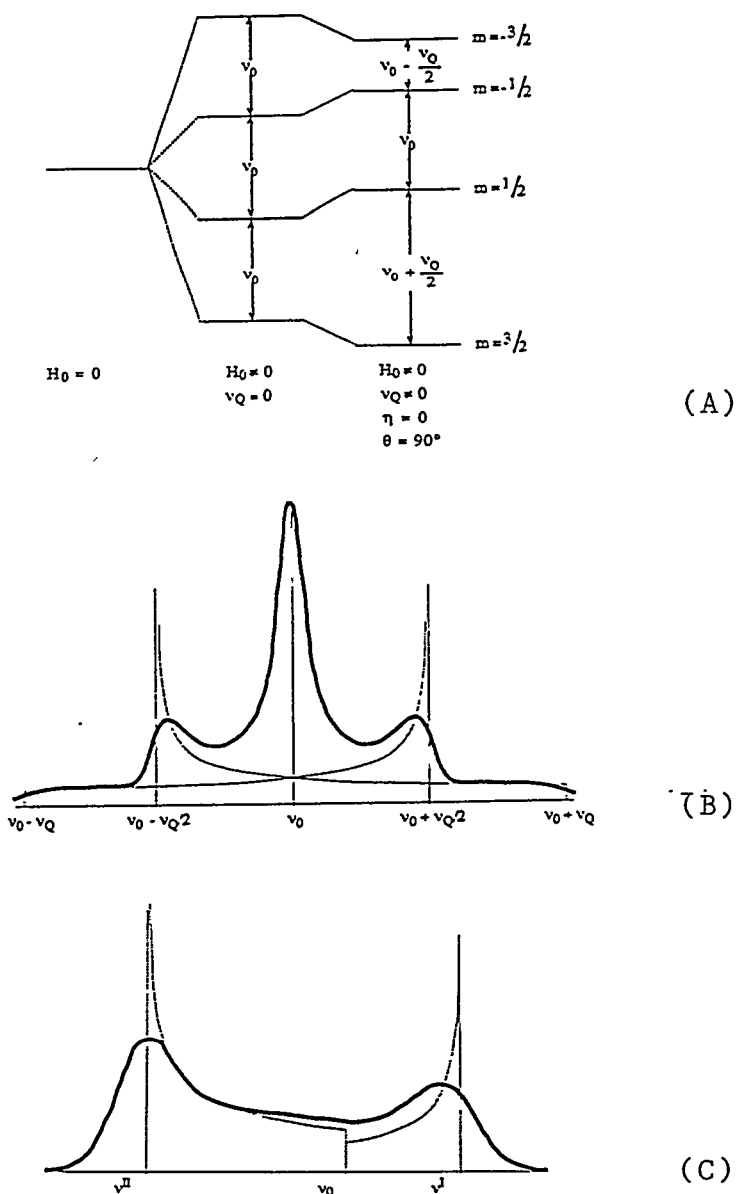


Fig. 2.3 (A) Energy level diagram for $I = 3/2$, (B) First order quadrupole spectrum, where the satellites are at $v_0 \pm \frac{v_Q}{2}$, (C) 2nd order quadrupole spectrum, where the separation $\Delta v = v^{\text{I}} - v^{\text{II}}$ are given in equation (2.40), and for $I = 3/2$, $\Delta v = \frac{25}{48} \frac{v_Q^2}{v_0}$

$$\Delta\nu = \nu' - \nu'' = \left\{ \nu_0 + \frac{\nu_Q^2}{16\nu_0} \left[I(I+1) - \frac{3}{4} \right] \right\} - \left\{ \nu_0 - \frac{\nu_Q^2}{9\nu_0} \left[I(I+1) - \frac{3}{4} \right] \right\}$$

(2.40)

for $I = 3/2$,

$$\Delta\nu = \frac{25}{48} \frac{\nu_Q^2}{\nu_0} \quad (2.41)$$

The power pattern for split central line due to the 2nd order quadrupole interaction are shown in Fig. 2.3(C) .

2.2.2.2.3 Hyperfine Interaction

Another important interactions in NMR is the magnetic interaction due to electron .Though FIC is usually an insulator with some exceptions of mixed electronic and ionic conductor, it is worth to consider this type of interaction.

The electrons could be in localized state or extended state or itinerant state. The 4 - f electrons in rare earth metal is localized on the ions to form a large magnetic moment. Such an unwanted substance in FIC would be a paramagnetic impurity, which affect the NSLR more or less. For 3d - electrons the local moments do not correspond to the extended or localized behavior. Due to this special combination of circumstances, the conduction electrons, called itinerant which form a collective state characterized by a periodically varying spin density (called spin density wave, SDW), with a wavelength that is incommensurate with the lattice spacing.

By confining the discussions to conduction electrons and unpaired (localized) electrons, equation (2.22) can be rewritten as,

$$H_{hf} = -\gamma_I \hbar \mathbf{I} \cdot \mathbf{H}_{eff} \quad (2.42)$$

where H_{eff} is the effective field produced by the electrons at the nucleus. They are conduction electron field, local field, transferred hyperfine field, and core field. Here the term 'local field' has narrow meaning such that it is due to the unpaired electrons on the other atoms or ions.

In diamagnetic materials, the first order effect of the electron-nucleus coupling vanishes due to the quenching of the orbital momentum and the zero value of the total spins. However, the applied field H_0 polarizes the electron clouds, which in turn produce a magnetic field at the nucleus proportional to H_0 . The total field the nucleus see can be described by ,

$$\mathbf{H} = H_0 \cdot (1 - \vec{\sigma}) \quad (2.43)$$

where 1 is the unit 3×3 matrix, and $\vec{\sigma}$ is the 3×3 , shielding tensor or chemical shift tensor. The principal values of chemical shift tensor can be related to the micro - structure and chemical bonding in a glass.

In metals, nucleus couples to the conduction electrons which is described by the Bloch wave function. Therefore each nuclear spin sees simultaneously the magnetic field produced by all the conduction electrons. These internal fields cause line shift, known as Knight shift [152], In the one electron approximation, the expression for Knight shift can be written as

$$K = 2\mu_B \left[H_{hf}(s)N_s(E_f) + H_{hf}(d)N_d(E_f) \right] + \left(\frac{1}{N_A\mu_B} \right) H_{hf}(0)\chi_o \quad (2.44)$$

where μ_B is the Bohr magneton, N_A is Avogadro's number, and N_s and N_d are s- and d-band density of states at the Fermi level respectively. $H_{hf}(s)$, $H_{hf}(d)$ and $H_{hf}(0)$ are the relevant hyperfine fields per electron at the nuclei, and arise from the following mechanisms: the Fermi-contact interaction [139,140] with unpaired s- electrons; core - polarization of the spin - paired s - orbitals due to d - electrons; d-electron orbital interactions. χ_o is an orbital VanVleck susceptibility

2.2.2.3 Nuclear Spin Lattice Relaxation

As was defined macroscopically in the Bloch equation (2.24). the nuclear relaxation process involves two process of approaching to the equilibrium, following the rf excitation: a spin-spin relaxation time T_2 , a characteristic time of approaching to the equilibrium in spin system, and a spin-lattice relaxation time T_1 , a characteristic time of approaching to the equilibrium in the whole spin-lattice system. The T_2 process does not involve any energy exchange with lattice, rather it is due to the dephasing of spins resulting from individual nuclei interacting with slightly different internal fields. Since the internal fields also determine the width of the NMR spectrum, a general relation holds between line width and spin - spin relaxation time as,

$$T_2 = (\delta\omega)^{-1} \quad \text{for Lorentzian line shape} \quad (2.45)$$

$$T_2 = (\sqrt{\ln 2} / \pi) / \delta\omega \quad \text{for Gaussian line shape} \quad (2.46)$$

where $\delta\omega$ is half width at half intensity of spectrum.

The microscopic relaxation of the nuclear spin system could be expressed in a simple form as,

$$R_1 = T_1^{-1} = E_c^2 f(\tau) \quad (2.47)$$

where R_1 is NSLR and E_c is coupling energy between nuclear spin and surroundings. The surroundings would be the other nuclear spin or heat reservoir, so called a lattice. A small perturbing rf would excite the nuclear spin which in turn excite the lattice by transferring energy to the lattice, while de-exciting itself. The excitation and de-excitation of nuclear spin is purely quantum mechanical in nature, though the one of lattice could be described as either quantum mechanically or semi classically.

In FIC-system if one consider FIC as a simple insulator, then the NSLR of the immobile-ion of insulator could be due to quasi particle excitation such as phonons. The NSLR of the diffusing mobile-ion would be due to the semi classical excitation due to the motion, so called a *motional relaxation*. Motion with spectral components near ω_0 can thereby induce transitions between the spin energy. With the exception of some favorable cases, the description of the motion of the lattice would be in the frame work of a classical picture, by using the idea of the random motions or stochastic fluctuations which modulates nuclear spin-lattice interactions. For a system undergoing random fluctuations, the microscopic dynamics can be described only by means of the correlation function of the atomic positions or its Fourier transform,

giving the spectralization of the random motion. Such a microscopic formulation of nuclear spin relaxation would require some approximations in practice, such as a *high temperature approximation* which assume the infinite specific heat of the lattice to form an ideal heat reservoir. Another important approximation is *spin temperature approximation*, when $T_2 \ll T_1$, as usually in the solid NMR. In most cases, the density matrix formulation applied, and is a completely general method for the systems in which the lattice is described classically and the resonance width is substantially narrowed by the motion of nuclei which is treated in the following section.

A general approach relating to the relaxation rates to the spectral densities of the motions which is modulating the various lattice functions is the 'weak collision theory' [153], where additional interaction to the Zeeman level and rf excitation are treated as time dependent perturbations causing transitions between the stationary energy levels of the spin system. Therefore the Hamiltonian of the spin and the lattice system can be written as ,

$$H = H_S + H_{sL}(t) + H_L \quad (2.48)$$

where s and L stands for spin and lattice respectively. The assumption is made that the correlation time is much less than the relaxation time so that many elementary processes of fluctuations are required to relax the nuclear magnetization, in particular,

$$\tau_c \ll T_2 \leq T_1 \quad (2.49)$$

Through a lengthy quantum-mechanical calculation [143], which we omit here, it can be shown that

$$\frac{1}{T_1} = -\frac{1}{\hbar^2 \text{Tr}(H_s^2)} \text{Re} \int_0^\infty dt \text{Tr} \left\{ \overline{[H_{sL}^*(t), H_s][H_{sL}, H_s]} \right\} \quad (2.50)$$

where the bar represents the average over a thermal equilibrium ensemble, and H_{sL}^* is the operator associated with H_{sL} in the Heisenberg representation and given by

$$H_{sL}^*(t) = e^{i(H_s + H_L)t/\hbar} H_{sL} e^{-i(H_s + H_L)t/\hbar} \quad (2.51)$$

One could now specify the spin-lattice coupling H_{sL} for dipolar, quadrupolar, or interaction to the electrons.

2.2.2.3.1 Dipolar Relaxation

The dipolar Hamiltonian in equation (2.10) can be written as

$$H_d = \sum_{q=-2}^2 FqAq \quad (2.52)$$

where

$$\begin{aligned} F^{(0)} &= \frac{1 - \cos^2 \theta}{r^3} & A^{(0)} &= \alpha \left[-\frac{2}{3} I_z S_z + \frac{1}{6} (I_+ S_- + I_- S_+) \right] \\ F^{(1)} &= \frac{\sin \theta \cos \theta \exp(-i\phi)}{r^3} & A^{(1)} &= \alpha [I_z S_z + I_+ S_+] \\ F^{(2)} &= \frac{\sin^2 \theta \exp(-2i\phi)}{r^3} & A^{(2)} &= \frac{1}{2} \alpha I_+ S_+ \\ \alpha &= -\frac{3}{2} \gamma_I \gamma_s \hbar^2 & \text{and } F(-q) &= F(q)^*, A(-q) = A(q)^+ \end{aligned} \quad (2.53)$$

Since the time dependence enters only through the inter-nuclear vector and not through the spin operators, the time dependence of the interaction is then expressed through the correlation function

$$G^{(q)}(t) = \sum_k \langle F_{ik}^{(q)}(0) F_{ik}^{(-q)}(t) \rangle \quad (2.54)$$

where the sum is over all spins and $\langle \dots \rangle$ means ensemble average. A more useful quantity is the Fourier transform of $G^{(q)}(t)$

$$J^{(q)}(\omega) = \int_{-\infty}^{\infty} G^{(q)}(t) \exp(-i\omega t) dt \quad (2.55)$$

On the assumption, and usually is the case, that the dipolar interaction is sufficiently weak to apply the perturbation theory, the results for like spins are given as [143],

$$\begin{aligned} \frac{1}{T_1} &= \frac{3}{2} \gamma^4 \hbar^2 I(I+1) [J^{(1)}(\omega_0) + J^{(2)}(2\omega_0)] \\ \frac{1}{T_2} &= \frac{3}{8} \gamma^4 \hbar^2 I(I+1) [J^{(0)}(0) + 10J^{(1)}(\omega_0) + J^{(2)}(2\omega_0)] \\ \frac{1}{T_{1\rho}} &= \frac{3}{8} \gamma^4 \hbar^2 I(I+1) [J^{(0)}(2\omega_0) + 10J^{(1)}(\omega_0) + J^{(2)}(2\omega_0)] \end{aligned} \quad (2.56)$$

The terms with ω_0 result from single spin flips caused by C and D term of H_d (equation 2.11) : terms with $2\omega_0$ come from flips of both spins via term E and F; the terms with $J^{(0)}(0)$ derives from the flip-flop term B of H_d .

2.2.2.3.2 Quadrupolar Relaxation

If the quadrupolar interaction can be considered as a weak perturbation on the Zeeman interaction, the associated spin relaxation rates due to the quadrupolar coupling may expressed in terms of the same spectral density functions as in the dipolar case.

$$\begin{aligned}\frac{1}{T_1} &= \frac{2}{30} \alpha \left[J^{(1)}(\omega_0) + 4J^{(2)}(2\omega_0) \right] \\ \frac{1}{T_2} &= \frac{3}{40} \alpha \left[3J^{(0)}(0) + 5J^{(1)}(\omega_0) + 2J^{(2)}(2\omega_0) \right] \\ \frac{1}{T_{1\rho}} &= \frac{3}{40} \alpha \left[3J^{(0)}(2\omega_0) + 5J^{(1)}(\omega_0) + 2J^{(2)}(2\omega_0) \right]\end{aligned}\tag{2.57}$$

where the constant α is defined by

$$\alpha = (z'e^2qQ/\hbar)^2 (2I+3) / [I^2(2I-1)]\tag{2.58}$$

where z' is the effective charge. Except for the above case the relaxation becomes very complex, leading to multi-exponential recovery of the nuclear magnetization due to non equivalent energy level spacing due to considerable quadrupolar modification of the Zeeman level. To see this effect, one can consider a rate equation for the populations of each energy level which is unequally spaced due to quadrupolar interaction. This rate equation is called as master equation.

$$\frac{dn_i(t)}{dt} = \sum_j (n_j(t)W_{ij} - n_i(t)W_{ji}) \quad (2.59)$$

To go further, one must assume a form for W_{ij} by postulating a relaxation mechanism or combination of relaxation mechanism. One can simply divide the relaxation mechanism as one with magnetic origin (e.g. magnetic dipolar) and one with electric origin (e.g. quadrupolar). The transition of the adjacent level ($\Delta m = \pm 1$) is allowed for the magnetic transition whereby electric transition is allowed for $\Delta m = \pm 1, \pm 2$. By solving the master equation [154] which is omitted here one have the "recovery law" for the nuclear magnetization. For $I = 3/2$ with saturating only the central line ($1/2 \leftrightarrow -1/2$) with two distinct initial conditions : (a) $t \ll T1$, (b) $t \gg T1$, where t is the duration of the rf irradiation. Then for each conditions one have,

$$\begin{aligned} a_{1/2} &= 0.5e^{-2W_1t} + 0.5e^{-2W_2t} \\ a_{1/2} &= \left(\frac{W_2}{W_1 + W_2}\right)e^{-2W_1t} + \left(\frac{W_1}{W_1 + W_2}\right)e^{-2W_2t} \end{aligned} \quad (2.60)$$

for the NSLR due to electric interaction where W_1 and W_2 corresponds to the transition $\Delta m = \pm 1, \pm 2$ respectively and $a_{1/2}$ is normalized nuclear magnetization. For the NSLR due to magnetic interaction,

$$\begin{aligned} a_{1/2} &= 0.1e^{-2W_Mt} + 0.9e^{-12W_Mt} \\ a_{1/2} &= 0.4e^{-2W_Mt} + 0.6e^{-12W_Mt} \end{aligned} \quad (2.61)$$

The single exponential recovery of nuclear magnetization can be obtained if one saturates whole spectrum for the magnetic interaction, then

$$a_{1/2} = e^{-2W_M t} \quad (2.62)$$

For the electric interaction, single exponential recovery is obtained when one saturates the superimposed central line and satellites and have condition of $W_1 = W_2 = W$, then

$$a_{1/2} = e^{-2/5(W_1+4W_2)t} = e^{-2Wt} \quad (2.63)$$

otherwise (if satellites are out, but one can saturate only the central line),

$$a_{1/2} = 2e^{-2W_2 t} - e^{-2W_1 t} \quad (2.64)$$

On the above, one should aware that the static part of the quadrupolar interaction cause the unequally spaced energy level and dynamic part of the interaction cause the population change among the levels.

2.2.2.3.3 *Electronic Relaxation*

Electronic contribution to NSLR can be approached by the concept of the generalized susceptibility [155] regardless of the state of the electrons, e.g. extended, itinerant or localized. For electrons in extended states, within the free electron approximation and assuming that only s- and d- orbitals contribute to the hyperfine interaction, the conduction electron contribution to the NSLR, T_{1e} is given by [156],

$$\frac{1}{T_{1e}T} = 4\pi\hbar\gamma K_B \left\{ [H_{hf}(s)N_s(E_F)]^2 + [H_{hf}(d)N_d(E_F)]^2 q + [H_{hf}(o)N_d(E_F)]^2 p \right\} \quad (2.65)$$

where $N_s(E_F)$ and $N_d(E_F)$ are the s - and d - band densities of states at Fermi level respectively, and p and q are constants determined by the nature of electron states at the Fermi level. $H_{hf}(s)$ is due to the Fermi - contact interaction with unpaired s - electrons at E_F , $H_{hf}(d)$ is the core polarization hyperfine field of paired s - orbitals due to the unpaired d - electron at E_F , and $H_{hf}(o)$ is the d - electron orbital interaction. The expression can be greatly simplified to

$$\frac{1}{T_{1e}} = R_{1e} = \frac{T}{K} \quad (2.66)$$

where the "Korringa constant" K depends on both $|\psi(0)|^2$ and $N(E_F)^2$. Korringa [157] first discovered a useful relation between the Knight shift and the relaxation rate caused by contact and core polarization contributions,

$$(\Delta\nu/\nu)^2 T_{1e}T = (\gamma_e/\gamma_n)^2 Sh / (4\pi K_B) \quad (2.67)$$

where g_e is the electron gyro magnetic ratio and S depends on the electronic structure.

2.2.2.3.4 Relaxation due to Paramagnetic Impurities

Electron spins of paramagnetic impurities create large fluctuating magnetic fields by continually flip - flopping between spin states. If the fluctuating fields have spectral components near the Lamor frequency, they can relax nearby spins, which can

in turn relax other spins in the sample via spin diffusion at low temperature. At higher temperature atomic diffusion will allow direct coupling between all the moving nuclei and the impurities. The result is a relaxation rate with a rather complex temperature dependence. The two most prominent features are : low temperature relaxation rates which do not go through the origin and have a slight frequency dependence, and relaxation maximums which can occur at various temperatures. The best way to deal with this usually unwanted relaxation process is sometimes simply to get very pure material. The related concepts of spin temperature and spin diffusion are useful in many NMR analysis. The spin temperature θ_s can be defined via

$$\frac{P_n}{P_m} = \exp\left[\frac{(E_m - E_n)}{k_B \theta_s}\right] \quad (2.68)$$

where P_x is the occupation probability of a spin state with energy E_x . The concept of a temperature is valid only when the state of the entire system is described through the occupation probabilities alone (i.e., when off-diagonal elements of the density matrix vanish). When $T_2 \ll T_1$, the concept is most useful in certain experiments in solids, where different spin temperatures can be assigned to different frames of reference. The most useful definition of the spin temperature for these purposes is found by simply inverting equation (2.2) to define the temperature θ_s

$$\theta_s = \frac{1}{\beta_s} = \frac{N\gamma^2 h^2 I(I+1)}{K_B M} H \quad (2.69)$$

spin lattice relaxation rates then represent the return of the spin temperature to

the equilibrium lattice temperature. Energy can be exchanged via mutual spin flips induced by the flip-flop term of the dipolar interaction which will eventually results in a uniform spin temperature. It was shown by Bloembergen [158] that the process does indeed follow a diffusion equation (Fick's law) with $D_{\text{spin}} = a^2/50T_2$, where a is the lattice parameter. Spin diffusion coefficients are usually rather small, on the order of 10^{-13} cm²/sec.

2.2.3 BPP and Beyond

In order to gain information about particle motion from nuclear relaxation rates some *model* that relates $G^{(q)}(t)$ to particle hopping time must be employed. A nearly exact expression for polycrystalline samples is [159]

$$G^{(q)}(t) = \frac{b_q^2}{4\pi} \sum_{\alpha, \beta} \frac{P_2(\cos \theta_{\alpha\beta})}{r_\alpha^3 r_\beta^3} P(r_\alpha, r_\beta, t) \quad (2.70)$$

where the b_q are constants, P_2 is a Legendre polynomial, and $P(r_\alpha, r_\beta, t)$ is the probability of a pair of spins being separated by r_β at time t given that they were separated by r_α at time zero. The most common approximation of $G^{(q)}(t)$, originally employed by Bloembergen, Purcell, and Pound (BPP) [94], uses only the first term in equation (2.69). Corresponding correlation function is taken to be

$$G^{(q)}(t) = G^{(q)}(0)e^{-|t|/\tau_c} \quad (2.71)$$

where τ_c is called correlation time which is characteristic of random motion. Fourier transform readily yields the BPP spectral densities

$$J^{(q)}(\omega) = G^{(q)}(0) \frac{2\tau_c}{1 + \omega^2 \tau_c^2} \quad (2.72)$$

$$G^{(q)}(0) = \frac{1}{2\pi} \int_{-\infty}^{\infty} J^{(q)}(\omega) d\omega$$

Relaxation rate predicted by the BPP approximation for hopping with a single activation energy at high temperature, is independent of ω_0 but proportional to τ_c , while at low temperatures $R_1 \propto 1/(\tau_c \omega_0^2)$. Slope of the high and low temperature in $\log(R_1)$ vs. $1000/T$ curves are proportional to the activation energy. The maximum of R_1 is proportional to M_2/ω_0 and occurs when $\omega_0 \tau_c \cong 1$. The relaxation rates in many systems do not show the predicted behavior of BPP. The most common deviation are low temperature relaxation rates with frequency dependence $R_1 \propto 1/\omega^s$, where $s < 2$, and asymmetric $\log(R_1)$ vs. $1000/T$ curves that predict higher activation energies at high temperatures. When this behavior is not ascribed to a *distribution of hopping rates* different ad-hoc correlation functions [160] are often used to fit the data. One such function is the "*stretched exponential*" introduced in section 1.2.3..

2.2.3.1 Beyond BPP

The inherent disorder in the glassy material enables one to have common treatment of relaxation rate. The introduction of the distribution of hopping times $r(t)$ which produces the measured R_1 via

$$R_1 = \int d\tau \rho(\tau) R_1(\tau) \quad (2.73)$$

where $R_1(t)$ is the relaxation of spin at a given site with dwell time t . Probably convincing support for the use of equation (2.72) has come from computer simulation [161] with distributions of both site and saddle point energies.

Probably the better way to describe the distribution of hopping time which has better connection to the physics of disorder, is the scheme of the distribution of activation energies. The resulting R_1 is given by

$$R_1 = \int dE_a g(E_a) R_1(E_a, Z(E_a)) \quad (2.74)$$

where $g(E_a)$ is a temperature independent normalized distribution of activation energy. A distribution of activation energies can be directly connected to the disordered structure, and produces many of the same features of R_1 vs. $1000/T$ plots not only in the glass but also in systems that do not follow normal NMR spectral densities. The weakness of the distribution of E_a is that it assumes temperature independent distribution which may not always be true. The formalism also may ignore the possible correlation effect among mobile species. Still the formalism of distribution of activation energy seems to provide more information about disordered system. The stretched exponential correlation function is also widely used, although the physical significance of the derived correlation time is not readily apparent.

2.2.3.2 NSLR in Glass

The simple extension of BPP with a distribution of activation energy is a rewriting the BPP expression of NSLR into the form of equation (2.74) and is treated in the section 3.4.3, although it is the main approach used in this work. In this section more general background of NMR in glass are discussed.

NMR in disordered material poses some difficulties both in theoretical approach and in interpretation of raw data of NSLR (e.g., recovery of nuclear magnetization to the equilibrium following the excitation). Therefore one has to have a correct way to interpret measured NSLR data, before inquiring the cause of the non exponential behavior of the relaxation in the disordered system. The more fundamental issue are asking why the glass show much faster NSLR than the crystalline phase of the same stoichiometry.

The ^7Li -NSLR of glassy material as in this work, has a merit that it shows exponential recovery of nuclear magnetization M_z in the pulsed NMR experiment. Therefore the recovery of the nuclear magnetization could be interpreted to have NSLR without any considerable ambiguity. On the other hand almost all the other nuclei (e.g. ^{23}Na , ^{11}B) in glass shows non exponential and/or multi exponential recovery of M_z . [162]. The reason why ^7Li -NSLR shows exponential recovery is explained by G. B. Jollenbeck et al. [162]: The nuclear quadrupole moments of ^7Li is small and de tuning of the nuclear energy levels via static quadrupole distortions which quenches the transport of spin temperature does not occur. Hence, common spin temperature is established in a very short times.

Since the glass net work (NWF) can be modified by alkali (NWM) which provide the mobile alkali ion, one tempt to distinguish the NSLR of mobile ion passing through the host net work and NSLR of immobile ion which belongs to the host net work. When the mobile ion is in motion (at elevated temperature), the first issue of

NSLR is the existence of NSLR maximum due to the motional relaxation. This should be satisfied when the correlation time of the motion is about the magnitude of the inverse of the Larmor frequency of the probing nuclei. Even though there is a distribution of correlation times due to disorder, the condition is satisfied by the most probable correlation time. The motional maximum of NSLR which is naturally expected for the mobile ion, could be expected for the immobile ion. This is because the main interaction between nuclei of the immobile ion and the lattice could be modulated by the mobile ion motion or at least it should be affected. In the former case the NSLR maximum of both mobile and immobile ion should occur around the same temperature or up to the activation energy of motion due to the interaction to the mobile ion. M. Rubinstein et al [163], G. B. Jollenbeck et al. [162], A. Avogadro et al.[164], and O. Kanert et al [165] reported the NSLR maximum of ^{11}B -NSLR in $\text{a-B}_2\text{O}_3$ at elevated temperature (~ 300 K), whereas J. Szeftel and H. Alloul [166,167] did not report it in the same material.

The next issue is the mechanism of NSLR e.g., at low temperature, where the mobile ion is practically frozen (below ~ 100 K) and the NSLR of both mobile and immobile ion may be treated in the same work frame. The classical motional relaxation is no more dominant and even be absent. In NSLR measurement of the glass, one is observing practically NSLR of an insulator in which relaxation mechanism would be a relaxation due to phonon. Though the observed NSLR in glass seems to show the power law behavior ($R_1 \sim T^S$) similar to the phonon relaxation in the ordered system, the observed rather weak field dependence in the glass would require NSLR mechanism specific to disordered system.

The phenomenological two level system (TLS) was introduced to explain NSLR mechanism in glass; for the magnitude and dependence on field (or Larmor frequency)

and temperature. Although TLS itself is a matter of a continuing debate, NSLR due to TLS is known to explain why glass has much faster NSLR than crystalline phase of the same stoichiometry, as well as the dependence on temperature and field. Therefore NSLR mechanism of nuclear spin flip process to be due to the localized low energy excitations of disordered mode (TLS) intrinsic to the glass is most widely accepted [162].

The model for TLS was taken to be an asymmetric double well potential (ADWP) with a broad distribution of the barrier height, V , between wells, $g(V)$ and of their energy difference Δ , $P(\Delta)$. Then the derived equation for NSLR is [165],

$$\frac{1}{T_1} = \delta \int_0^{\Delta_{\max}} d\Delta \int_0^{V_{\max}} dV \frac{P^2(\Delta)g(V)}{\cosh^2(\Delta/2K_B T)} \frac{\tau}{1 + \omega^2 \tau^2} \quad (2.75)$$

where, δ is the strength of TLS-nucleus coupling and Δ_{\max} and V_{\max} are the maximum energy difference and maximum barrier height. Below 1K, tunneling process occur and above 1K excitations are assumed to be thermally activated, therefore [165],

$$\tau(\Delta, V, T) = \tau_0 \sec h(\Delta/2K_B T) \exp(V/K_B T) \quad (2.76)$$

The NSLR above T_g is also reported by Marco Villa et al. [168] where the mechanism is described as: (1) field independent region just above T_g ($\sim T_g + 50$ K) where defect motion ($10^{-8} < \tau_{\text{defect}} < 10^{-10}$) enhance the NSLR and $\omega \tau_{\text{defect}} \ll 1$ practically gives no field dependence (2) field dependent region ($\sim T_g + 100$ K) suggest the contribution of mainly re orientation motion of the tetrahedra (e.g., BO_4)

2.3 Model for Ionic Conduction

2.3.1 Free Ion Type Model

True dc-conductivity can not be observed due to the accumulation of ionic charge on the electrodes. However, at very low frequency the conductivity becomes frequency independent (dc plateau) and one can assume the value at the plateau as the dc conductivity with the following discussions..

In FIC dc conductivity is dominated by the long range drift of the light cations which move by thermally activated hops over energy barriers. By assuming that the ions are almost free, one can use the Drude - model to describe the conductivity.

$$\sigma_{dc} = (Ze)n\mu \quad (2.81)$$

where Ze is the charge of the carrier. If one can increase the mobility m , or the charge density n , the dc-conductivity should be improved. Such an effort has been done extensively on glassy-FIC. The mobility of the ions, μ , can be expressed in terms of the diffusion constant D by the Nernst - Einstein relation [170]. In a random walk description of the activated hopping motion over the energy barrier E_a the diffusion constant can be expressed in terms of the jump distance λ and the jump frequency ν as $D = a \lambda^2 \nu$ where the jump frequency ν is assumed to be thermally activated. One has,

$$\begin{aligned} \mathbf{J} &= \sigma \mathbf{E} \\ &= (Ze)n\mu \mathbf{E} \\ &= (Ze)nD(Ze)/k_B T \mathbf{E} \end{aligned}$$

$$\begin{aligned}
&= \{(Ze)^2 n a v \lambda^2 / k_B T\} E \\
&= \frac{(Ze^2) n a \lambda^2 v_0}{k_B T} \exp(-Ea/k_B T) E
\end{aligned} \tag{2.82}$$

As seen on the above formulation, free ion type model exploits the relaxation time approximation and the assumptions of quasi free, and independent charge carrier. Thus, equation (2.81) would have to be modified to describe the conductivity in glassy FIC to include effects due to disorder and possible correlation among ions.

The connection between the contribution of the mobile ions and the one of the polarizable host lattice has been explored through an empirical relation, so called "BNN relation" after Barton, Nakajima and Namikawa [48,49],

$$\sigma(0) = p \Delta \varepsilon \varepsilon_0 \omega_m \tag{2.83}$$

where ω_m is the frequency of the dielectric loss peak. P is a constant of proportionality close to the unity and $\Delta \varepsilon$ is the dielectric strength, $\Delta \varepsilon = \varepsilon(0) - \varepsilon_\infty$. It was observed that ω_m shows Arrhenius behavior vs. temperature with the same activation energy as for dc conductivity. The validity of the relation (2.83) gives some experimental evidence that the mechanism of ac-conductivity is not different from the mechanism of the dc conductivity. The BNN relation has been interpreted such that P is the ratio of average drift velocity of the current charge to average accumulation velocity of bound charge [11].

At this point, it is worth while to list the general features of the ac conduction in glassy-FIC, which can not be understood on the basis of the simple models discussed above:

i) $\sigma'(w) \sim w^s$, with $0 < s < 1$

where s may frequency or temperature dependent which apparently approach to the unity at low temperature and high frequency. As s approaches unity at low temperature, the ac conductivity becomes practically independent of the temperature.

ii) Gradual transition to a frequency- independent conductivity at ω_m , the frequency-independent conductivity being defined as σ_{dc} . Whenever dc conductivity is measurable there is always a dielectric loss peak, when there is no σ_{dc} measurable, s seems to approach to unity.

iii) ω_m and $\sigma(0)$ are usually Arrhenius with the same activation energy.

2.3.2 Hopping Model

2.3.2.1 Hopping Models in Disordered System

As was seen in the previous section, the free-ion type model which adopt Drude type expression and thermally activated hopping motion of ionic charges is too simplified. A number of models have been proposed which try to incorporate effects due to disorder and correlation in the ionic motion. All the above models rely on the basic assumption that ions move through the lattice by thermally activated hops. Therefore we should first review the approximations involved in a hopping model; the

frame of the immobile structure (either ordered or disordered) should be sufficiently open to insure an abundance of physically interconnected and accessible sites and unhindered movement of ions through relatively large windows connecting these sites. The glass, due to its inherent disorder and open structure appears to satisfy this condition and even the lack of interconnection of available sites the percolation effect may enable the conduction. The fundamental parameter in hopping motion is the probability of the individual hopping which is used to formulate appropriate master equations for the hopping rate. In the simplest approach the individual hopping probability is assumed to be time independent and the sequence of hops is assumed to be a Markovian process. In a realistic formulation of a hopping model in glassy FIC, one should take into account the following effects on the hopping rate :

- i) The inherent disorder in glassy material
- ii) The interactions among mobile ions, e.g., coulomb interaction
- iii) Forward and backward hopping sequence which may introduce correlation affecting the hopping rate, giving rise to effect sometimes called 'bounce back effect' and 'caterpillar mechanism'

In order to incorporate the effects listed above, several models have been proposed. The one adopted by us [54 - 57] includes the effect of disorder by allowing for a distribution of activation energies and consequently a distribution of exponential correlation functions with different correlation times (in homogeneous correlation function). The coupling model, introduced by Ngai [104], includes mostly correlation effects by means of a phenomenological model whereby the hopping probability is assumed to be time dependent leading to a non exponential single homogeneous

correlation function. The diffusion controlled model, introduced by Elliot [185 - 187] and the jump relaxation model introduced by Funke [172] deal mostly with the "bounce back effect" and "caterpillar mechanism".

2.3.2.2 Simple Hopping Model

The ionic motion can be considered to consist of vibrations about local equilibria with occasional hopping from one equilibrium configuration to another. A simple example of hopping ion is one in which a mobile ion in FIC moves from one site to another, but the remaining ionic configurations remains unchanged. Therefore one has a simple picture shown in Fig. 2.4.

Considering site i , the potential difference and local electric field due to the applied electric potential V is given by

$$\Delta V_i = \frac{V}{2} \cdot \frac{d}{l} = \frac{Ed}{2} \quad (2.84)$$

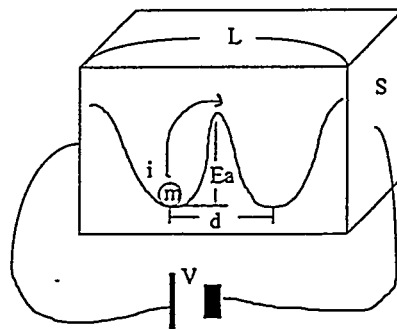


Fig. 2.4 Consider a sample of length l and area of cross section S which is loaded by voltage V . Let E_i be the activation energy required for hopping at site i .

where E is the electric field acting on site i . The electric current through the cross section of area S can be written as

$$J_i = \frac{eN}{S} \cdot (v_+ - v_-) \quad (2.85)$$

where n_+ and n_- denote the hopping rates of incoming and outgoing charge carrier through the area S respectively and N is the number of ions on the surface S . The barrier height that a charge carrier at site i has to overcome the activation energy E_i , plus or minus the extra barrier due to the applied voltage.

$$\begin{aligned} v_+ &= v_0 \exp\left(-E_i / k_B T\right) \cdot \left(1 + \frac{e\Delta V_i}{k_B T}\right) \\ v_- &= v_0 \exp\left(-E_i / k_B T\right) \cdot \left(1 - \frac{e\Delta V_i}{k_B T}\right) \end{aligned} \quad (2.86)$$

where we have expanded the exponential function for $V_i \ll k_B T$. The equation (2.85) and (2.86) then give

$$J_i = \frac{Ne}{S} v_0 \exp\left(-\frac{E_i}{k_B T}\right) \cdot \frac{2e\Delta V_i}{k_B T} \quad (2.87)$$

Let n be a number of carrier per unit area, $n = N/S$. Using equation (2.84), one finally has,

$$J_i = \frac{ne^2 d^2}{k_B T} \cdot v_0 \exp\left(-\frac{E_i}{k_B T}\right) \cdot \Delta E_i \quad (2.88)$$

Therefore , by counting the six possible directions in space (i.e., $\tau = (6v)^{-1}$) conductivity is given by

$$\sigma = \frac{ne^2 d^2}{k_B T \tau} v = \frac{ne^2 d^2}{6k_B T \tau} \quad (2.89)$$

which is identical with the result of the almost free - ion model (see equation 2.81 or equation 1.4).

2.3.2.3 Hopping Model with Distribution of Hopping Frequencies and Percolation Scheme

Starting from equation (2.89) one can introduce modifications into the simple hopping model. If there is a distribution of energy barriers then the total current can be calculated by averaging the current due to ion i (equation 2.88) over the distribution of ions having different hopping frequencies. This implies the assumption of a random diffusion and no correlation effects nor "bounce back effects" , one has

$$J = \sum_i P_i J_i = P \frac{ne^2}{k_B T} \langle d^2 \rangle_{av} \left\langle \tau_0 \exp\left(\frac{E_i}{k_B T}\right) \right\rangle^{-1} E \quad (2.90)$$

where P is the percolation fraction defined as:

$$P = \frac{\int_0^{E_{\max}} Z(E) dE}{\int_0^{\infty} Z(E) dE} \quad (2.91)$$

and $Z(E)$ is the distribution of probabilities to find the activation energy E . The idea behind the model is the following: in order to have dc conductivity one has to assume that there are a fraction of ions which can move from one end to the other of the sample (or at least to move over a macroscopic distances). The lowest barriers will allow ions to drift faster. If one has a distribution of barriers corresponding to the different lattice sites there will be a minimum number of barriers, i.e., the ones from zero up to E_{\max} , which allow for the ions to "percolate" through the sample without having to go over barriers higher than E_{\max} . The fraction of barriers from zero to E_{\max} with respect to the total number, defines the percolation factor P (see equation 3.27).

The factor P should depend on the lattice structure. For our glassy FIC we take P to be adjustable parameter since the fraction of barriers, and therefore the fraction of ions which give rise to percolation determined a lot on the short and intermediate range order of the glass. There are occasional hops over barriers higher than E_{\max} but these should not be important for dc conductivity, since the ions can percolate around these barriers. The average hop length of the ions in the direction of the field is $\langle d^2 \rangle_{\text{ave}} = d^2/6$ and average correlation time τ_{ave} is calculated using the distribution of barriers up to the cut off E_{\max} :

$$\sigma'(0, T) = \frac{nPe^2 d^2}{6k_B T} \cdot \frac{1}{\tau_{\text{av}}} \quad (2.92)$$

with

$$\tau_{\text{av}} = \int_0^{E_{\max}} \frac{1}{6\nu} \cdot \frac{Z(E)}{P} dE \quad (2.93)$$

being the average time between jumps in the direction of the electric field.

2.3.2.4 Other Hopping Models; The Coupling Model

There are a number of microscopic models which go beyond the simple hopping model and incorporate effects due to correlation among hopping ions. Besides the diffusion controlled model [185 - 187] and the jump relaxation model [172] already cited. We quote the effective medium approximation [177], the continuous time approximation [181] and the extended pair approximation [182]. Although these models are elegant and sophisticated, they do not lead to simple general formulas which can be easily tested with both NMR and conductivity results and will therefore not be considered here. On the other hand, a special attention is devoted below to the semi phenomenological coupling model since it leads to some simple predictions which can be tested on the basis of our experimental results. The main assumption and predictions are listed below.

The model based on time dependent relaxation rate which is constant if there is no correlation effect. Therefore the rate is actually constant in a very short time defined as t_c after which the correlation effect comes in:

$$W(t) = W_0 \equiv \tau^{-1} = v_{\infty} \exp\left(-\frac{Ea}{k_B T}\right) \quad \omega_c \tau < 1 \quad (2.94)$$

$$W(t) = W_0 (\omega_c t)^{-n} \quad \omega_c \tau > 1 \quad (2.95)$$

$$W(t)\phi(t) = d\phi / dt \quad (2.96)$$

where constant relaxation rate, $W_0 \propto m^{-1/2}$ and $\phi(t)$ is the correlation function. The correlation function is given by

$$\phi(t) = \exp\left(-\frac{t}{\tau_0}\right) \quad \omega_c \tau < 1 \quad (2.97)$$

$$\phi(t) = \exp\left[-\left(\frac{t}{\tau^*}\right)^\beta\right] \quad \omega_c \tau > 1 \quad (2.98)$$

where τ^* is given by

$$\tau^* = \tau_0 \exp\left(\frac{E_a^*}{k_B T}\right) = \left[(1-n)\omega_c^n \tau_c\right]^{\frac{1}{1-n}} \quad (2.99)$$

where $\tau_c = \tau_0 \exp(Ea/k_B T)$, and the β is related to n by,

$$\beta = 1-n \quad (2.100)$$

Thus n in equation (2.99) and (2.100) is measure of ion - ion correlation.

The most important predictions is about the microscopic activation energy which is given by [188],

$$\beta_{NMR} E_{a_{NMR}}^* = \beta_\sigma E_{a_\sigma}^* = E_a \quad (2.101)$$

The above prediction should be tested for various glass systems and compositions.

CHAPTER III. EXPERIMENTAL DETAILS

3.1 Sample Preparation

The sulfide glass samples are made in a two step process. The first is the preparation of the vitreous net work former (GeS_2 and B_2S_3), and the second is the binary (or ternary) preparation. The binary preparation is done by reacting net work modifier to net work former. The ternary is prepared by adding salt dopant to prepared binary, which dopant addition is known to increase the ionic conductivity. Mixture of several net work former can be prepared as well as mixture of several net work modifier which is not considered here. In this work, we avoid using commercially available B_2S_3 and GeS_2 , but these are prepared from the high purity raw materials.

3.1.1 Lithium Thio germanate Glasses

High purity v- GeS_2 were synthesized from Ge metal (3N, Cerac) and sulfur (5N, Cerac) using a solid state reaction. Since the materials used in this study are air- and moisture- sensitive, a glove box (<1 ppm H_2O and O_2) was used for all handling of glasses and starting materials. An initial charge of Ge metal and sulfur powder was inserted into a previously dried quartz tube.

The tube was sealed with a stopcock assembly, removed from the glove box, and evacuated through a liquid N_2 trap and then sealed with a gas torch. The tube was heated to 1000°C for 12 hours in a furnace, and then quenched to room temperature. When the v- GeS_2 was removed from the tube, it consisted of a homogenous transparent yellow rod. $x\text{Li}_2\text{S} + (1-x)\text{GeS}_2$ glasses in the $0.35 \leq x \leq 0.55$ were prepared by

weighing appropriate amounts of $v\text{-GeS}_2$ (prepared as described above) and Li_2S (Cerac, 3N), mixing together and melted in a vitreous carbon crucible using a muffle furnace (Thermolyne) inside the glove box. Furnace temperature was $850\text{ }^\circ\text{C}$ and weight loss due to evaporation of the melts was below 3 wt % when the melting time is kept low. Finally, the melts were quenched into pre-heated stainless ($\sim 150\text{ }^\circ\text{C}$) steel molds. The last step of the preparation is the vacuum sealing the powdered sample in quartz tube for NMR measurement, and sputtering the disk shape molded sample with gold for conductivity measurement. All the process requires extreme care in the glove box, i.e., the possible magnetic impurity was carefully avoided for NMR samples.

3.1.2 Lithium Thioborate Glasses

The starting materials were reagent grade powers of Li_2S (Cerac, 99.9%) and prepared B_2S_3 of high purity. Appropriate amounts of the reactants are weighed and thoroughly mixed in a glove box. The mixture was transferred to a covered vitreous carbon crucible and melted in an electric furnace at about $900\text{ }^\circ\text{C}$ depending on composition. Melting times of 5 - 10 minutes were adequate to obtain clear melts. These melts were quenched between two stainless steel blocks. The binary mixtures were homogenized by swirling of the crucible, and also by quenching, breaking up and re melting.

Commercially available B_2S_3 is generally of very low purity with high contamination due to oxygen and water. Preparation of high purity B_2S_3 has been much researched by D. Bloyer[118] at Iowa State University, whose method was used to prepare the sulfide glass samples.

3.2 Conductivity Measurement by Impedance Spectroscopy

Impedance Spectroscopy (IS) is a relatively new and powerful method of characterizing many of the electrical properties of materials and their interfaces with electronically conducting electrodes. The general approach is to apply an electrical stimulus of a known voltage or current to the electrodes and observe the responds of the resulting current or voltage. The stimulus can be in the form of a continuous or a pulsed sinusoidal function , therefore the observation can be done in the frequency domain and in the time domain. Different methods have their own advantage and disadvantage. Since the applied voltage is much smaller than the thermal voltage $V(T)$ ($= k_B T/e$), the measurement reveals the electrical properties of the sample to an excellent approximation.

In this work, the measurement of complex impedance at constant temperature is done by applying a sinusoidal voltage to the specimen and measuring the magnitude and phase angle of the current through the specimen. The four terminal method was used to measure the input voltage and the output current of the specimen as shown in Fig. 3.1. The measurement of the output current has instrumental limitation. In present work, the Solatron 1260 Impedance Gain-Phase Analyzer (Schlumberger Instruments) was used, which performance is summarized below.

- resistance: 1 Ω to 100 $M\Omega$
- capacitance: 1 pF to 1 mF
- frequency: up to 32 MHz (50K frequencies per sweep)

The temperature range of measurements depend on the probe design which should protect the sample from oxygen and water. The details of the probe design

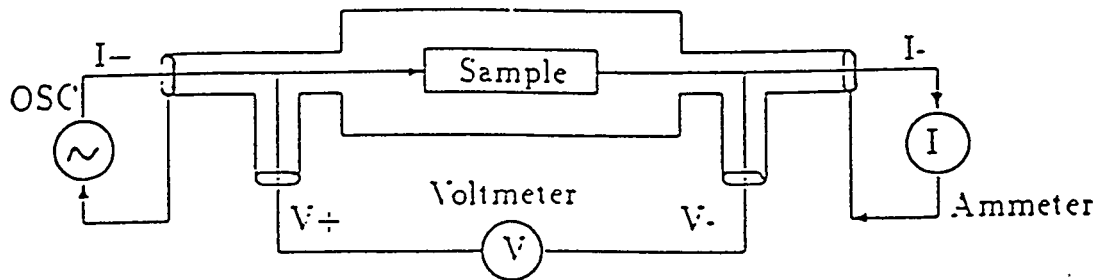


Fig. 3.1 Principle of the four terminal measurement

appears in the Ph.D. thesis of H. P. Patel [46] and omitted here. The temperature range could be covered from ~ 100 K to ~ 500 K. Overall instrumental limit with the available sample dimension allowed lower limit of conductivity measurement of about $10^{-11} (\Omega\text{cm})^{-1}$. The glass sample of size 20 mm (diameter) \times 1 mm (thickness) is sputter coated with gold electrodes (~ 50 nm thickness) and loaded in the probe inside of the glove box.

The calibration of the probe (sample holder and connecting coaxial cables to the analyzer) was done by built-in features of Solatron Analyzer. The fully automated Impedance Spectroscopy workstation is shown in the Fig. 3.2, and the probe (conductivity cell) is shown in the Fig. 3.3.

The measured magnitude and phase of the complex impedance at several different temperature (of $0.35\text{Li}_2\text{S} + 0.65\text{GeS}_2$) can be converted into the complex conductivity, by considering the cell constant k_0 ($= d/S$, where d is thickness and S is the area of the sample), since the impedance is given by

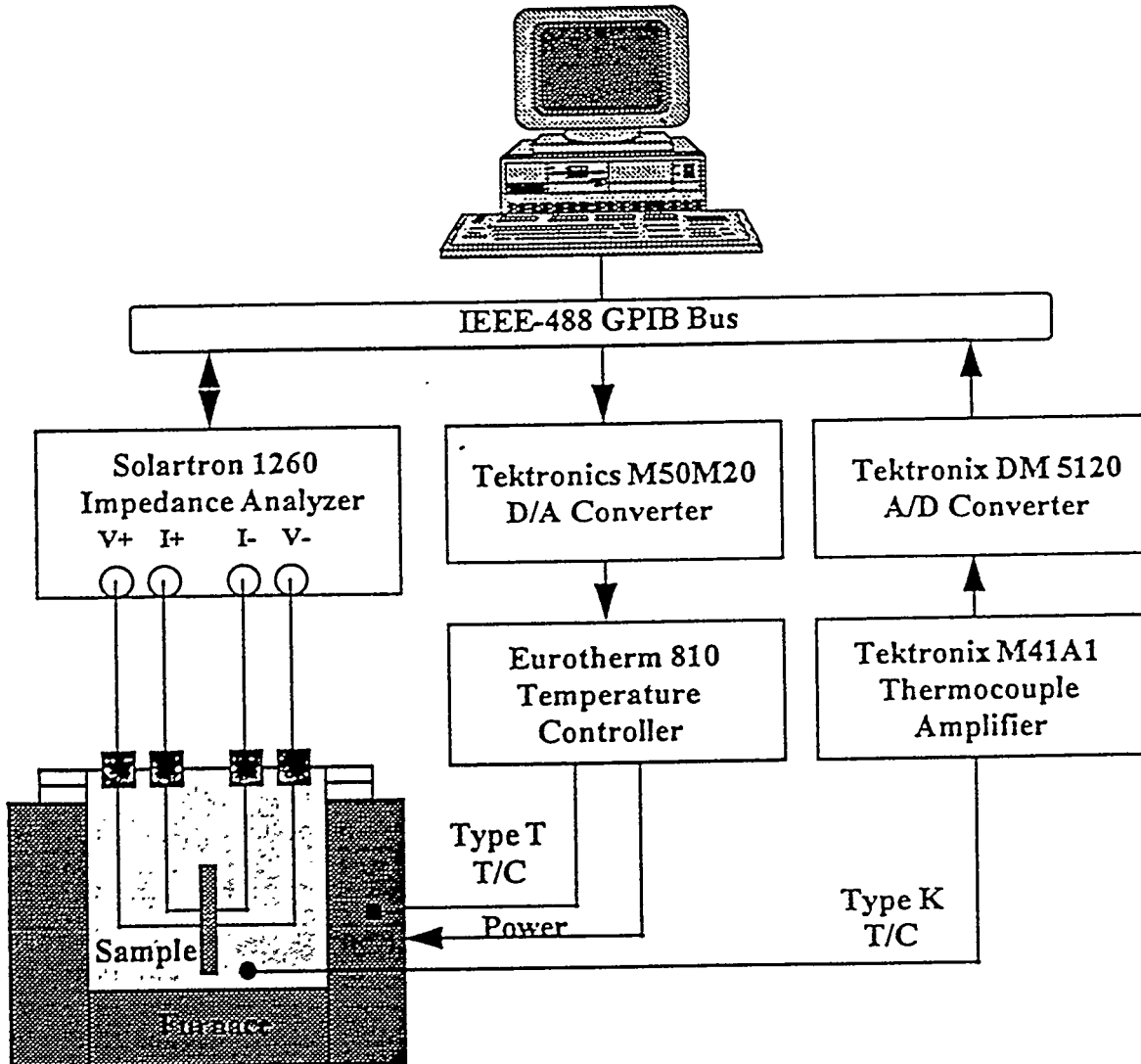


Fig. 3.2 Impedance Spectroscopy work station set up (taken from reference No. 46)

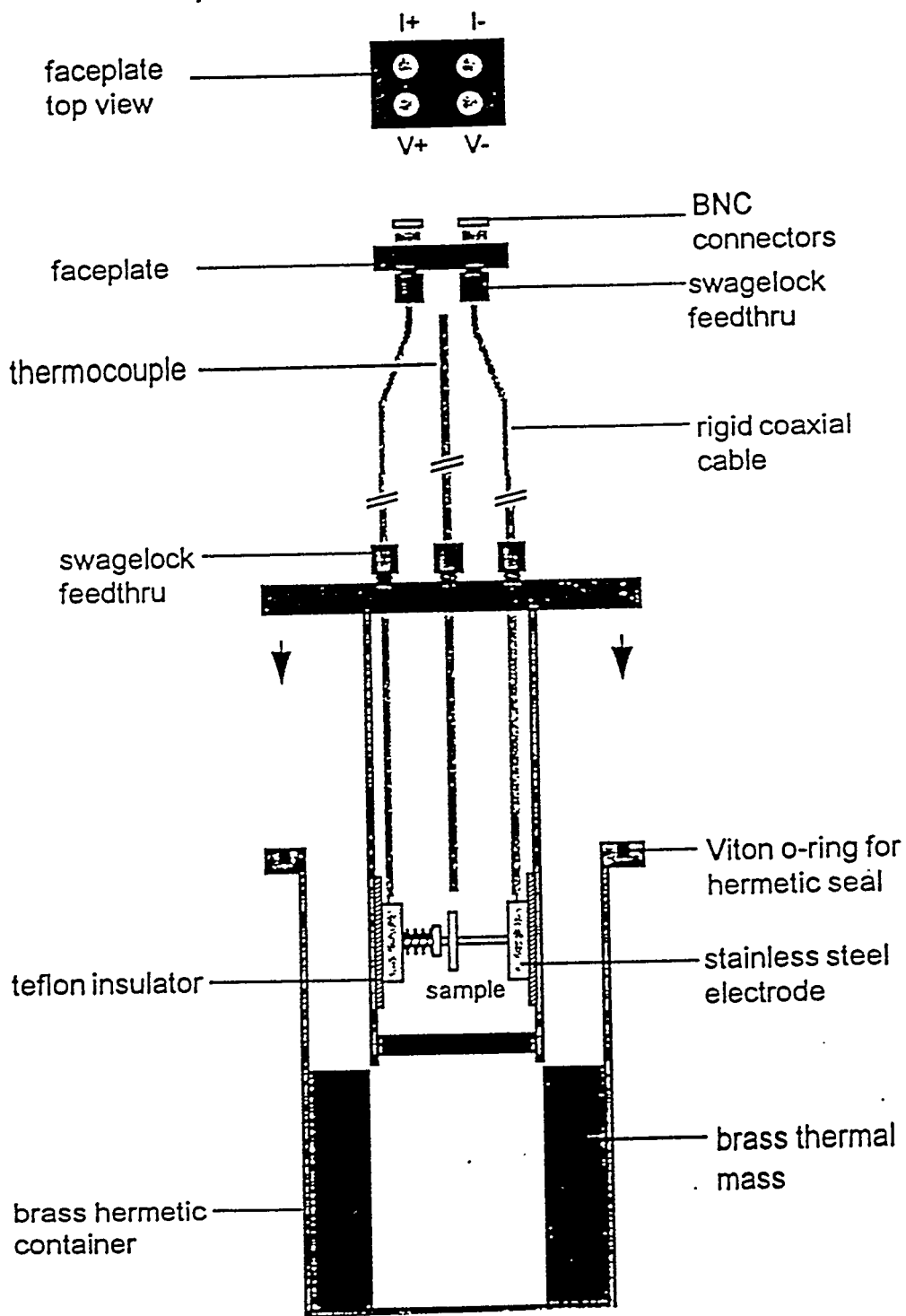


Fig. 3.3 Variable temperature conductivity cell (taken from reference No. 46)

$$Z^* = \frac{V_{\text{input(stimuli)}}^*}{I_{\text{output(response)}}^*} = \frac{d}{\sigma^* \cdot S} = k_0 / \sigma^* \quad (3.1)$$

Therefore the complex conductivity is given by

$$\begin{aligned} \sigma' &= \frac{k_0}{|Z|} \cos \theta \\ \sigma'' &= \frac{k_0}{|Z|} \sin \theta \end{aligned} \quad (3.2)$$

In an ideal lossy material, both the conduction and polarization of species occur, and these causes the ohmic losses and energy storage. The simple model of ideal lossy material would be RC-circuit, the complex impedance of such a circuit is given by

$$Z^* = \frac{R}{1 + (\omega RC)^2} + i \frac{\omega R^2 C}{1 + (\omega RC)^2} \quad ; \quad \tau = RC \quad (3.3)$$

The complex impedance plot (Z' vs. Z'') shows semi circle for ideal lossy material (one may use simple RC-circuit), whereas the glassy fast ionic conductors shows deviation from the semi circle. This behavior is dependent on the relaxation behavior of the material, therefore it provides a tool to investigate the relaxation behavior of the glassy fast ionic conductors. Since Impedance Spectroscopy observes the macroscopic electrical properties, microscopic study of ion-dynamics is needed to understand the fast ionic conduction in the glassy materials.

3.3 Measurement of Nuclear Spin-Lattice Relaxation Time

Understanding the NMR measurements requires knowledge of both method and instrumentation to have reliable NMR data. A simple description of the NMR experiment is on and off of the transmitting a radio frequency (rf) signal to a tuned sample coil placed in the magnet pole and observing the responding signal from the sample. One can transmit either a continuous rf signal or a pulsed rf signal at resonance frequency of nuclei, whereas the detection of response signal can be done by an absorption or a dispersion mode. The pulsed NMR spectrometer will be described in this section following the inversion recovery method of measuring T_1 , which is a simple introduction to the pulse NMR experiment. The more detailed experimental procedures will be discussed after a brief description of the NMR instruments.

3.3.1 Inversion Recovery Method of Measuring T_1 .

As mentioned in the previous chapter, in the rotating frame spins will precess with angular velocity $\omega = \gamma H_1$ around a rf field H_1 oscillating at ω_0 . In the experiment an rf field along the x' axis is produced by a sample coil perpendicular to the Zeeman field H_0 . During the time t , the rf magnetic field H_1 is applied, the magnetization will precess through an angle $\theta = \omega t$ about the x' axis. In the inversion recovery method of measuring T_1 the rf field is first left on just long enough to invert the magnetization; this is a 180° or π pulse. The magnetization then begins to relax back to equilibrium by exchanging energy with the lattice. After a time τ the magnetization is measured by again turning on the rf field long enough to rotate the spins through 90° , i.e., a $\pi/2$ pulse is applied. The magnetization is now in the x - y

plane and will precess about H_0 creating a changing magnetic flux in the coil, inducing a measurable voltage proportional to the magnetization.

The transverse magnetization decays in a time T_2^* , which can be quite shorter and is often due to inhomogeneous fields at the sample. The envelope of the oscillating decay signal is the "free induction decay" better known as the FID, where "free" means no rf field is applied while the spins are decaying. The spins gradually relax back to equilibrium and the process begins again with a 180° pulse followed by a 90° sampling pulse delayed by a time τ greater than the previous values. In this way the "recovery curve" $M(\tau)$ is obtained, from which T_1 is readily determined using the Bloch equations [2.24]. Other methods of measuring relaxation times are more appropriate in different situations, but this simple example is sufficient to introduce some of the requirements placed on the instrumentation.

3.3.2 NMR Pulse Spectrometer

NMR pulse spectrometers are designed to deliver specified sequences of high power radio-frequency (rf) magnetic field pulses to the sample and then to quickly receive the micro volt level signals induced by the spin system. Six Ames Laboratory spectrometers which differ only in detail were used in this study in order to span a large frequency range. A block diagram of the spectrometer on which the majority of measurements were made is shown in figure 3.4.

3.3.2.1 Pulse Generation and Transmission

The pulse sequencer initiates a measurement by sending a series of logic pulses

TORGESON/HORNUNG/ADDUCI PULSE NMR SPECTROMETER

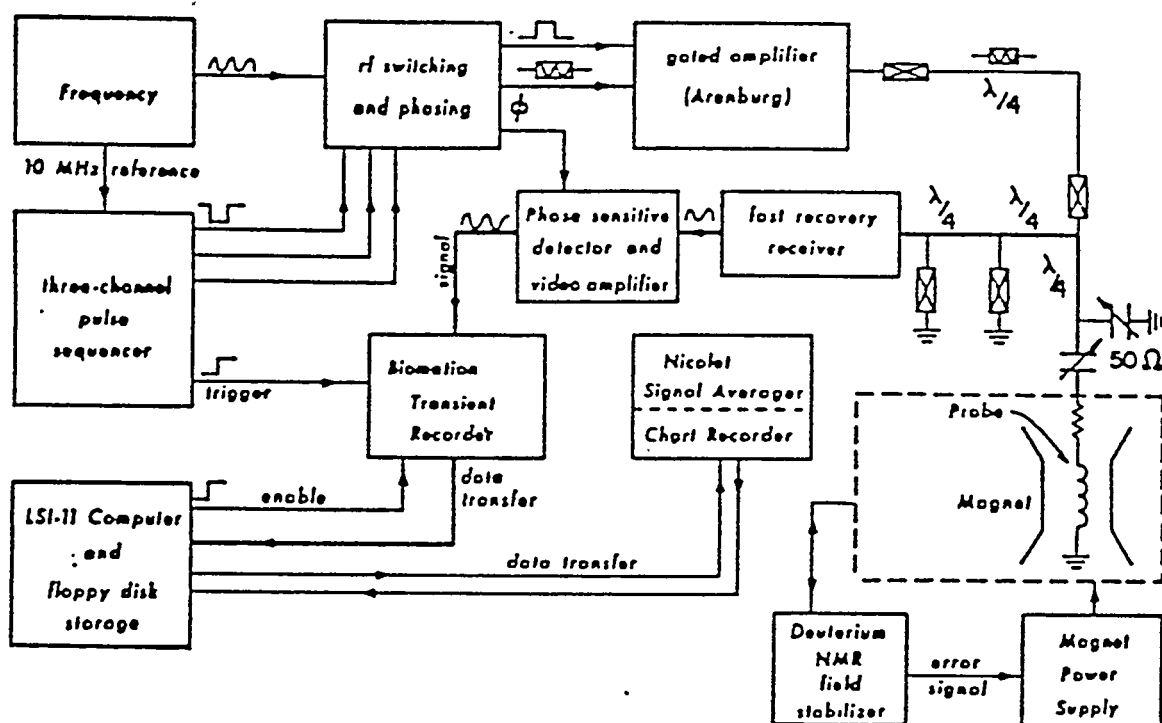


Fig. 3.4 Block diagram of phase coherent pulse NMR spectrometer. The present set up is modified a bit such that the Biomatron transient recorder and Nicolet signal averager is substituted by softwares. Further software control and data acquisition based on personal computers instead of LPI11 is underway.

to the "rf switch" which turns the rf pulses on and off. The microprocessor based pulse programmer was designed as a general purpose NMR spectrometer controller capable of producing standard pulse sequences for the measurements of NSLR and NMR spectra in a solid. The programmer also provides the facilities of an automatic time base advance function for relaxation time measurements. Each of its four analog adjustable pulse channels has a range of 0.5 to 80 microseconds over six ranges. The toggle switch associated with each pulse channel can be used to manually enable or disable a channel output. Three programmable trigger channels produce 100 nano second pulses, which can be issued under program control and used for triggering data acquisition equipment. The experimental repetition rate can be set from 0.001 to 999 seconds per each measuring sequence by the slow clock.

The pulse programmer triggers the rf switch which allows a pulse of rf voltage with a selected phase with respect to a reference frequency to be passed from a frequency synthesizer to a gated rf power amplifier. A low phase noise synthesizer is used which also provides a coherent time base for the programmer. The combination of a continuous phase coherent source and a time base which is definitely related to the phase of the rf pulse is therefore created. These are important criteria for the stability of multiple pulse measurements and phase sensitive detection.

The rf pulse is amplified to approximately a kilowatts by a gated power amplifier or transmitter. This transmitter produces an rf pulse magnetic field to satisfy the rotating frame condition of $H_{rf} > H_{local}$ in the sample.

The duplex circuit [145] is used to couple the transmitter output, pulse NMR probe and receiver preamplifier together, consisting of $\lambda/4$ cables and crossed diode switches, directs the rf power pulses to be transferred from the amplifier to the probe, with minimal voltage leaking to the sensitive receiver, yet does not reduce the smaller

signal coming from the probe to the receiver. During transmission of the rf pulse, the shunt diodes at the end of $\lambda/4$ cable at the receiver preamplifier input creates a high impedance path in the direction of the receiver so that essentially all of the rf power is transferred to the probe, which is tuned to 50Ω resistance at the resonance frequency. The low level voltage from the sample probe will see a high impedance path back towards the transmitter power amplifier due to the presence of the series diodes but low impedance in the direction of the receiver.

3.3.2.2 Pulse NMR Probe

The pulse NMR probes consisted mainly of a single coil, two tuning capacitors, a cylindrical dewar pipe, a cylindrical heater, dual thermocouple and tuning box as shown in figure 3.5. The unique design by D. R. Torgeson allows the very short distance from the pickup coil to the tuning circuit thus optimizing the capability and tunability of the probe. The heater was wound non-inductively and was made from manganin wire. The low temperatures were attained by blowing a chilled nitrogen gas by boiling of liquid nitrogen. Two copper - constantan thermocouples were installed near the sample to monitor and control the temperature. The automatic feedback control of temperature was accomplished using an Omega programmable three term temperature controller and heater current switching circuit. The rf coil was made from the #16 copper coil for ^7Li and ^{11}B NMR experiment and #18 platinum wire for ^{23}Na

NMR experiment. For the use of super conducting magnet for the high field NMR experiments, commercial Oxford CF-1200 continuous transfer, variable temperature chambers were used which had capability of temperature control from the liquid He temperature to 500K by a continuous flow of liquid He or liquid N_2 .

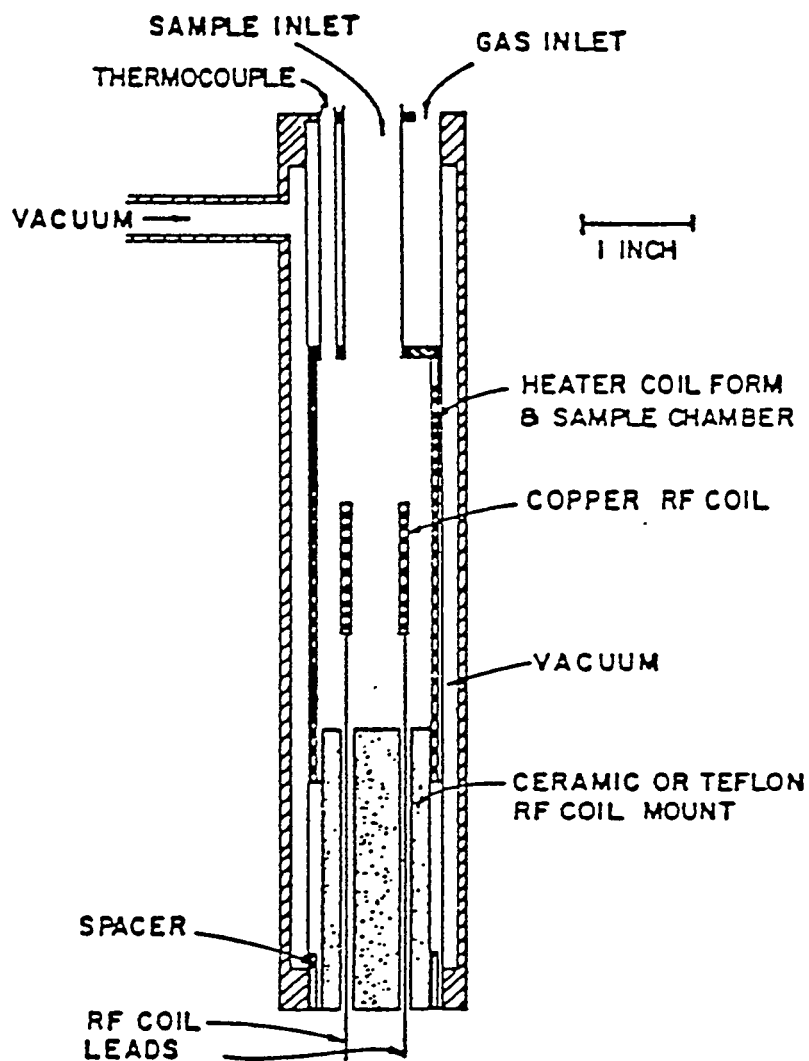


Fig. 3.5 Variable temperature probes designed by D.R. Torgeson. Direct connection of rf tuning circuit at the bottom of this probe prevents from possible loss of signal and from an interference of unwanted noise from outside.

3.3.2.3 Receiver

The receiver consisted of a preamplifier, three limiting amplifier stages followed by a quadrature phase sensitive detector. One operational problem which all pulse NMR spectrometers have is the saturation of the receiver during and for a period of time after the rf pulse due to an unavoidable overload of the preamplifier and following rf stages, within the receiver resulting in a "dead time" after application of a high power pulse. Because the transient signals in solids decay extremely fast, experiments with solids require fast recovery receivers. The receiver unit employed in our experiments is a version of the one designed by Adduci et al.[189] in the Ames Laboratory.

3.3.2.4 Magnet

The static magnetic field H_0 was produced by a 37.5 cm diameter pole, Varian Associates electromagnet which can supply a maximum field strength of 2.5 Tesla. The field drift was controlled by Hall effect regulator. For fields greater than 2.5 T, measurement were made using Oxford Instruments super conducting magnets. At present the two Oxford super conducting magnets are set to 3.7 Tesla and 8.2 Tesla respectively.

3.3.3 Experimental Procedure and Data Processing

The motion of the nuclear magnetization described by the Bloch equations was discussed in chapter II. The NMR experimental procedure will be described in more

detail in this section. Another common method of NSLR measurement other than the inversion recovery method (see 3.3.1) is the saturation comb $(\pi/2)_n - \tau - \pi/2$ pulse sequence. This sequence enables the operator to prepare the initial non-equilibrium state of the spin system via n preparatory pulses. Whenever the nuclear magnetization recovery is not single exponential, one should examine carefully the possible sources of the non-exponential recovery. This can be done by changing the number of preparation pulses, the pulse width or the pulse intensity. For the case of exponential recovery, the recovery of the magnetization is described by

$$M_z(\tau) = M_0 [1 - \exp(-\tau/T_1)] \quad (3.4)$$

Using a saturation comb does not require one to wait many (5 to 10) T_1 time periods until the equilibrium magnetization is restored naturally to full equilibrium. The saturation comb method is faster than the inversion recovery method. Thus this method is useful when one must signal average many transient signals in the computer memory due to poor signal to noise ratio or when the T_1 is quite long.

The spin-spin relaxation time T_2 is a characteristic time for magnetic interactions between the spins. Following a $\pi/2$ pulse, the magnetization in the x' - y' plane is observed to decay in time exponentially with the time constant T_2^* and is defined as

$$1/T_2^* = 1/T_2 + 1/T_2' \quad (3.5)$$

The first term is due to the dipole-dipolar interaction between the spins, and the second term results from the combined contributions due to the spin - lattice relaxation

process and in homogeneity in the magnetic field from either the detailed shape of the sample particles or from the spacial variations of the field in the magnet. When diffusion is negligible, the two pulse Hahn [190] spin-echo pulse sequence can be used to reduce or eliminate field in homogeneity effects, yielding an exponential decay of the amplitude of the successive spin echoes with the natural relaxation time T_2 . Therefore one is measuring the rephasing time of the nuclear spin due to the local dipolar field produced by the neighboring nuclei. When there is diffusion or any other source of the modulation of spin-spin interactions, the rephasing will not be exponential but may be expressed as a product of exponential and some function of time $f(t)$. A measurement of $f(t)$ will provide the information of the diffusion or any other source of the modulation of spin - spin interactions. A general expression for the amplitude of the spin echoes observed in the presence of the diffusion[192]

$$M(\tau) = M_0 \exp\left(-\frac{2n\tau}{T_2}\right) \cdot \exp\left(-\frac{2nD\gamma^2 G^2 \tau^3}{3}\right) \quad (3.6)$$

where n is the number of π pulse repetitions in the Carr - Purcell - Meiboom - Gill (CPMG) sequences, $[(\pi/2)_x - (\tau - \pi_y - \tau \text{ echo})_n]$, which eliminates the accumulation of small errors in pulse width of Hahn echo sequence. D is a diffusion coefficient, here γ is the gyro magnetic ratio of the nucleus and G is the magnitude of the field gradient.

3.4 Methods for Data Analysis and Computer Program

3.4.1 KWW Stretched Exponential Model

The analysis of conductivity data and NSLR data using the KWW stretched exponential correlation function approach and the distribution of activation energies approach were done using software package written in the FORTRAN language. The integration of the stretched exponential was done with Dishon's formula [193]. The FORTRAN programs for both NSLR and conductivity approaches can be found in Appendix. The use of the KWW correlation function which was used to obtain the fitting parameters, will be discussed below

The NSLR is related to the spectral density function $J(\omega_L)$ of the fluctuations of local magnetic and electric fields due to the cation hopping. The NSLR R_1 is given by

$$R_1 = C [J(\omega_L) + 4J(2\omega_L)], \text{ where} \quad (3.7)$$

$$J(\omega_L) = \text{Re} \int_{-\infty}^{\infty} dt f(t) \exp(-i\omega_L t) = \text{Re} \int_{-\infty}^{\infty} dt \exp[-(t/\tau_{\text{eff}})^\beta] \exp(-i\omega_L t) \quad (3.8)$$

where C in (3.7) is the strength of the interaction between nuclei and its environment.

The correlation function, $f(t)$, describes the time decay of some lattice function due to the diffusion of cation. The lattice is referred as any substances other than nuclei in the system.

By using the stretched exponential correlation function in equation (1.5) as the correlation function in equation (3.8), with the help of Dishon's formula [193], one has

$$\frac{1}{T_1} = 2\pi c \frac{Z}{\omega} [Q_\beta(Z) + 4Q_\beta(2Z)] \quad (3.9)$$

where $u = t/\tau$ and $Z = \omega\tau$ and

$$Q_\beta(Z) = \frac{1}{\pi} \int_0^\infty \exp(-u^\beta) \cos(Zu) du = \frac{1}{\pi} \sum_{n=1}^{\infty} (-1)^{n+1} \frac{\Gamma(1+n\beta)}{n! Z^{1+n\beta}} \sin\left(\frac{n\pi\beta}{2}\right) \quad (3.10)$$

therefore one has fitting parameters β , C , τ_0^* and E_a^* , which is a measure of the disorder, interaction strength between nuclei and lattice, effective correlation time and effective activation energy, respectively. Therefore, by measuring NSLR as a function of temperature and NMR Lamor frequency, we can deduce the correlation function $f(t)$ and related parameters of the cation-motion in FIC glasses.

Complex conductivity is related to the complex dielectric function as seen in equation (8). And the dielectric function is given by its correlation function as in equation (9) [77],

$$1/\varepsilon(\omega)^* = (1/\varepsilon_\infty) \left[1 - \int_0^\infty dt \exp(-i\omega t) (-d\varphi(t)/dt) \right]$$

where, $\varphi(t)$ is a correlation function probed by conductivity measurement. From equation (8) and (9) one has

$$\sigma(\omega) = \frac{\varepsilon_0 \varepsilon_\infty \int_0^\infty \cos(\omega t) \varphi(t) dt}{\left[\int_0^\infty \sin(\omega t) \varphi(t) dt \right]^2 + \left[\int_0^\infty \cos(\omega t) \varphi(t) dt \right]^2} \quad (3.11)$$

By using the stretched exponential correlation function in equation (1.5) into equation (3.6) and with the use of Dishon's formula [193], one has

$$\sigma' = \varepsilon_0 \varepsilon_\infty \frac{\omega}{\pi Z} \frac{Q_\beta(Z)}{\left(Q_\beta(Z) \right)^2 + \left(V_\beta(Z) \right)^2} \quad (3.12)$$

where

$$Q_\beta(Z) = \frac{1}{\pi} \int_0^\infty \exp(-u^\beta) \cos(Zu) du = \frac{1}{\pi} \sum_{n=1}^{\infty} (-1)^{n+1} \frac{\Gamma(1+n\beta)}{n! Z^{1+n\beta}} \sin\left(\frac{n\pi\beta}{2}\right) \quad (3.13)$$

$$V_\beta(Z) = \frac{1}{\pi} \int_0^\infty \exp(-u^\beta) \sin(Zu) du = \frac{1}{\pi} \sum_{n=1}^{\infty} (-1)^{n+1} \frac{\Gamma(1+n\beta)}{n! Z^{1+n\beta}} \cos\left(\frac{n\pi\beta}{2}\right) \quad (3.14)$$

where $u = t/\tau$ and $Z = \omega\tau$. Therefore by measuring ac conductivity as a function of temperature, one again is able to deduce the correlation function $\phi(t)$ and related parameters β , ε_∞ , τ_0^* and E_a^* which is a measure of disorder, dielectric constant at infinite frequency, correlation time and activation energy, respectively.

3.4.2 Limiting Behavior of Stretched Exponential Correlation Function

The difficulty involved in the use of stretched exponential function is in the evaluation of the integration. Therefore one can use numerical method as in the previous section or estimating its limiting behavior [54]. From equation $\varphi(t)$, for $\omega \rightarrow 0$, one has an expression of dc conductivity from the limiting behavior

$$\sigma(\omega \rightarrow 0) = \sigma_{dc} = e_0 e_{\infty} / \int_{-\infty}^{\infty} dt \varphi(t) = e_0 e_{\infty} / \tau_{eff} \quad (3.15)$$

where, τ_{eff} is effective correlation time of corresponding correlation function. For exponential correlation function τ_{eff} can be defined as a correlation time τ . The non-exponential KWW correlation function itself can be represented as sum of exponential, in this case τ_{eff} is the average τ or $\langle \tau \rangle$. Considering the ${}^7\text{Li}$ spin-lattice relaxation rate at high temperature and high ion jumping rate or short correlation times then $\tau \ll \omega_L^{-1}$, the correlation function has decayed essentially to zero, and one has from equation (3.8),

$$R_1 \propto J(0) = 2 \int_{-\infty}^{\infty} dt f(t) = 2\tau_{eff} \quad (3.16)$$

From the above two equations, one expects,

$$(R_1)_{\text{high temperature}} \propto \sigma_{dc}^{-1} \quad (3.17)$$

If the KWW function is used to express both the conductivity $\phi(t)$ and NMR $f(t)$ correlation functions, then one should expect

$$\varphi(t) \propto f(t) \propto \exp[-(t/\tau_{\text{eff}})^\beta] \quad (3.18)$$

with

$$\tau_{\text{eff}} = \tau_0 \exp(Ea^*/k_B T) \quad (3.19)$$

using equations (3.4), (3.6), and (3.11) the following limiting behavior can be deduced for high temperature and rapid ion hopping and short correlation times

$$\omega_L \tau_c \ll 1, \quad R_1 \propto \tau_{\text{eff}}, \quad \sigma(\omega) = \sigma_{\text{dc}} \propto \tau_{\text{eff}}^{-1} \quad (3.20a)$$

for low temperatures and slow ion hopping and long correlation times

$$\omega_L \tau_c \gg 1, \quad R_1 \propto \omega_L^{-(1+\beta)} \tau_{\text{eff}}^{-\beta}, \quad \sigma(\omega) \propto \omega^{(1-\beta)} \tau_{\text{eff}}^{-\beta} \quad (3.20b)$$

and for an intermediate temperature

$$\omega_L \tau_c \sim 1, \quad R_{1\text{max}} \propto \exp(Ea^*/k_B T_{\text{max}}) \quad (3.20c)$$

where Region I, II and III of Fig. 1.4 corresponds to $\omega_L \tau_c \ll 1$, $\omega_L \tau_c \sim 1$, and $\omega_L \tau_c \gg 1$ respectively. Similar limiting behavior is expected also with coupling model, since the model also employs stretched exponential correlation function.

3.4.3 Distribution of Activation Energies and Percolation Scheme

The ^7Li NSLR is affected by all microscopic motions the ions in thus provides the essential information for the microscopic ion dynamics in a glassy fast ion conductor. The disorder in a glass can be characterized with a Gaussian distribution of activation energies

$$Z_{NMR}(Ea) = \frac{1}{\sqrt{2\pi}E_b} \exp\left[-\frac{(E_m - Ea)^2}{2E_b^2}\right] \quad (3.21)$$

where E_b is the half width around E_m the mean or center of the distribution. The ion jumping rate r is a function of Ea and T at the ion location in the glass which is thermally activated and of the form

$$r(Ea, T) = 1/\tau = r_0 \exp\left(-\frac{Ea}{k_B T}\right) \quad (3.22)$$

where k_B is the Boltzman constant and T is the absolute temperature in Kelvin. The attempt frequency $r_0 = 1/\tau_0$ can be deduced from the oscillation frequency, f_{osc} , of the ion mass m dwelling in the one dimensional potential well, which could be approximated by a simple sinusoidal function of the form

$$V(x) = \frac{Ea}{2} \sin\left(\frac{2\pi}{d}x - \frac{\pi}{2}\right) \quad (3.23)$$

where E_a is the height of the barrier or the activation energy and d is the interwell distance. Then one can have f_{osc} near the origin $x \cong 0$,

$$f_{\text{osc}}|_{x \cong 0} = \frac{1}{2\pi} \sqrt{\frac{k}{m}} \Big|_{x \cong 0} = \frac{1}{2\pi} \sqrt{\frac{V''(x)}{m}} \Big|_{x \cong 0} \approx \frac{\sqrt{E_a / 2m}}{d} \quad (3.24)$$

where k is a spring constant. The total attempt rate depends upon the number of possible jump directions $z (= 6)$ at each ion site times the f_{osc} deduced from the one-dimensional sinusoidal potential barriers, therefore

$$\tau_0 = \tau_0^{-1} = \frac{1}{z \cdot f_{\text{osc}}} = \frac{d}{6\sqrt{E_a / 2m}} \quad (3.25)$$

The NSLR is given by the simple extension of the BPP type relaxation

$$R_1(\omega, T) = A^2 \int_0^{\infty} \left[\frac{\tau/z}{1 + \omega^2(\tau/z)^2} + 4 \frac{\tau/z}{1 + 4\omega^2(\tau/z)^2} \right] Z_{\text{NMR}} dE_a \quad (3.26)$$

where A is the strength of the nuclear spin interactions and Z_{NMR} the Gaussian distribution of activation energies[56,57]. For the calculation of dc conductivity, a simple hopping model was used with the substitution of the single correlation time by the average correlation time by the Gaussian distribution up to the percolation threshold.

$$\sigma_{\text{dc}} = \frac{npe^2 d^2}{zk_B T \langle \tau \rangle} \quad (3.27)$$

where n is the concentration of the ionic charge carrier, $e = 1.6 \times 10^{-19}$ coulomb is the Li ion charge, $\langle \tau \rangle$ is the average correlation time by the Gaussian distribution up to the percolation threshold E_c

$$\langle \tau \rangle = \left(\frac{1}{p} \right) \int_0^{E_c} \tau_0 \exp\left(-\frac{Ea}{k_B T} \right) \cdot Z_{NMR} dEa \quad (3.28)$$

$$p = \int_0^{E_c} Ea \cdot Z_{NMR} dEa$$

where p is the percolation fraction and represents the fraction of all ions which contribute to long range ion motion derived by truncating Z_{NMR} at energy E_c . Those ions whose motion is characterized by hops of lower energy from essential 0 up to E_c are those ions which are not trapped in deep energy traps above E_c and can not contribute to long range motions.

CHAPTER IV. RESULTS AND DISCUSSIONS

4.1 $x\text{Li}_2\text{S} + (1-x)\text{GeS}_2$

In this section we present and analyze data of NSLR and conductivity in lithium thio germanates with three compositions ($x = 0.35, 0.45, \text{ and } 0.55$). Differences in the effective correlation times from the two techniques were observed as well as non-Debye behavior of relaxation in both measurements. The NSLR showed non BPP (Bloembergen, Purcell and Pound) behavior and the characteristics of the motional relaxation. The conductivity showed almost Arrhenius behavior of dc plateau and dispersive behavior which approaches a power law at low temperature and/or at high frequency.

In order to explain the NSLR and the conductivity and the difference in effective correlation times, both models, i.e., the phenomenological KWW approach and the distribution of activation energies, were tested.

It is shown that the dc conductivity in FIC can be calculated essentially from the distribution of activation energies obtained from the NMR relaxation data with a cut-off for the maximum barrier probed by the long range ionic diffusion. From the fit one obtains the fraction P of percolating ions as a function of the composition of the sample.

The phenomenological KWW approach, on the other hand, although useful in analyzing the data, does not provide any valuable microscopic insight. The main predictions of the coupling model [188] are also tested and found to be only in partial agreement with the data.

4.1.1 ^7Li Nuclear Spin Lattice Relaxation Measurements

The ^7Li - NSLR vs. temperature is shown in Fig. 4.1 for one of the three samples ($x = 0.35$) at three different resonance frequencies. Similar results were obtained for the other samples with composition $x = 0.45$ and $x = 0.55$ and those will be shown in the following paragraphs together with the theoretical fitting curves. The main features of the data in Fig. 4.1 are: (i) the slopes of the $\log R_1$ vs. $1000/T$ plot are different on the high and low T side of the maximum. This is a clear indication of departure from BPP model with single exponential correlation function. (ii) the frequency dependence on the low temperature side of the maximum is less pronounced than the $R_1 \propto \omega^{-2}$ dependence predicted by the BPP model. (iii) the magnitude of the relaxation rate R_1 at the maximum is larger than predicted for nuclear dipole - dipole interaction while it is consistent with a relaxation mechanism driven by fluctuations of the quadrupole interaction with the electric field gradient in the disordered lattice.

4.1.2 Conductivity Measurements

The measurements of the ac conductivity are shown in Fig. 4.2 plotted as a function of frequency at fixed temperatures for the same sample used in the NMR study. Again, similar results were obtained for the other two samples ($x = 0.35$ and 0.45) and will be shown in the following. In Fig. 4.3 we plot the same conductivity data vs. temperature at fixed frequency. The dc conductivity is obtained from the frequency independent plateau in Fig. 4.2. The deviations from the dc plateau at very low frequency in Fig. 4.2 is due to electrode polarization effect of accumulated ions

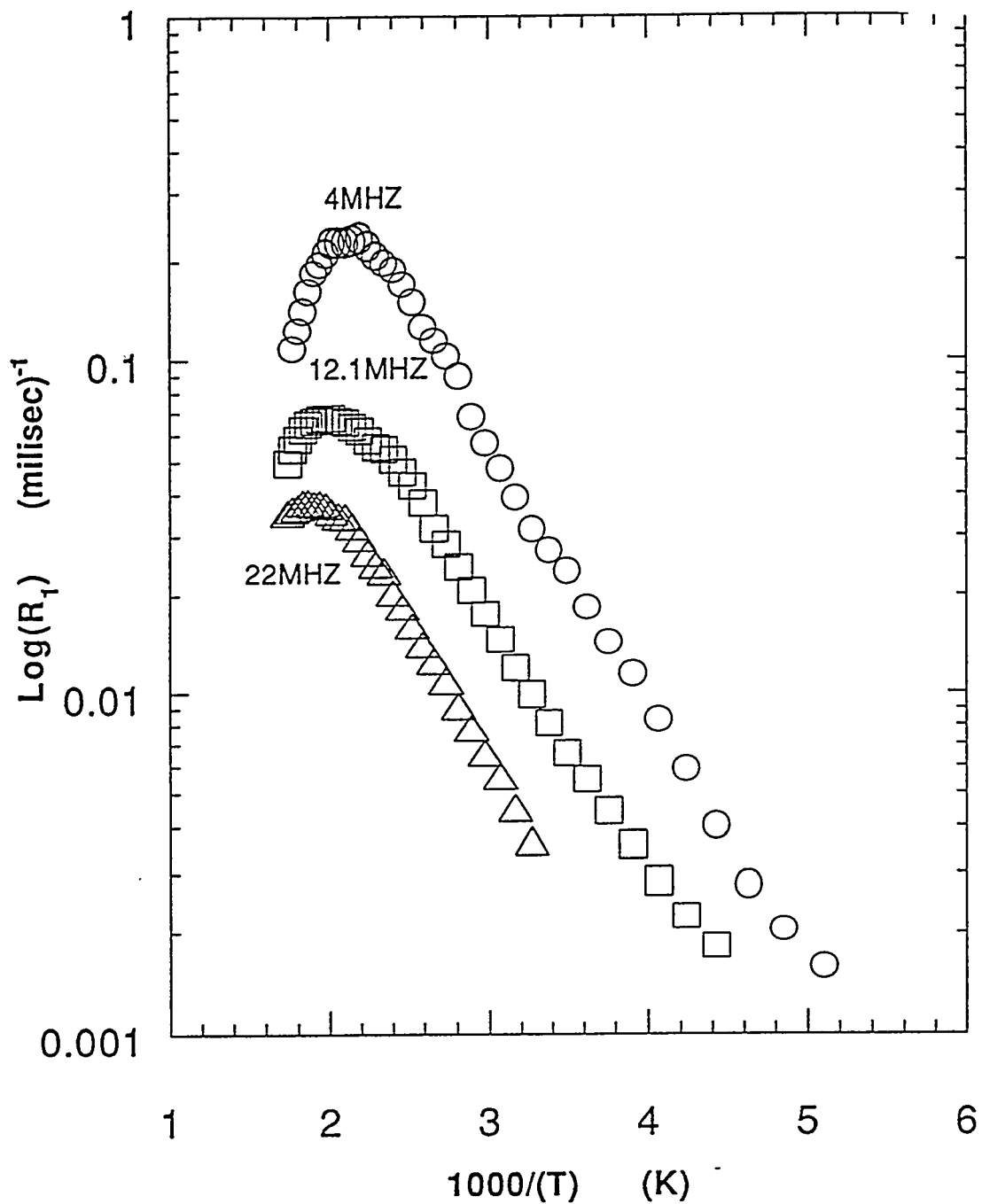


Fig. 4.1 ${}^7\text{Li}$ NSLR at 4, 12.1 and 22 MHz in logarithm of the relaxation rates as a function of reciprocal temperatures in $0.35 \text{Li}_2\text{S} + 0.65\text{GeS}_2$; data show BPP type of maximum and asymmetry about maximum in R_1 curve.

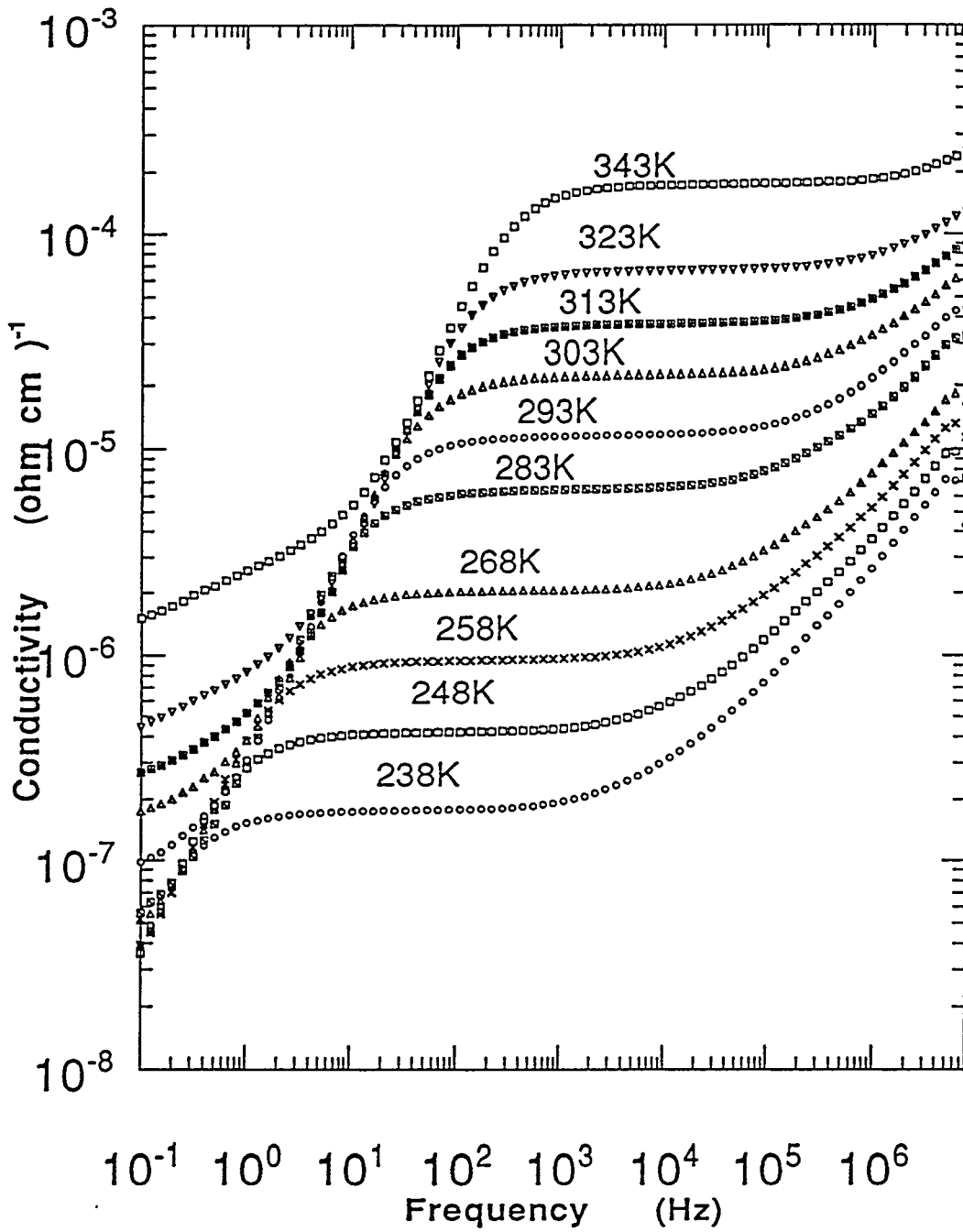


Fig. 4.2 The real part of ionic conductivity of $0.35 \text{ Li}_2\text{S} + 0.65 \text{ GeS}_2$ vs measurement frequency for several temperatures.; data shows electrode polarization at low frequency, d.c. plateau in the middle range and dispersive behavior at higher frequency.

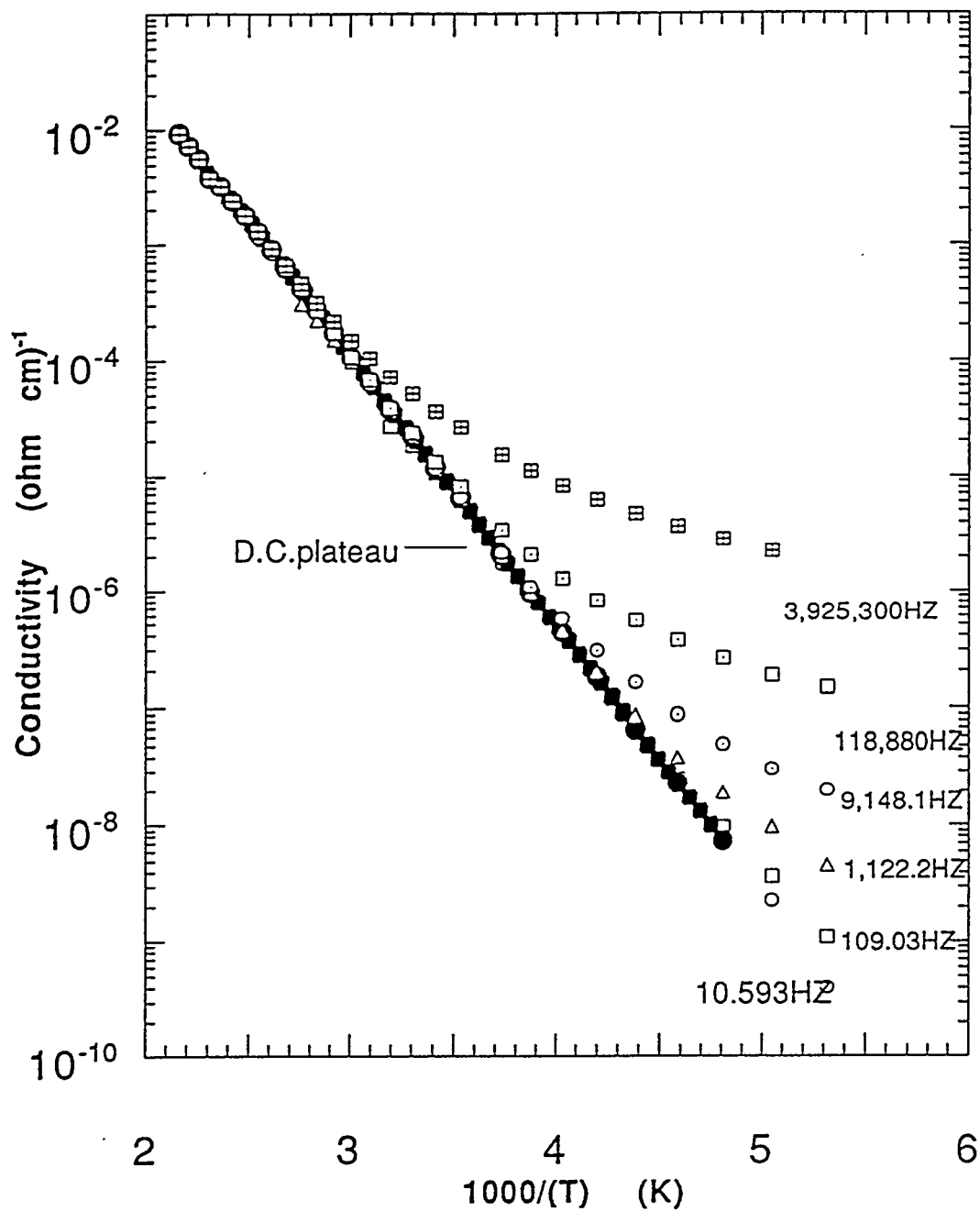


Fig. 4.3 Arrhenius plot of the real conductivity data shown in Fig. 4.2 of $0.35 \text{Li}_2\text{S} + 0.65 \text{GeS}_2$; dc - plateau shows almost Arrhenius behavior, while the data at higher frequency show strong deviations from the simple Arrhenius behavior.

on the electrode, and it should be disregarded. The main features of the data in Fig. 4.2 and 4.3 are: (i) the onset of the frequency dependence is a function of temperature. The frequency dependence goes as ω^s with the exponent s becoming close to unity for the lowest temperatures and highest frequencies. (ii) Apparent Arrhenius behavior of the dc conductivity. The apparent Arrhenius behavior is largely due to the narrow temperature range in which the conductivity is plotted. As will be shown later, measurable deviations from Arrhenius behavior can be observed in dc conductivity at high temperature in some FIC.

4.1.3 Direct Comparison of Correlation Times from NMR and Conductivity

Before proceeding to a detailed analysis of both NMR and conductivity data in terms of the two models outlined in section 2.3, it is worthwhile to point out that there is an obvious and direct evidence that the correlation times measured in NMR is orders of magnitude different from the one measured in conductivity.

The NSLR data in Fig. 4.1 convey a direct information about the correlation time τ of the Li ionic motion which is believed to drive the NSLR through the modulation of the electric field gradient. In fact the maximum NSLR is observed when the correlation frequency τ^{-1} is of the order of the Larmor resonance frequency. Thus from the condition $\omega_L \tau \approx 1$ at the maximum in the curves in Fig. 4.1, one can get three values at three different temperatures. These data are plotted in Fig. 4.4 and 4.5 for the $x = 0.35$ sample and also for the other two samples at $x = 0.45$ and 0.55 .

A similar direct information can be obtained from the conductivity data in Fig. 4.2. In fact the frequency at which the conductivity starts deviating from the dc plateau corresponds to the condition $\omega \tau \approx 1$. The onset of dispersion in the ac

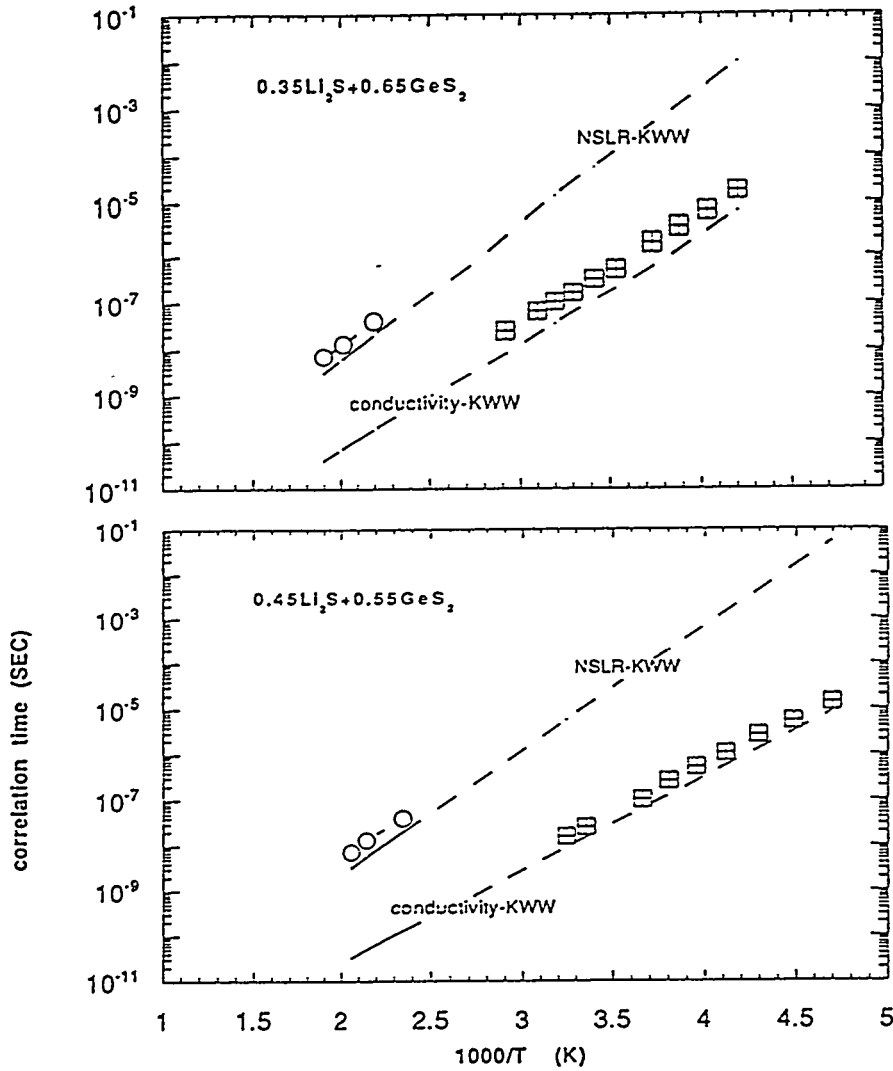


Fig. 4.4 Correlation times τ in $0.35 \text{Li}_2\text{S} + 0.65\text{GeS}_2$ and $0.35 \text{Li}_2\text{S} + 0.65\text{GeS}_2$ from $\omega\tau \sim 1$ at the maximum of NSLR vs. $1000/T$ plot and (circle) and from the onset of the conductivity dispersion (square). The lines are from the calculation using parameters from KWW fit to NMR and conductivity data. The lines should help to extrapolate the data so that they overlap in temperature. Unfortunately experimental difficulties prevented up to now to get data directly for both σ_{dc} and NSLR in the same temperature range.

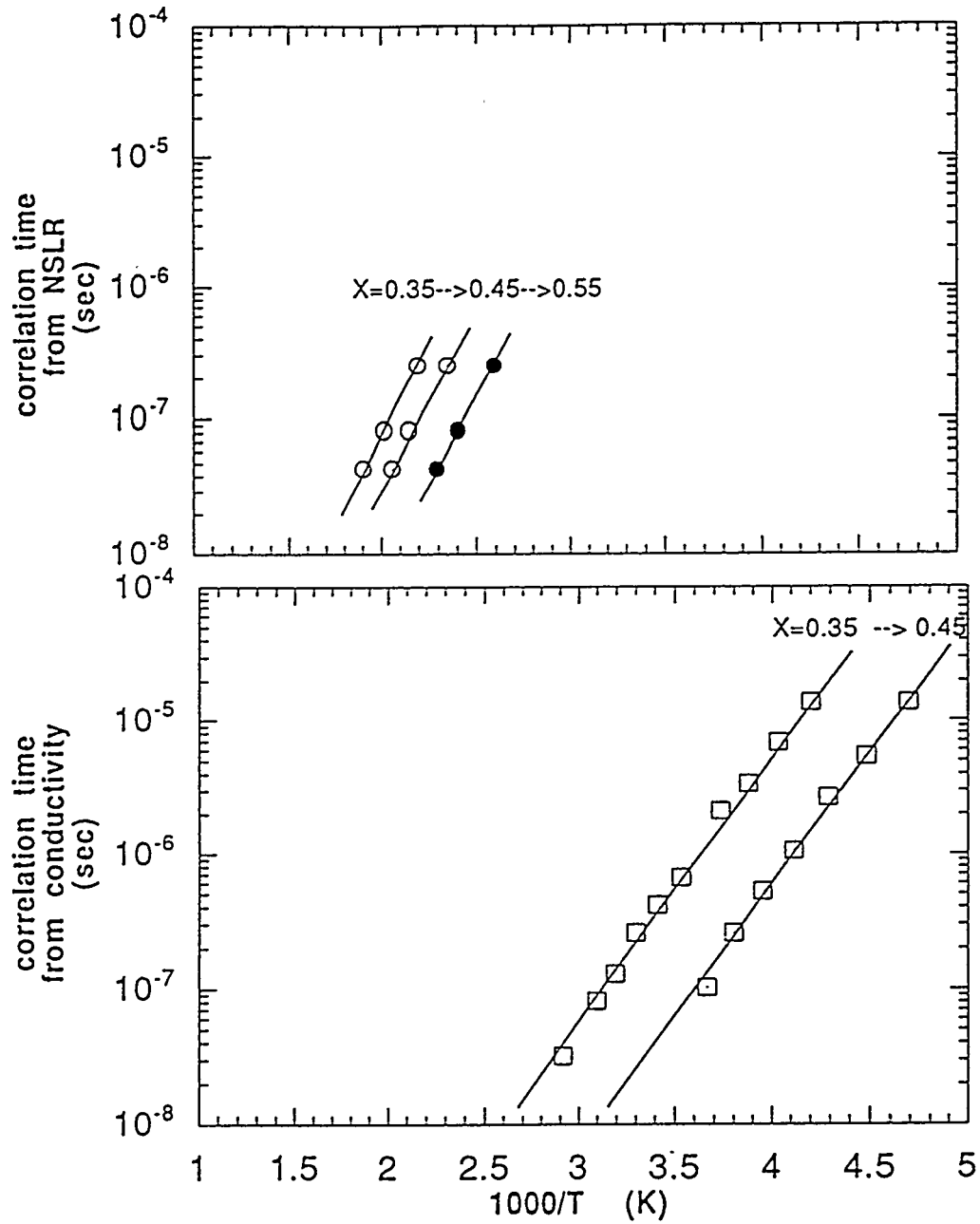


Fig. 4.5 Data of correlation times in Fig. 4.4 are re plotted to show the dependence from composition.

conductivity shows dependence on composition in $X \text{Li}_2\text{S} + (1-X)\text{GeS}_2$; $X=0.35, 0.45$ and 0.55 . The values of τ obtained from the onset of dispersion in Fig. 4.2 are plotted also in Fig. 4.4 and 4.5 vs. temperature for $x = 0.35$ and $x = 0.45$ samples. Clearly in the presence of non exponential decay of the correlation function or alternatively in the presence of distribution of correlation times the exact meaning of the τ plotted in Fig. 4.4 and 4.5 is not known. However, it certainly does represent a value which relates to the hopping frequency of the Li ion as probed by NMR and conductivity respectively. The mere fact that these two sets of τ 's are different by more than one order of magnitude indicates that the correlation is not a simple exponential, and that the two techniques do probe the Li motion in a different way. This is going to be one of the main point to be clarified by the analysis of the data presented in the following sections.

4.1.4 Analysis of the Data with the Phenomenological KWW Correlation Function and the Coupling Model

As was described in the section 3.4, we used the Dishon's formula for the numerical integration of the stretched exponential correlation function which does not have analytic solution except that for $\beta = 0.5$. For the fitting procedure for the NSLR and conductivity data, IMSL (see the Appendix) software package was used for the optimization process. FORTRAN language was used for the fitting programs and calculations. The measurements of impedance and conversion to the conductivity data was done with the software package developed by H. K. Patel and S. W. Martin [46].

The curves fitting the NSLR data according to equation (3.9) (Fig.4.6, 7 and 8) are in good agreement with the data except for deviations below about 200K.

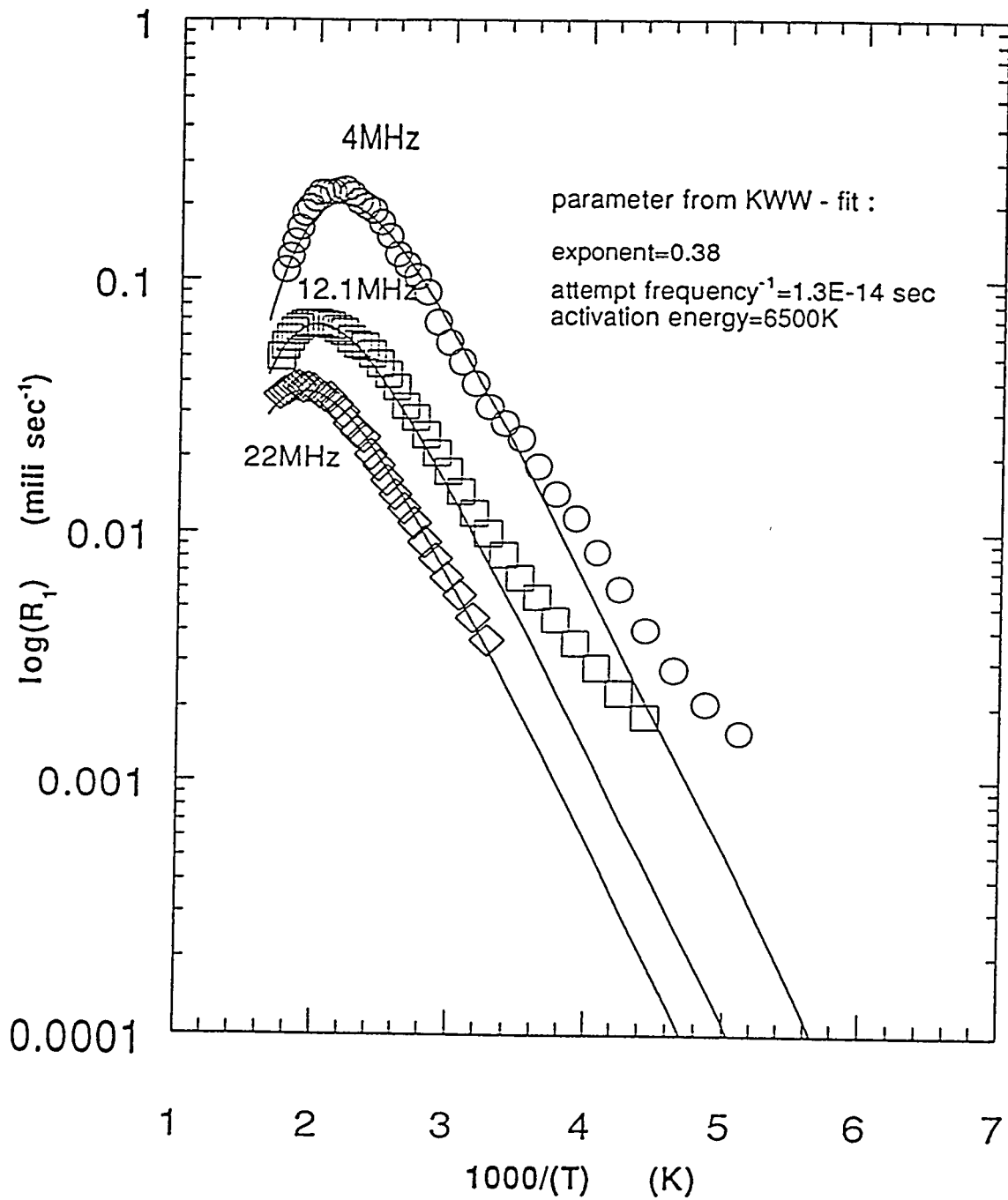


Fig. 4.6 ⁷Li spin lattice relaxation rate in 0.35 Li₂S + 0.65GeS₂. The solid line represent theoretical fit of equation (3.7) and (3.8) with the parameters shown inside graph and Table 4.1.

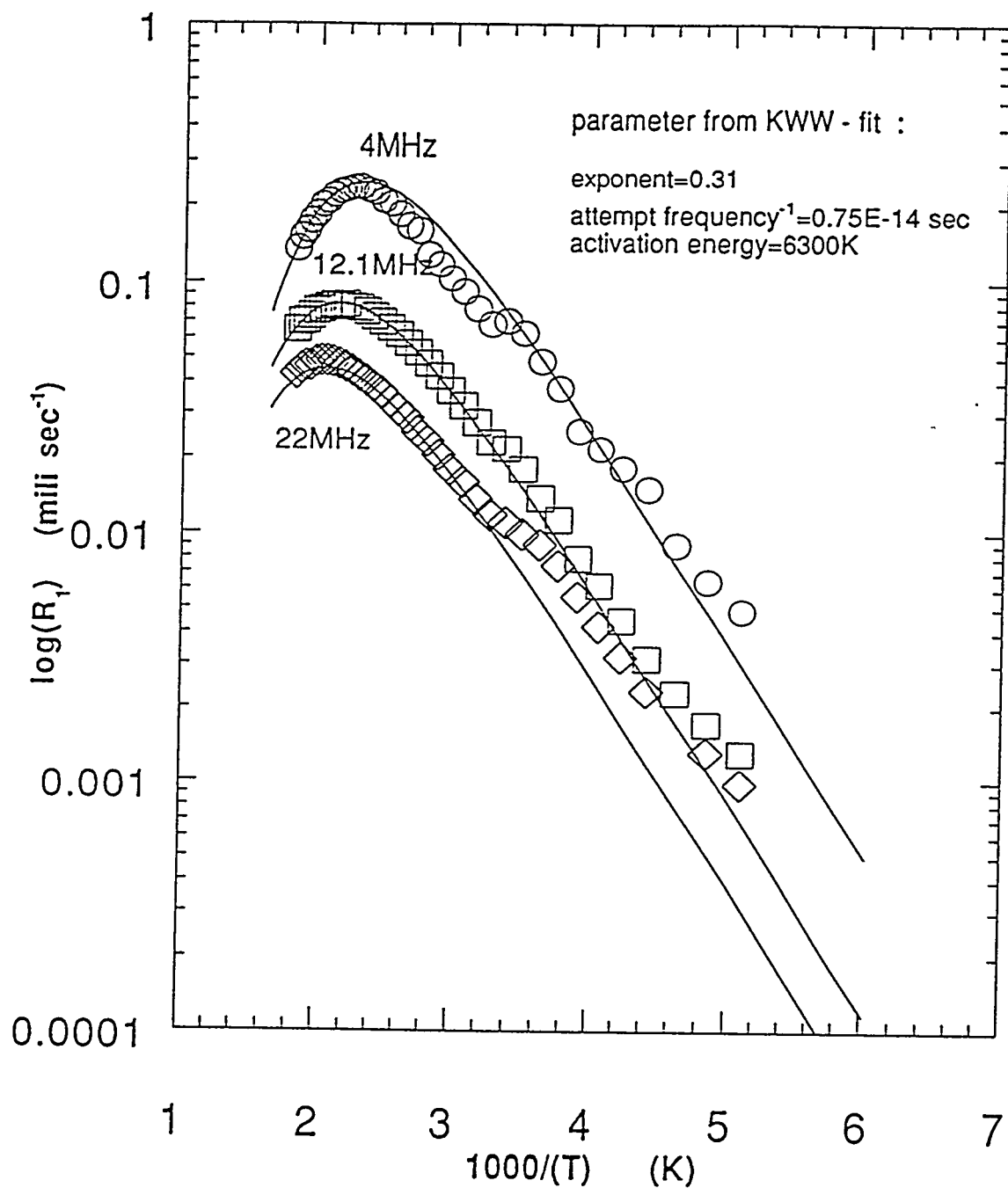


Fig. 4.7 ${}^7\text{Li}$ spin lattice relaxation rate in $0.45\text{Li}_2\text{S} + 0.55\text{GeS}_2$. The solid line represent theoretical fit of equation (3.7) and (3.8) with the parameters shown inside graph and Table 4.1.

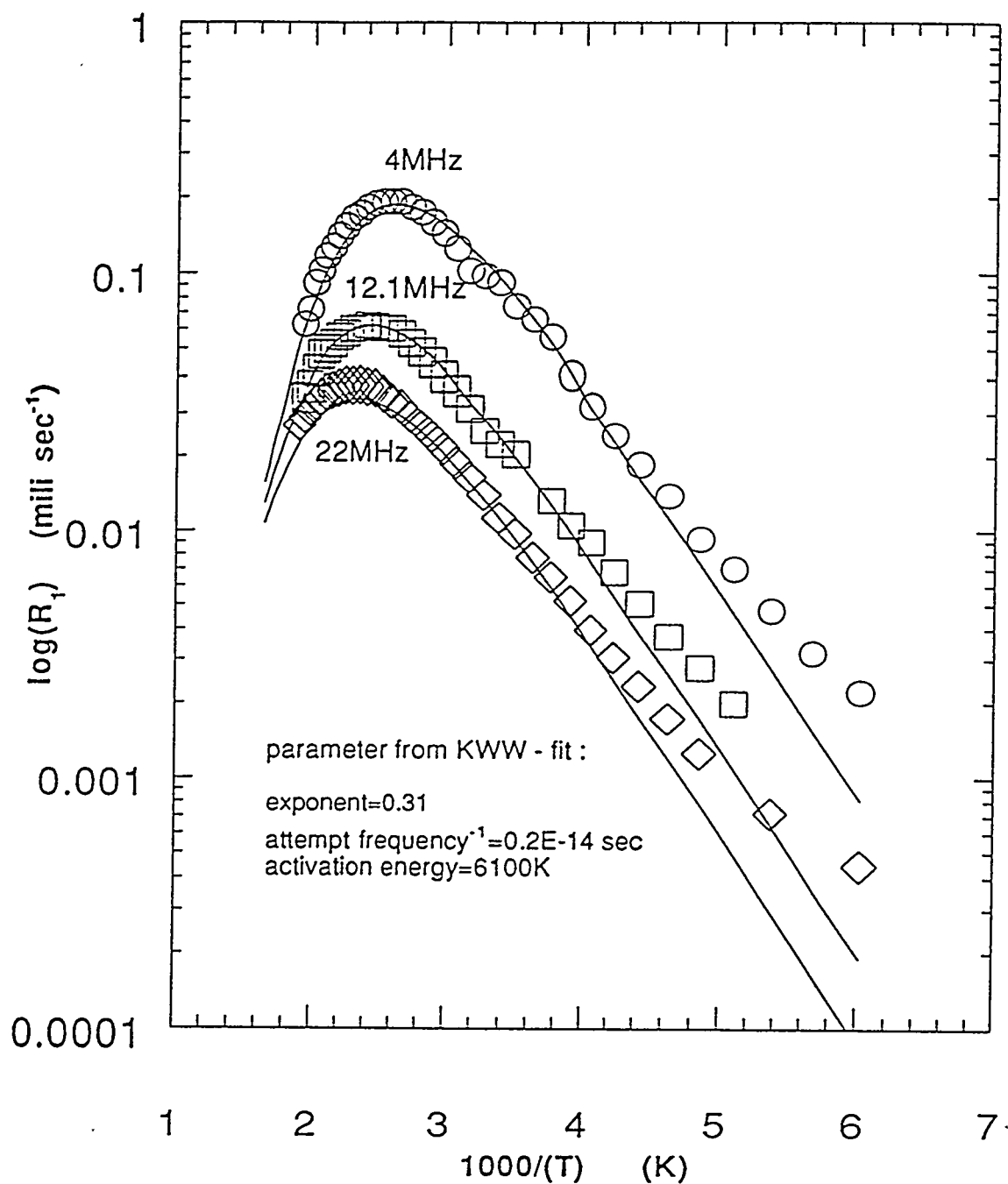


Fig. 4.8 ^7Li spin lattice relaxation rate in $0.55 \text{Li}_2\text{S} + 0.45\text{GeS}_2$. The solid line represent theoretical fit of equation (3.7) and (3.8) with the parameters shown inside graph and Table 4.1.

The deviation could either indicate a failure of equation (3.9) at low temperature or the presence of an extra relaxation mechanism at low temperature. The parameters obtained from the fit are summarized in Table 4.1.

The curves of best fit of the conductivity according to equation (3.12) are shown in the Fig. 4.9 and 4.10. The fits are good excepts for the data at low temperatures. The deviations from the fitting curves observed at low temperature for both NMR and conductivity could indicate that when the Li ion motion "freezes" other mechanisms which are not properly included in the KWW formalism become operative. The fitting curves are compared with the experimental data vs. temperature in

Table 4.1 Experimental Parameters obtained from KWW - Model for NSLR measurements.

	x = 0.35	x = 0.45	x = 0.55
A (rad / sec) ²	6.5×10 ⁹	6.2×10 ⁹	6.1×10 ⁹
τ ₀ * (sec)	1.3×10 ⁻¹⁴	7.5×10 ⁻¹⁵	2.0×10 ⁻¹⁵
Ea* (K)	6500	6300	6100
β	0.38	0.31	0.31

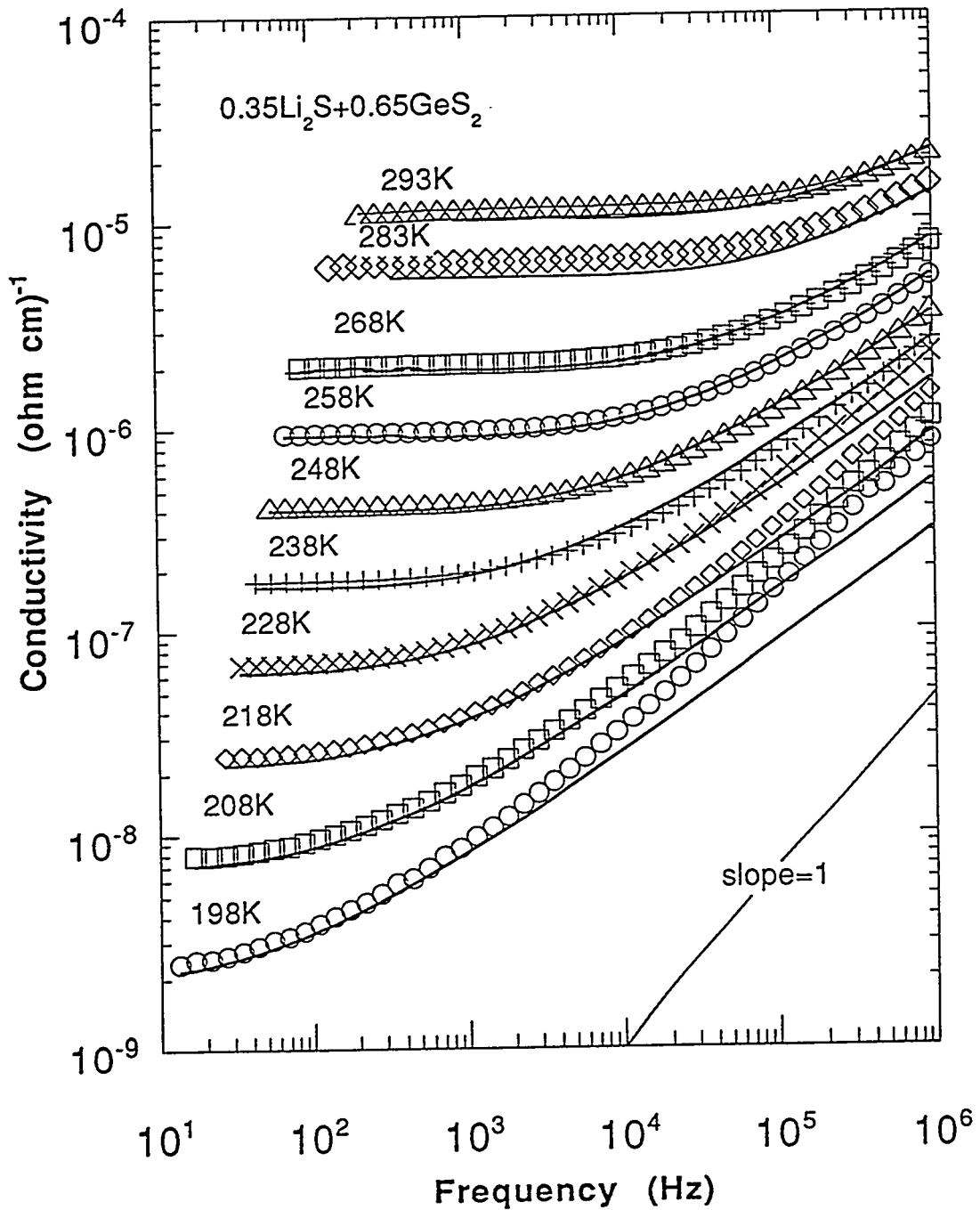


Fig. 4.9 The real part of ionic conductivity of $0.35 \text{Li}_2\text{S} + 0.65\text{GeS}_2$ vs. measurement frequency for several temperatures. The solid lines represent theoretical fit of equation (3.12) with the parameters shown inside graph and in Table 4.1.

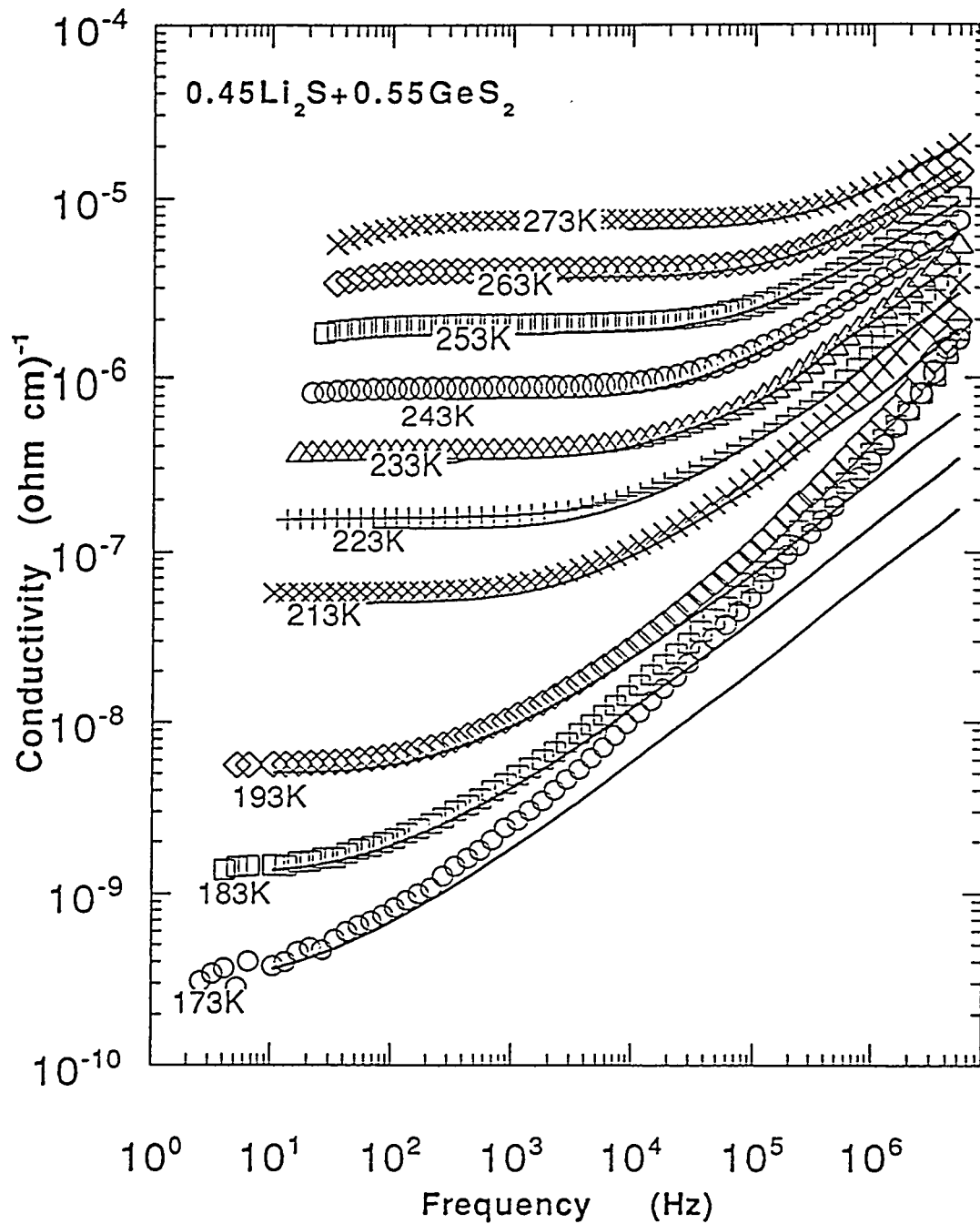


Fig. 4.10 The real part of ionic conductivity of $0.45\text{Li}_2\text{S} + 0.55\text{GeS}_2$ vs. measurement frequency for several temperatures. The solid lines represent theoretical fit of equation (3.12) with the parameters shown inside graph and in Table 4.1.

Fig. 4.11 and Fig. 4.12. Here we see that the disagreement between experiments and theory is more pronounced at low temperature and at high frequencies.

An extra contribution to the ac conductivity is often attributed to the low energy excitations in the disordered material [50], the so called two level systems of still ill-known microscopic origin [194]. The low energy excitations may be negligible at a elevated temperature where the long range ionic motion is dominant. Therefore the parameters for the motion of the ionic charge carrier should be obtained from the high temperature region while the extra conductivity at low temperature and at high frequency should be neglected. The parameters obtained from the fit of the conductivity are shown in the Table 4.2 and of the NSLR to the KWW - model are presented together in Fig. 4.13 in order to facilitate their comparison.

Table 4.2 Experimental Parameters obtained from KWW - Model for conductivity measurements.

	x = 0.35	x = 0.45
ϵ_{∞}	3.4	1.2
τ_0^* (sec)	1.9×10^{-15}	1.9×10^{-15}
Ea^* (K)	5230	4730
β	0.43	0.44

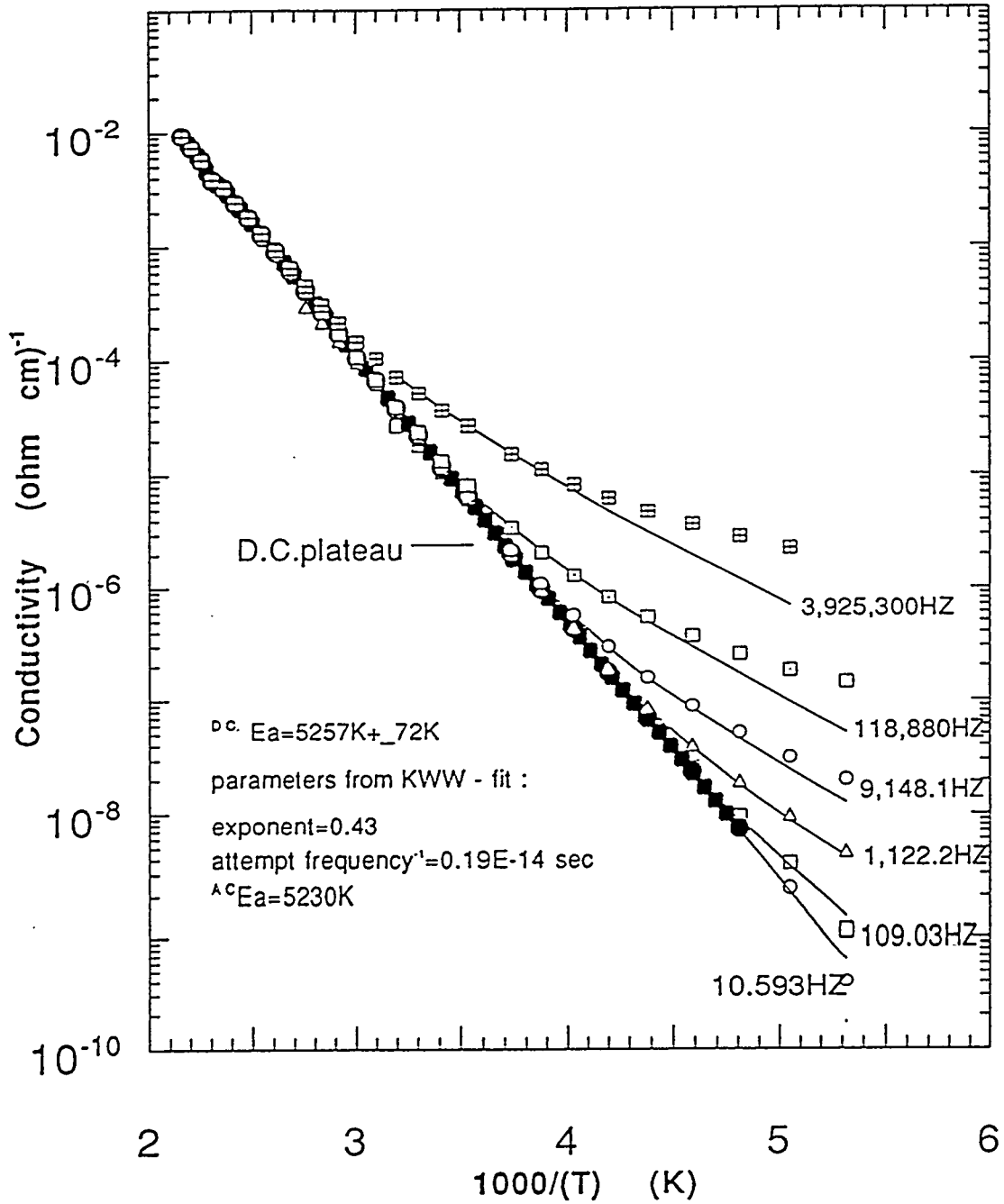


Fig. 4.11 Arrhenius plot of the real conductivity data shown in Fig. 4.2 or 4.9 of $0.35 \text{Li}_2\text{S} + 0.65\text{GeS}_2$. The solid line represents theoretical fit of equation (3.8) and (3.11) with the parameters shown inside graph and in Table 4.1.

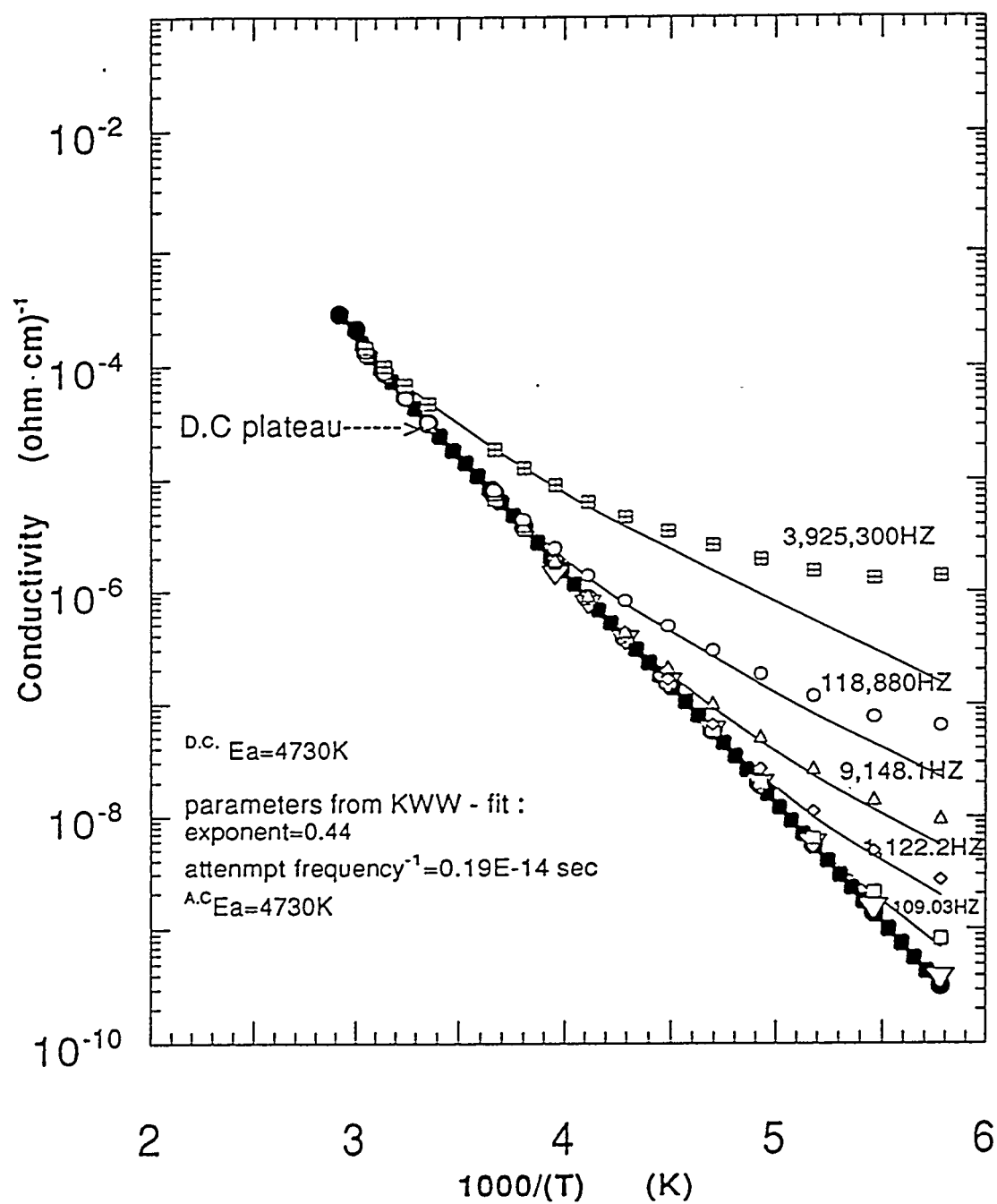


Fig. 4.12 Arrhenius plot of the real conductivity data shown in Fig. 4.10 of 0.45 $\text{Li}_2\text{S} + 0.55\text{GeS}_2$. The solid line represent theoretical fit of equation (3.8) and (3.11) with the parameters shown inside graph and in Table 4.1.

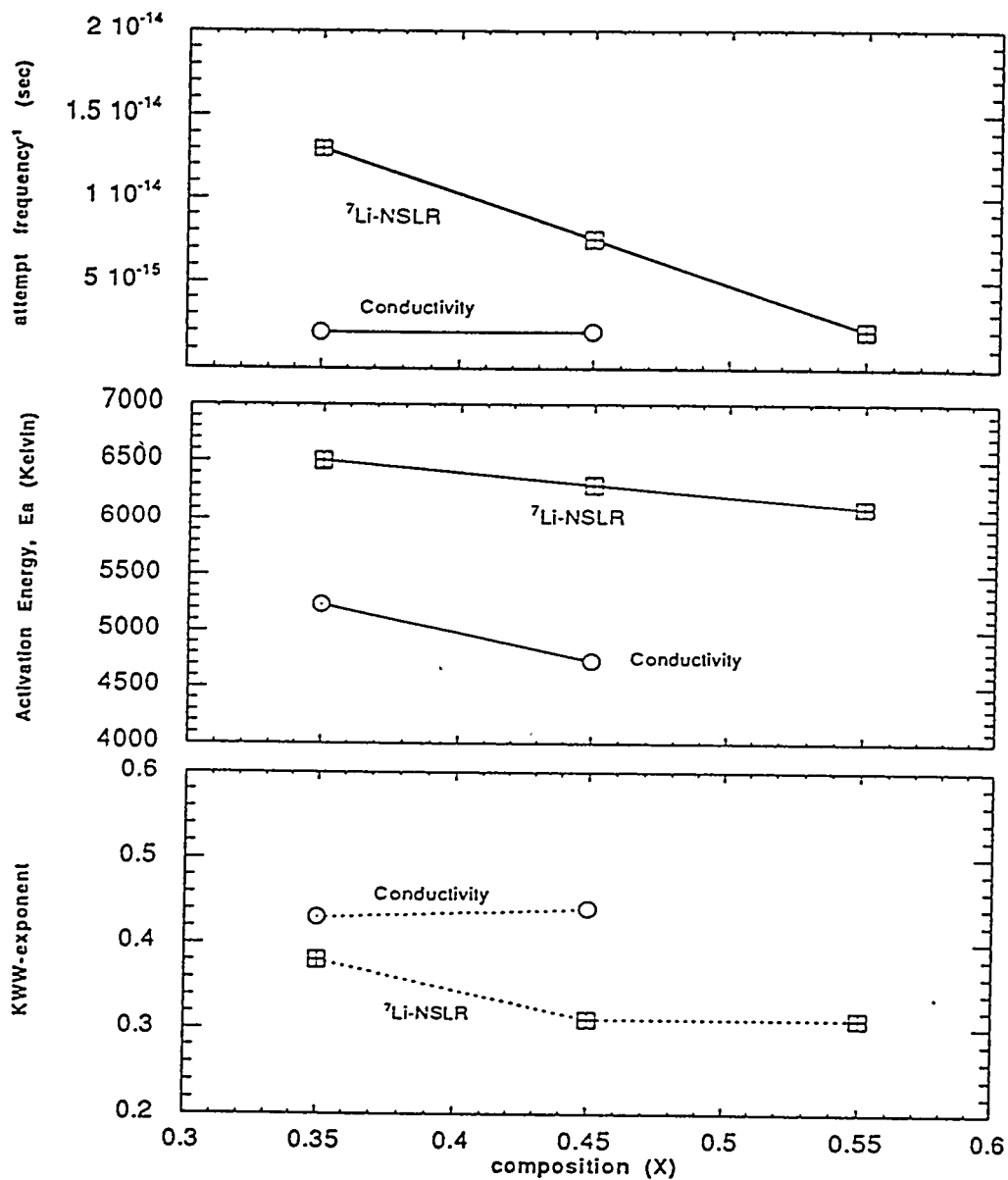


Fig. 4.13 The parameters from the fit using KWW - model vs. composition x to the NMR and conductivity data in $x\text{Li}_2\text{S} + (1-x)\text{GeS}_2$ ($x = 0.35, 0.45$ and 0.55). From the top τ_0^* , E_a^* and β vs. composition x are shown, where '*' indicate the effective value.

From the comparison of the parameters in Fig. 4.13, it can be seen that all three parameters i.e., τ_0^* , Ea^* and β obtained in the KWW model are different in NMR and conductivity. The difference of the parameters leads to a different effective correlation time τ^* which was already evidenced in the direct comparison discussed in section 4.1.3.

Since both NSLR and conductivity are determined (except for the low temperature, high frequency region) by the motion of the Li ion, the observed differences in the correlation functions must be related to a different mechanism by which the two techniques probe the Li ion dynamics. As was pointed out in the referenced work [54] the correlation function which is involved in the NSLR formulas is the local position - position correlation function of the Li ion while the correlation function involved in conductivity is the macroscopic polarization - polarization correlation function; therefore a difference in the two correlation functions is not surprising.

As was discussed in section 2.3.3 the KWW formalism has been interpreted by Ngai in terms of a phenomenological model which attributes a physical significance to the parameters τ_0^* , Ea^* and β . We are going to test some of the predictions of the coupling model against our experimental values. First let us check the prediction in equation (2.101) whereby the true single-ion activation energy barrier should not be identified either with the Ea^* from NMR or from conductivity but with the quantity $Ea = \beta_{NMR} Ea_{NMR}^* = \beta_{\sigma} Ea_{\sigma}^* \beta$. The prediction is approximately verified from the data in Table 4.1 and 4.2. One would conclude that the microscopic barrier is $Ea \cong 2300$ K for $x = 0.35$ and $Ea \cong 2000$ K for $x = 0.45$. Another predictions of KWW formalism and coupling are that the slope of $\log R_1$ vs. $1000/T$ on the low temperature

side of NSLR data should be E_a since in the low frequency region NSLR probes the short time part of the correlation function. From equation (2.99) and (2.100) we have,

$$\frac{(\tau_0^*)_{\text{NMR}}}{(\tau_0^*)_{\sigma}} = \frac{(\beta^{1/\beta})_{\text{NMR}}}{(\beta^{1/\beta})_{\sigma}} \left(\omega_c \tau_0 \right)^{\frac{\beta_{\sigma} - \beta_{\text{NMR}}}{\beta_{\sigma} \beta_{\text{NMR}}}} \quad (4.1)$$

From the parameters in Table 4.1 and 4.2 we can derive the cross - over frequency ω_c predicted by the coupling model (see equation (2.94 - 2.96)). One finds $\omega_c \tau_0 = 3.5 \cdot 10^3$ for $x = 0.35$; $\omega_c \tau_0 = 3.1 \cdot 10$ for $x = 0.45$. The cross - over time $t_c = \omega_c^{-1}$ obtained above is of the order of 10^{-15} sec to 10^{-17} sec for $\tau_0 \approx 10^{-14}$ sec. These values of t_c are unreasonably short to have a correct physical meaning of cross - over times in Ngai's coupling theory [188].

Finally one should point out that the KWW formalism and the coupling model predict a strictly Arrhenius behavior for the dc conductivity. As will be seen in the next paragraph, the experimental data, in some cases, do show a slight deviation from Arrhenius behavior which could not be explained with the coupling model.

4.1.5 Analysis of the Data with a Distribution of Activation Energies and the Percolation Model

We turn now to the analysis of the data based on the assumption that the Li ions move independently with thermally activated hopping motion but that the energy barriers are different in different sites of the lattice. The NSLR is given by the simple extension of the BPP type relaxation

$$R_1(\omega, T) = A^2 \int_0^{\infty} \left[\frac{\tau/z}{1 + \omega^2 (\tau/z)^2} + 4 \frac{\tau/z}{1 + 4\omega^2 (\tau/z)^2} \right] Z_{NMR} dEa \quad (4.2)$$

where A is the strength of the nuclear spin interactions and with the Gaussian distribution of activation energies Ea's [50,57]

$$Z_{NMR}(Ea) = \frac{1}{\sqrt{2\pi}E_b} \exp \left[-\frac{(E_m - Ea)^2}{2E_b^2} \right] \quad (4.3)$$

where Eb is the half width around Em, and the correlation times in the equation (4.2) are thermally activated form of

$$\tau = \tau_0 \exp \left(+\frac{Ea}{k_B T} \right) \quad (4.4)$$

where k_B is the Boltzman constant and T is expressed in Kelvin. Then the total rate on the ionic hopping is z times the f_{OSC} of equation (3.24), where z is assumed to be 6 for the simple harmonic oscillator's of depth Ea and site distance d, which is extending in space. As was mentioned in the previous section, the site distances should not change much (therefore in the range of $2A^\circ \sim 6A^\circ$) to affect the whole calculation of the NSLR. Actually the calculation does not show considerable deviations if one use a reasonable estimation (site distances to be in the range of $2A^\circ \sim 6A^\circ$) of the

prefactor of the correlation time. Here we used $d = 3.7 \text{ \AA}$ to be the site distance, which is estimated from the crystal structure of the di thio germanate [138]. Therefore we could use the equation (4.2) with the IMSL optimization package in the VAX computer to fit the NSLR data (see appendix). The fitting parameters are the width E_b and the average E_m for the Gaussian distribution function of the activation energies. The fittings of equation (4.2) with equation (4.3) to the NSLR are shown in the Fig. 4.14, 15 and 16 for $x = 0.35, 0.45$ and 0.55 respectively. By using parameters from the fitting, the distribution of the activation energies are plotted for $x = 0.35, 0.45$ and 0.55 , as shown in the Fig. 4.17. By using the distributions of activation energies derived from NMR (Fig. 4.17) we estimate now the dc conductivity.

For the calculation of dc conductivity, the simple hopping model is used in which we replace the single correlation time with the correlation time averaged over the Gaussian distribution up to a cut - off energy E_c . One has:

$$\sigma_{dc} = \frac{nPe^2d^2}{zk_B T \langle \tau \rangle} \quad (4.5)$$

where n is the concentration of the ionic charge carriers, $e = 1.6 \times 10^{-19}$ coulomb, $\langle \tau \rangle$ is the average correlation time:

$$\langle \tau \rangle = \left(\frac{1}{P} \right) \int_0^{E_c} \tau_0 \exp\left(-\frac{E_a}{k_B T} \right) \cdot Z_{NMR} dE_a \quad (4.6)$$

$$P = \int_0^{E_c} E_a \cdot Z_{NMR} dE_a$$

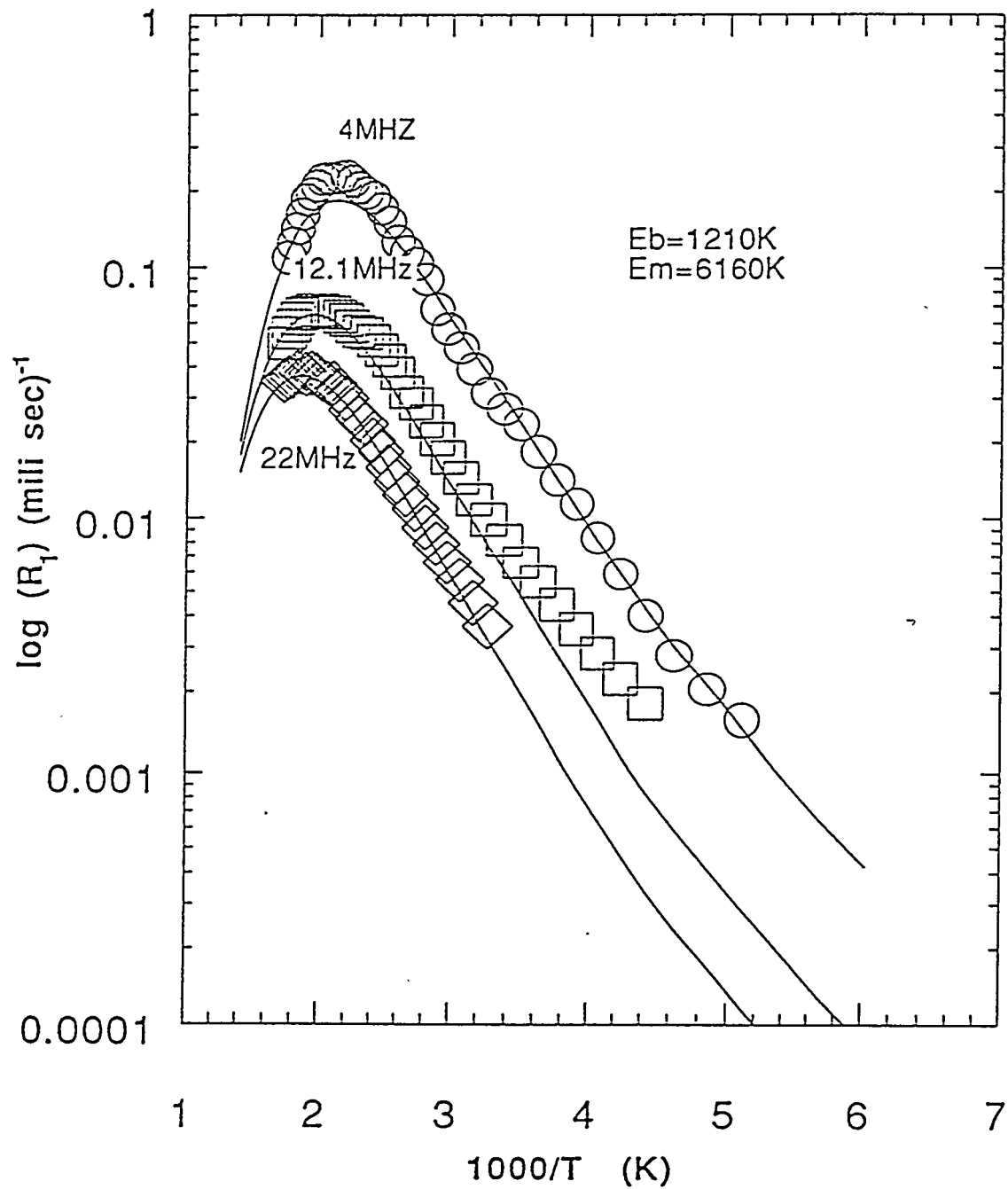


Fig. 4.14 ${}^7\text{Li}$ spin lattice relaxation rate in $0.35 \text{Li}_2\text{S} + 0.65\text{GeS}_2$. The solid line represent theoretical fit of equation (3.20) and (3.25) with the parameters shown inside graph.

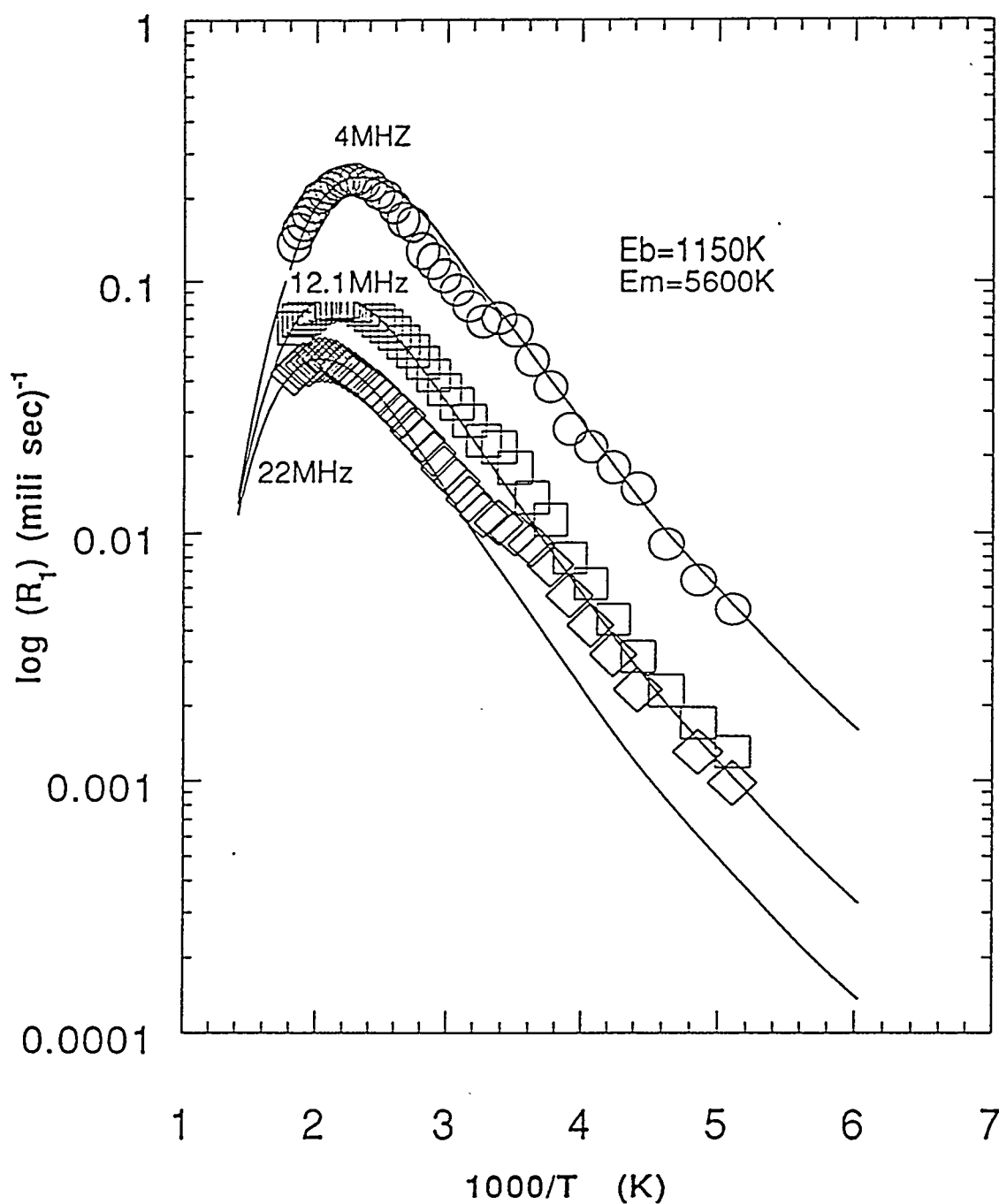


Fig. 4.15 ${}^7\text{Li}$ spin lattice relaxation rate in $0.45 \text{Li}_2\text{S} + 0.55\text{GeS}_2$. The solid line represent theoretical fit of equation (3.20) and (3.25) with the parameters shown inside graph.

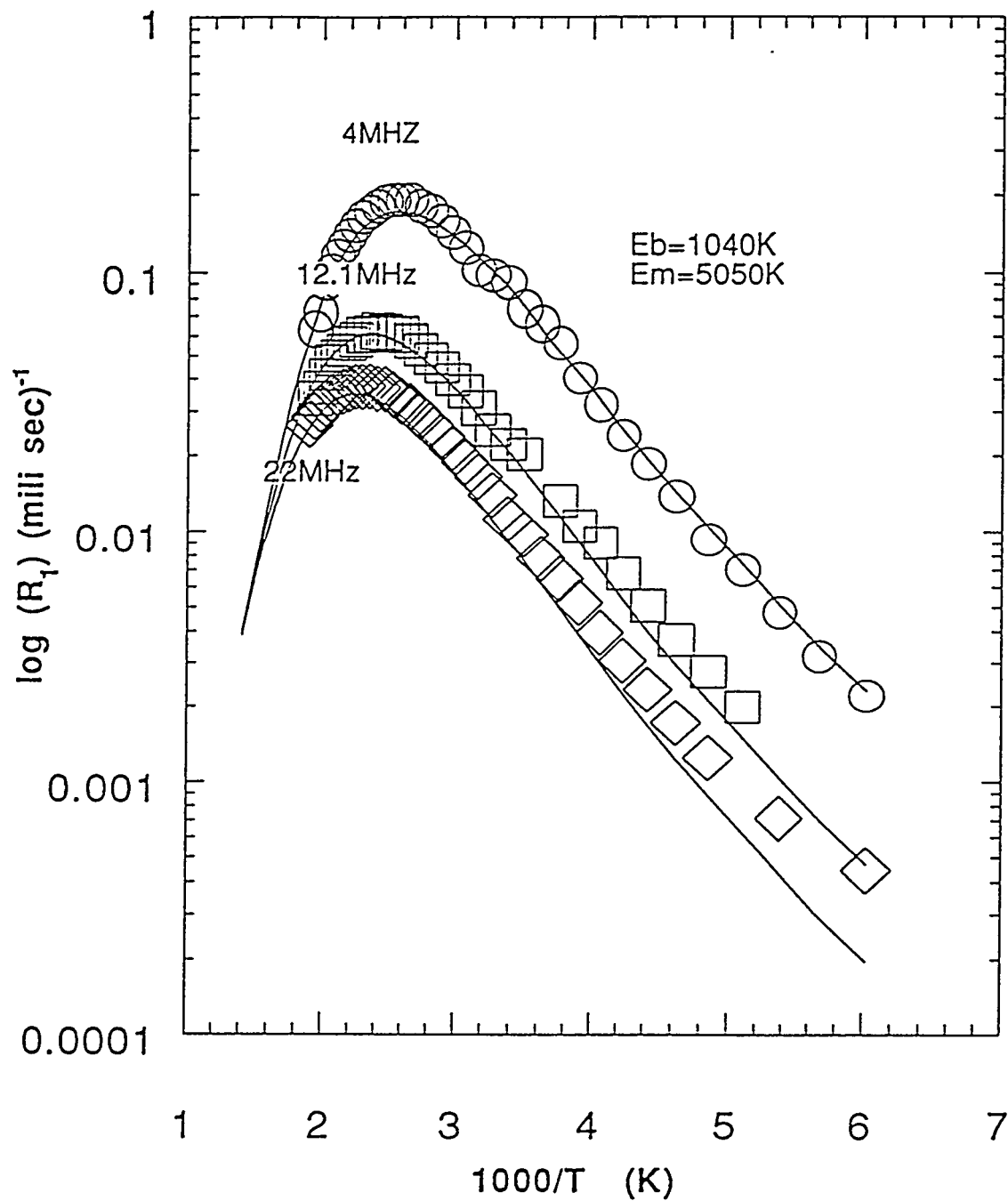


Fig. 4.16 ${}^7\text{Li}$ spin lattice relaxation rate in $0.55 \text{Li}_2\text{S} + 0.45\text{GeS}_2$. The solid line represent theoretical fit of equation (3.20) and (3.25) with the parameters shown inside graph.

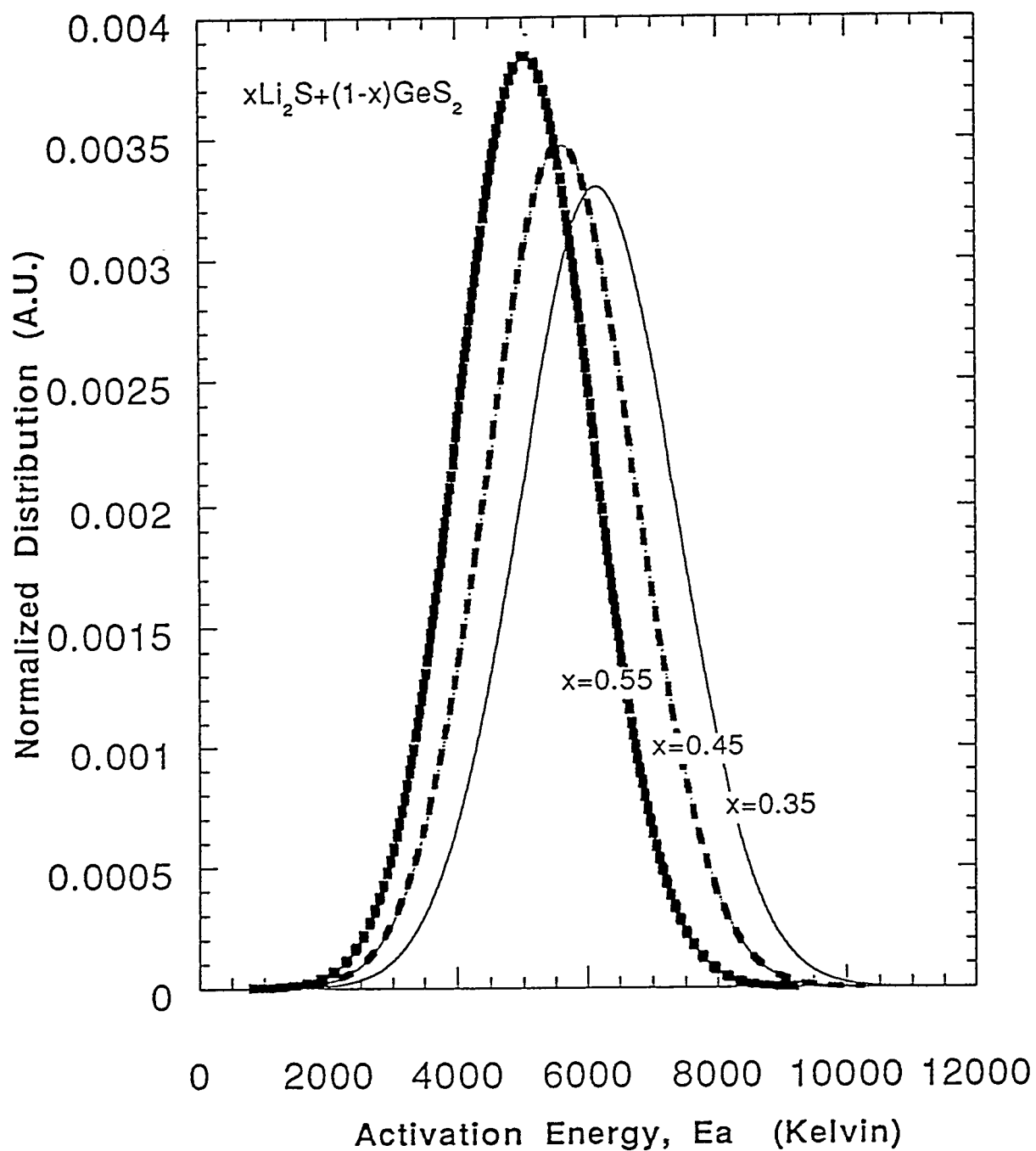


Fig. 4.17 Distribution of activation energies in the motion of Li^+ in $x\text{Li}_2\text{S} + (1-x)\text{GeS}_2$. ($x=0.35, 0.45$ and 0.55) derived from NMR relaxation.

where we define P as the percolation fraction. The site distance was estimated from the measured density of the glasses; $d = 2.59 \text{ gm/cm}^3$ for $x = 0.35$ and $d = 2.48 \text{ gm/cm}^3$ for $x = 0.45$. The average τ is determined by the width E_b around E_m , and by the percolation fraction P , which is chosen as a fitting parameter to bring the calculated value of dc conductivity in agreement with the measured one.

The fitting to the measured dc conductivity yields $P \sim 0.35$ for lithium thio germanate and lithium chrolo borate [56] which shows similar dc behavior, and $P \sim 0.25$ for lithium thio silicate[57] which has better conductivity than the thio germanate and chrolo borate. The measured and fitted dc conductivity are shown in Fig. 4.18 and 19 for $x=0.35$ and 0.45 respectively, with the distribution of activation energies cut off at E_c . It is noted that the percolation fraction obtained here are consistent with theoretical estimates for simple cubic lattices [28]. Also we find that $E_c \geq E_a^{dc}$ which is also reasonable.

Here we revisit the problem of the consequences of using the distribution of activation energies on the dc conduction. With the distribution of correlation times one should observe a deviation from Arrhenius behavior of dc conductivity. In Fig. 4.20 the Arrhenius plot for several calculated dc conductivities with a distribution of correlation times are shown for;(I) for the low ionic conductor as oxide glass, (II) for the intermediate conductor as thio germante glass and (III) very highly conductive glass as silver thio borate. In the graph, one can clearly see the almost-Arrhenius, slightly non Arrhenius and non Arrhenius behavior of the dc conductivity for each cases. Therefore one can argue that the observed behavior of almost-Arrhenius is due to the fact that the measurements are performed mostly on low conductivity glasses, and moreover in a limited range of the temperature where the non Arrhenius behavior

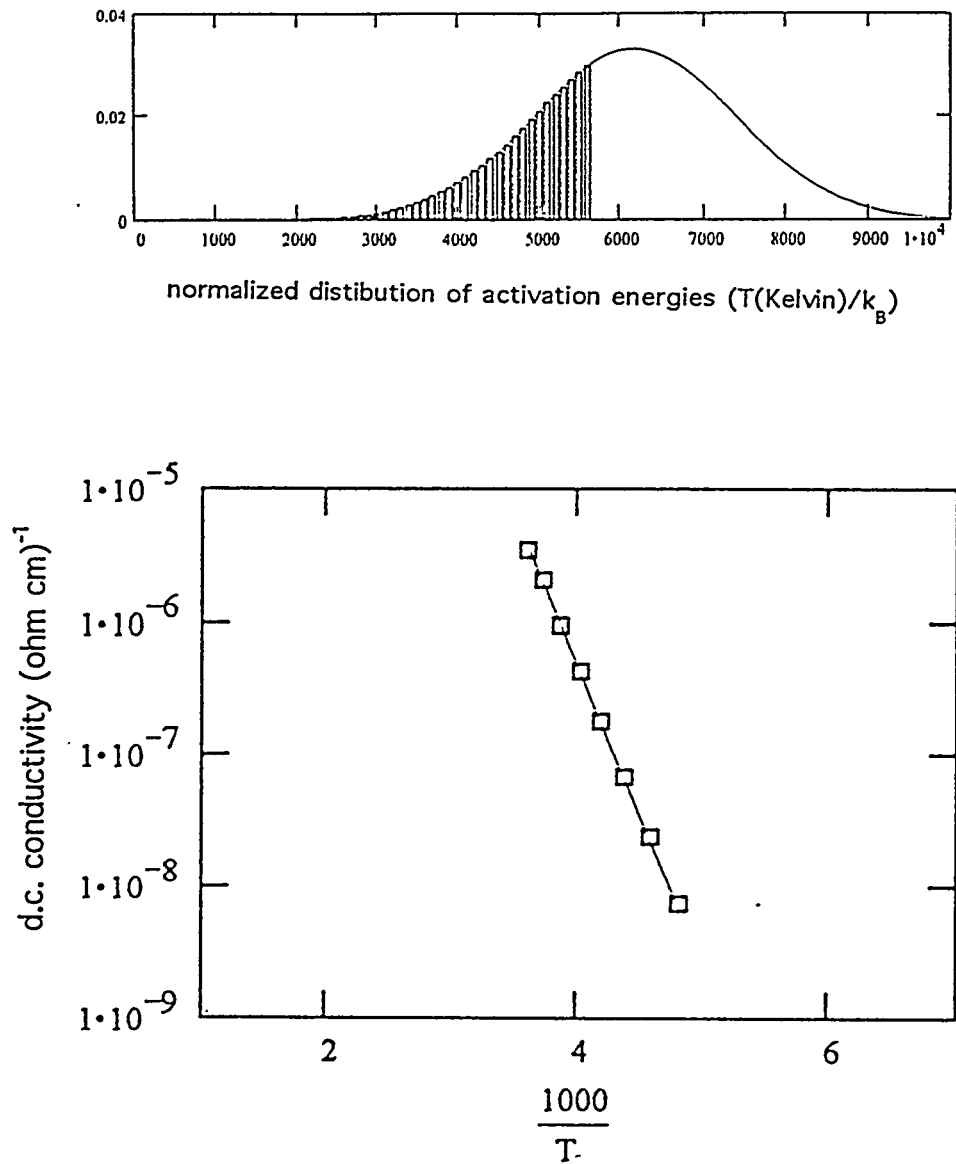


Fig. 4.18 Fit of Gaussian distribution, Z_{NMR} , with peak position $E_m = 6160$ K and width $E_b = 1210$ K (Top graph), in $0.35 \text{ Li}_2\text{S} + 0.65 \text{ GeS}_2$. Truncation at $E_c = 5600$ K gives the dc conductivity from the striped fraction $P = 0.34$ which is shown in the second graph (curve), as a function of inverse temperature, T . The squares represents experimental data.

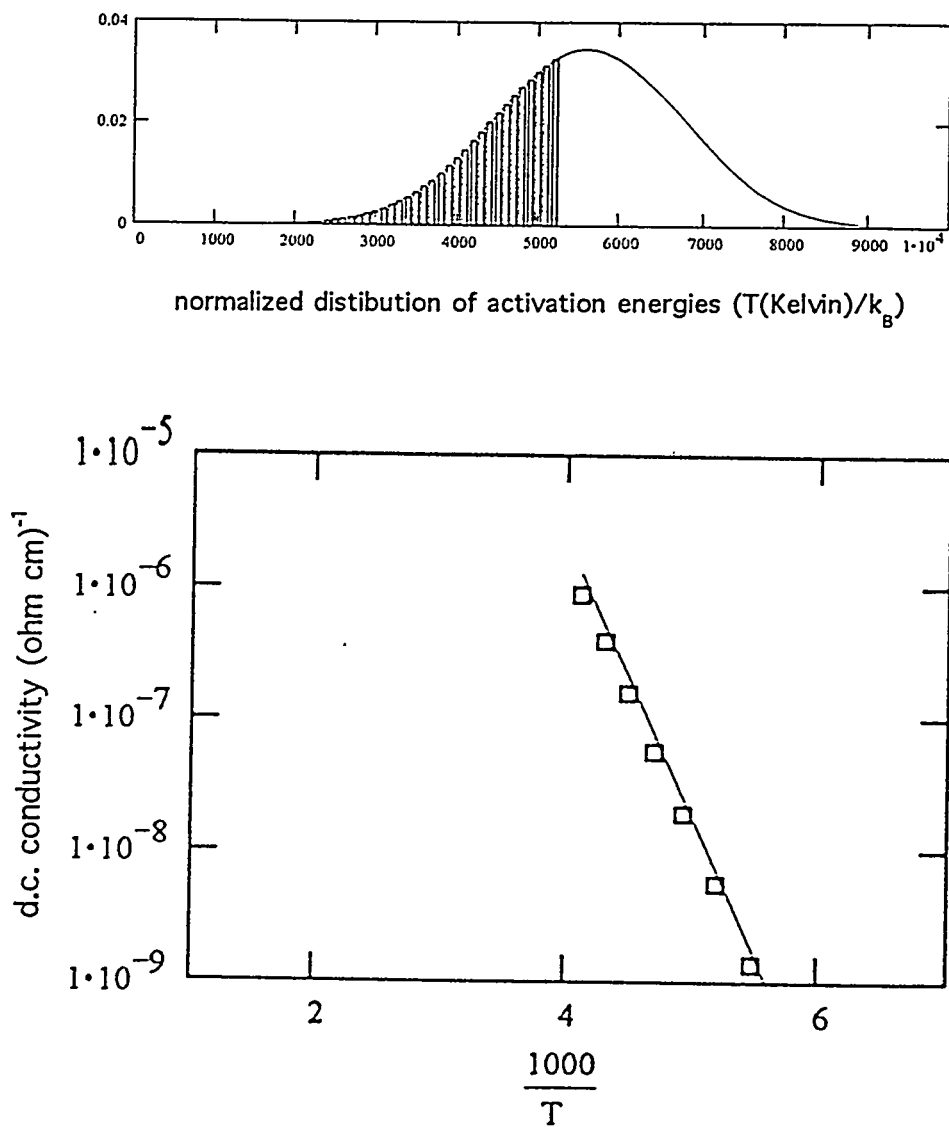


Fig. 4.19 Fit of Gaussian distribution, Z_{NMR} , with peak position $E_m = 5600$ K and width $E_b = 1150$ K (Top graph), in $0.45 \text{ Li}_2\text{S} + 0.55 \text{ GeS}_2$. Truncation at $E_c = 5200$ K gives the dc conductivity from the striped fraction $P = 0.38$ which is shown in the second graph (curve), as a function of inverse temperature, T . The squares represents experimental data.

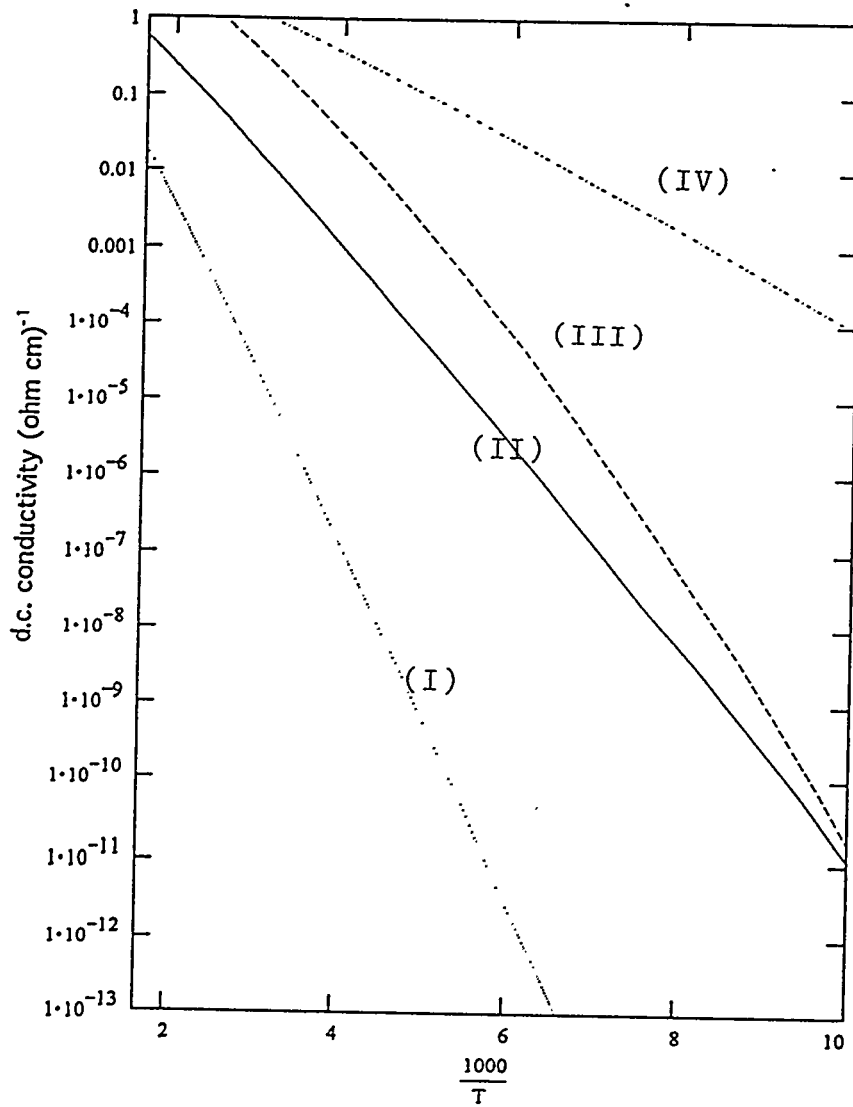


Fig. 4.20 The calculated d.c. conductivity vs inverse temperature using simple hopping model of equation (3.26) and (3.270 for various values of peak and width for the distribution of activation energies with percolation effect. The parameters for calculations ($E_m / E_b / P$) are: (I) 7000 K / 1800 K / 0.24 (II) 4000 K / 1000 K / 0.26 (III) 2000 K / 500 K / 1.0 (IV) 2000 K / 500 K / 0.24 respectively.

is difficult to observe within the experimental error. Clear deviations from Arrhenius behavior were indeed observed recently by J. Kincks et al. [196]. The results are shown in Fig. 4.21. We believe that this observation strongly supports the model adopted here of a distribution of activation energies.

4.2 $x\text{Li}_2\text{S} + (1 - X)\text{B}_2\text{S}_3$

In this section we present and analyze data of NSLR and conductivity in lithium thio borates with two compositions ($x = 0.65$ and 0.70). The NSLR in $\log R_1$ vs. $1000/T$ plot showed two distinct maxima. For the main maximum the NSLR showed non BPP behavior. The dc conductivity showed slight deviations from Arrhenius behavior. Dispersive behavior which seems to approach a power law (conductivity vs. frequency in a log-log plot looks linear) at low temperature and/or at high frequency were observed as was in lithium thio germanate glasses.

It is shown that both NMR and conductivity data can be explained in terms of a distribution of activation energies with two distinct maxima. It is shown that the motion of Li - ion hopping to the non-bridging sulfurs of BS_4 - environment and BS_3 -environment feels different (but weakly overlapping) distribution of activation energies, thus revealing two distinct motional maxima in ^7Li - NSLR. This simply means that one SRO group has slightly higher average activation energy than the other SRO group. The ^{11}B - NSLR in the BS_3 structural units and in the BS_4 structural units were measured separately. Each maximum corresponds to the motional relaxation maximum in the ^{11}B in BS_3 and in the BS_4 structural units respectively. From the fit of ^{11}B - NSLR we could conclude that the relaxation of ^{11}B is not due to Li ion motion but rather to a local rearrangement of BS_3 (BS_4) groups which can be triggered by the hopping of Li ions in the proximity.

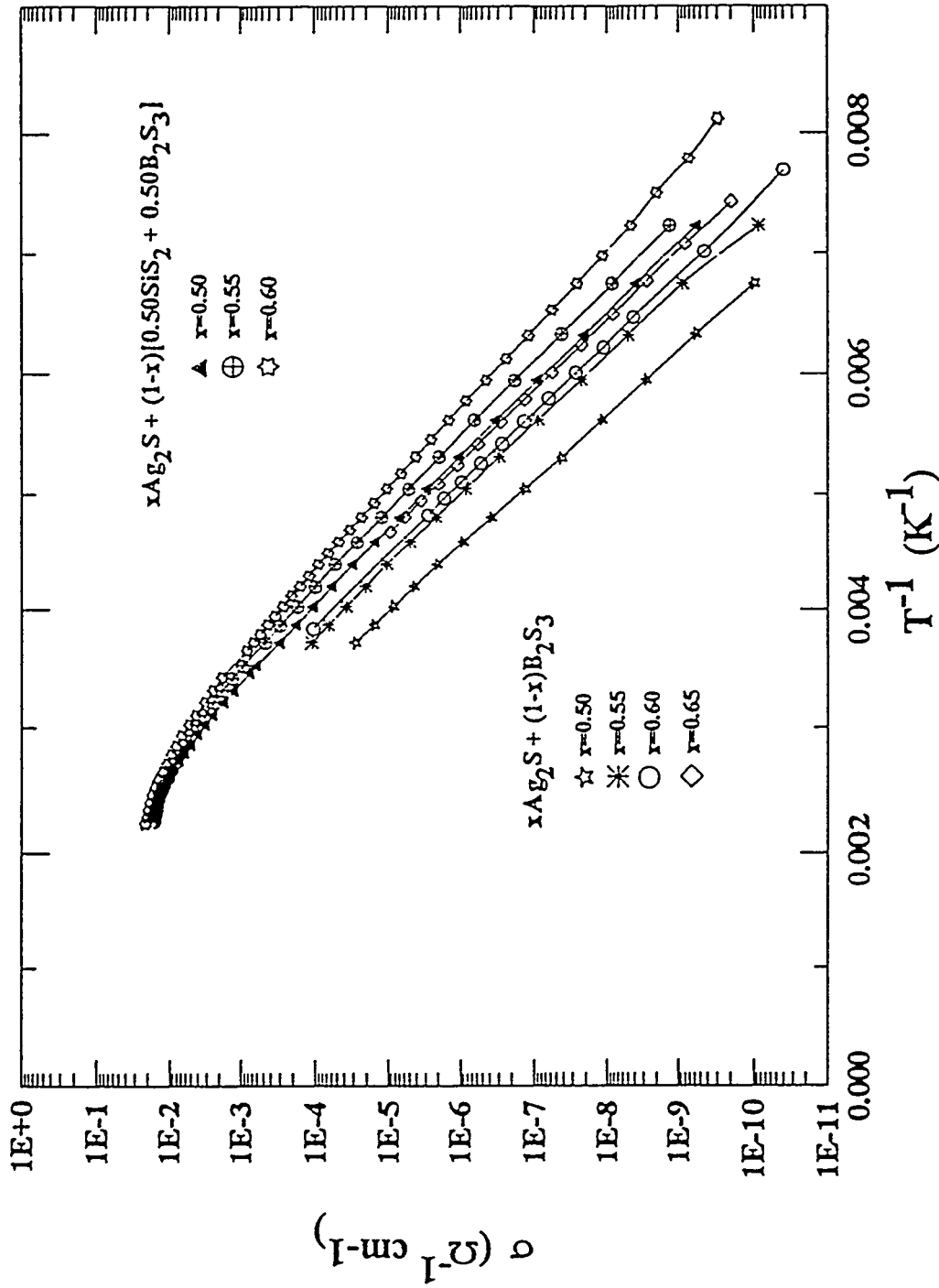


Fig. 4.21 Observed deviation of d.c. conductivity from Arrhenius behavior in $x\text{Ag}_2\text{S} + (1-x)[0.5\text{SiS}_2 + 0.5\text{B}_2\text{S}_3]$, by J. Kincs et al.

4.2.1 ^7Li Nuclear Spin Lattice Relaxation Measurements

The ^7Li NSLR vs. temperature is shown in Fig. 4.22 for two samples ($x = 0.65$ and 0.70) at three different resonance frequencies. The data in Fig. 4.22 are similar to the one observed in lithium thio germanate glasses (see section 4.1.1), except for the secondary maximum in $\log R_1$ vs. $1000/T$ plot. Four different batches of samples prepared with the same method were measured and showed the same features. The recovery of the ^7Li nuclear magnetization in thio borate glasses was found to be exponential down to the 90% of signal intensity for all temperatures, except at temperatures in the vicinity of the secondary maximum. This is shown in Fig. 4.23, for the higher resonance frequency (40 MHz) for which the signal to noise ratio is best. NSLR in Fig. 4.22 were obtained by the observed exponential decay of nuclear magnetization for the first 90% of decay.

4.2.2 Conductivity Measurements

The measurements of the dc conductivity are shown in Fig. 4.24 for $x = 0.70$. The main features of the data are again similar to the one for lithium thio germanates, except that now the departure from a simple activated Arrhenius behavior is more evident at high temperatures. This non Arrhenius behavior is a central finding of the present work because it strongly supports the model of distribution of activation energies.

4.2.3 Interpretation of the Anomalous ^7Li NSLR Curves

In order to put in the evidence the anomaly in the ^7Li NSLR data in Fig. 4.22, we try first to fit the data with a KWW correlation function. As was discussed

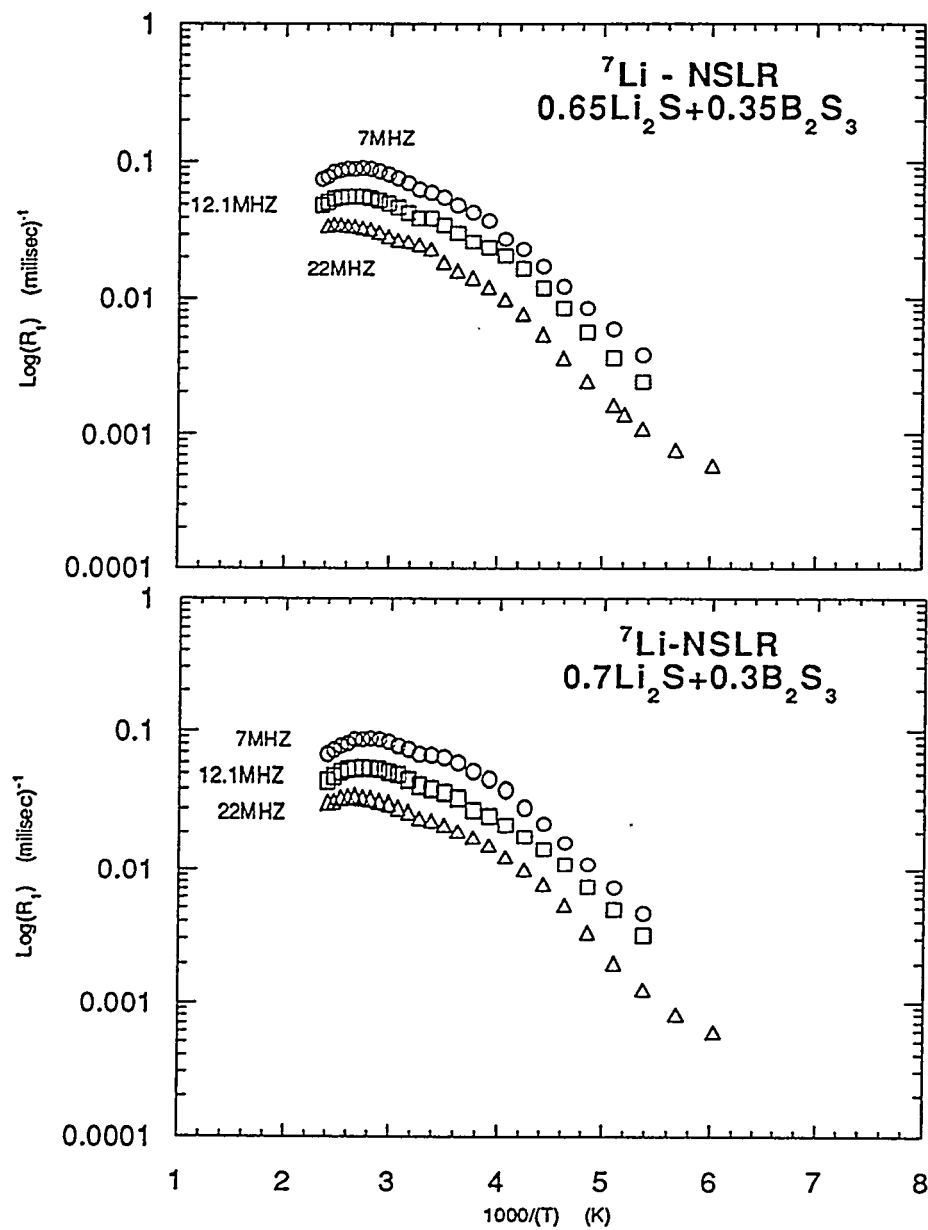


Fig. 4.22 ${}^7\text{Li}$ NSLR at 7, 12.1 and 22 MHz in logarithm of the relaxation rates as a function of reciprocal temperatures in $0.65 \text{Li}_2\text{S} + 0.35\text{B}_2\text{S}_3$ (upper graph) and $0.70 \text{Li}_2\text{S} + 0.30\text{B}_2\text{S}_3$.

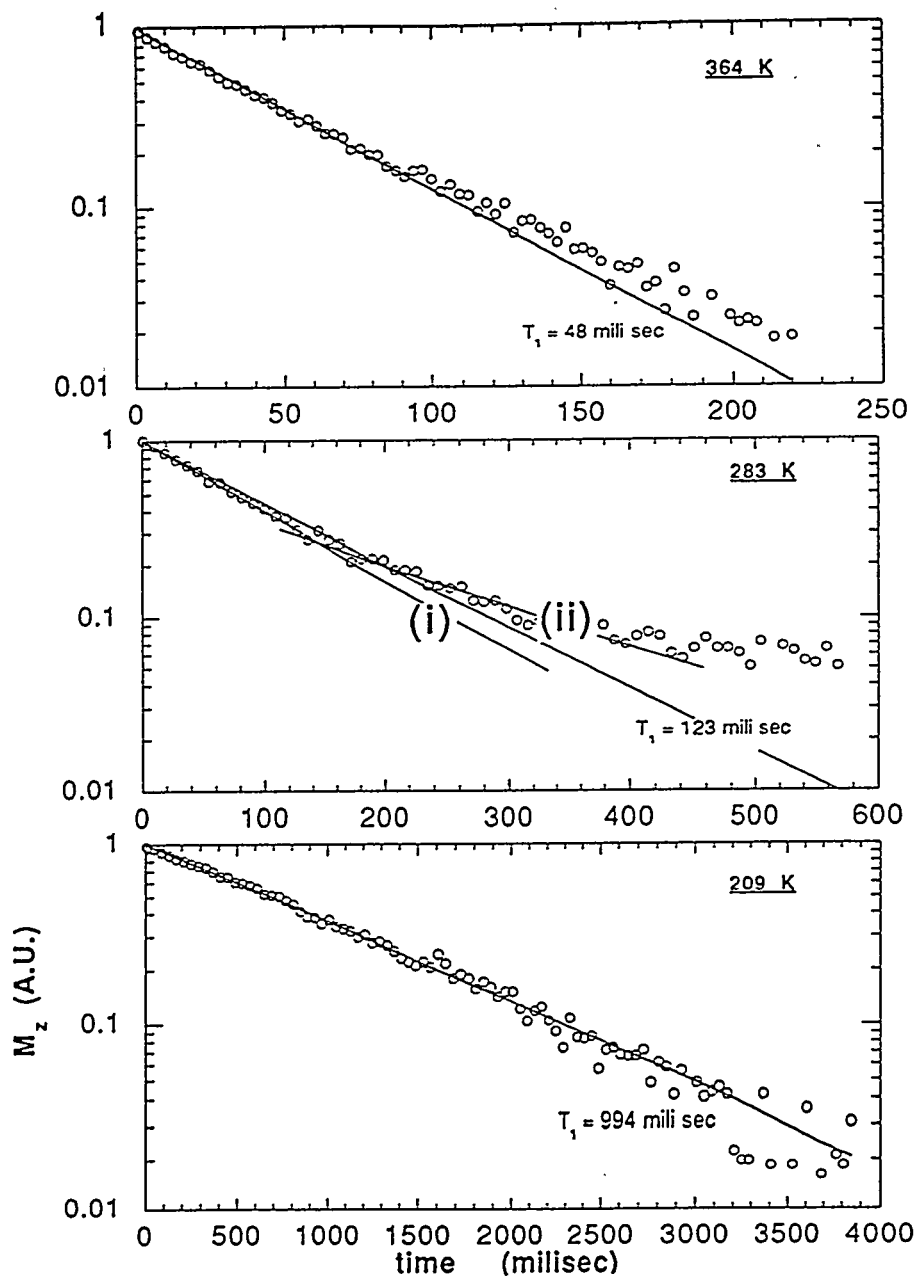


Fig. 4.23 Logarithmic ${}^7\text{Li}$ recovery vs. time (in mili sec) in $0.70 \text{ Li}_2\text{S} + 0.30 \text{ B}_2\text{S}_3$ measured at 40 MHz, at three different temperatures 364 K, 283 K and 209 K. The solid line represent the single exponential decay of nuclear magnetization along the direction of external magnetic field.

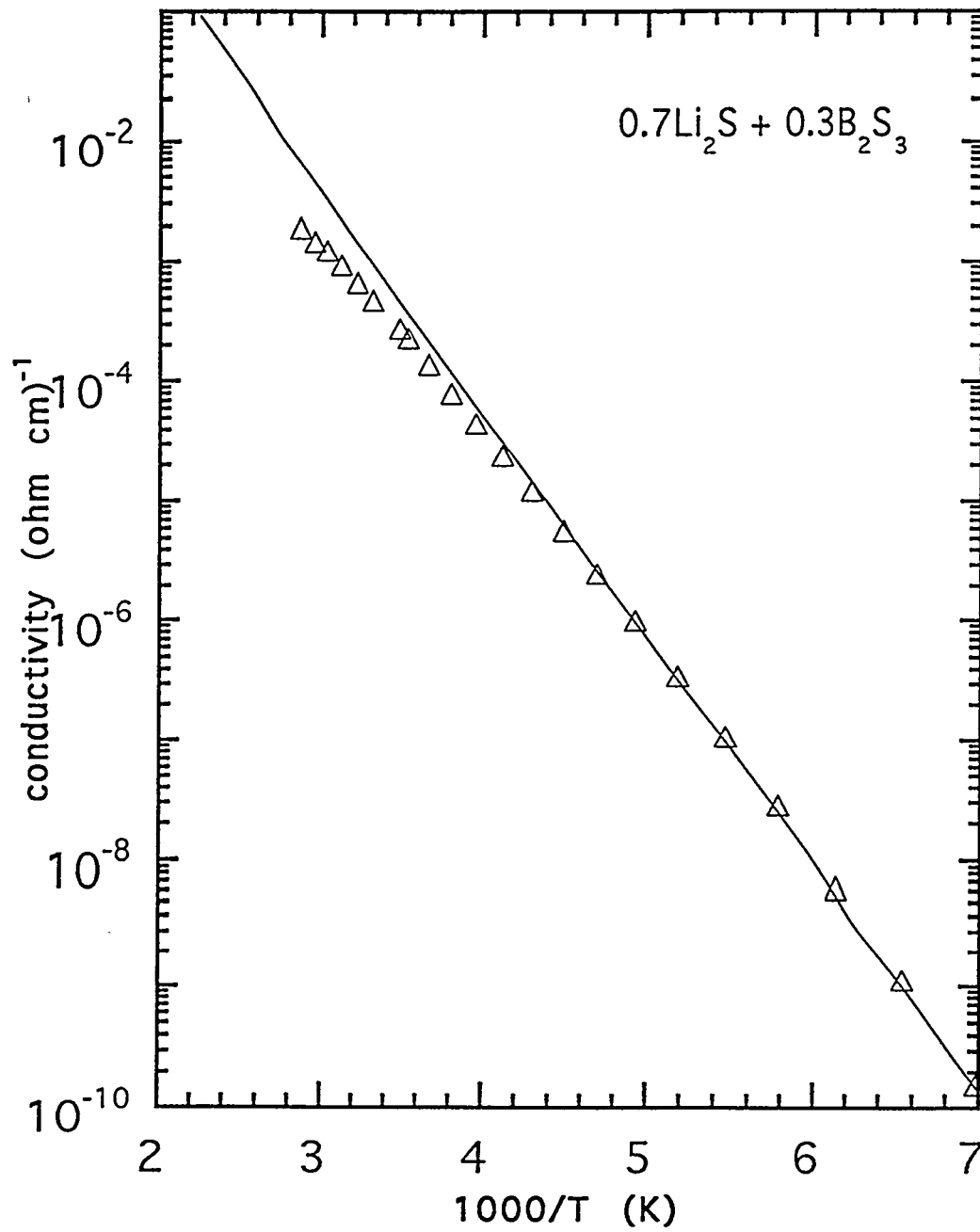


Fig. 4.24 Experimental d.c. conductivity in 0.70 Li₂S + 0.30B₂S₃ vs. reciprocal temperature shows continuous deviation from Arrhenius behavior.

before this fit is practically equivalent to the fit in terms of a single Gaussian distribution of activation energies. The curves fitting the NSLR data according to equation (3.9) and (3.12) shows "extra relaxation" which is one order of magnitude smaller than the main relaxation described by equation (3.9) and (3.12). The fitting were done to the data in the vicinity of the first maximum, and then the assumed extra relaxation rate or "extra NSLR" were obtained by subtracting the predictions of equation (3.9) and (3.12) from the raw data of NSLR (since NSLR is additive).

The ${}^7\text{Li}$ ($I = 3/2$) spectrum shown in Fig. 4.25 does not reveal any structure which could come from an extra phase. The spectrum consists of central line transition ($1/2 \leftrightarrow -1/2$), and a broad wing due to the powder distribution of satellite transitions shifted by the first order quadrupole interactions. The independence of the width of the broad wing from the external magnetic field supports the above arguments. It is noted that the broad satellite signal may also contain a distribution of quadrupole interactions due to different local ν_Q and η for different Li ion sites. The broad wing disappears at around 250K because of motional narrowing in agreement with the correlation times inferred from the NSLR data.

The possibility that the extra NSLR contribution is due to paramagnetic impurities was ruled out by chemical analysis of the sample which shows less than 10 ppm of Fe, Co and Ni and less than 0.5 ppm of Mn and Cu. The possibility of the cross relaxation of ${}^7\text{Li}$ with ${}^{11}\text{B}$ was also ruled out as an explanation of the extra NSLR because it would give a sizable contribution only at frequencies lower than 4 MHz contrary to the experimental results.

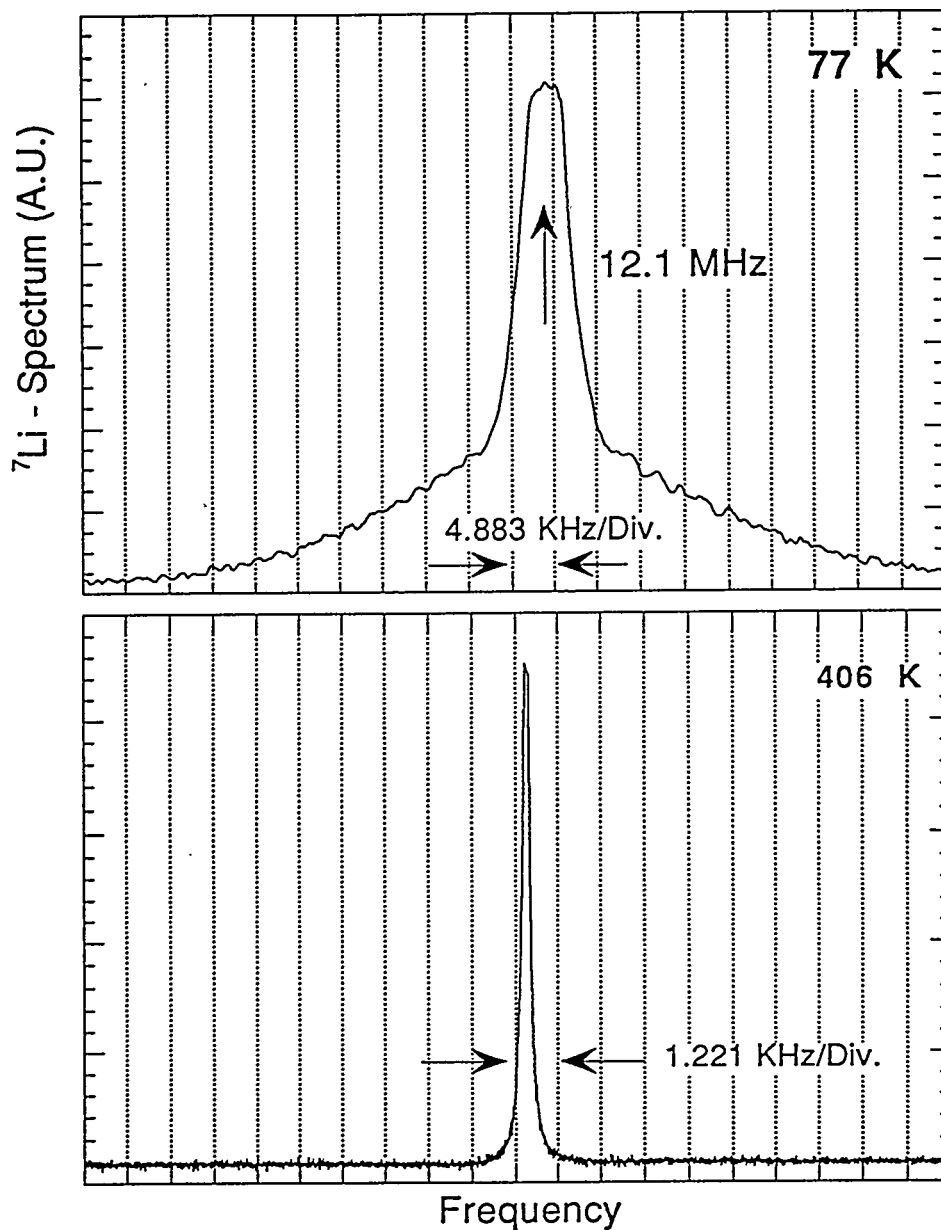


Fig. 4.25 ${}^7\text{Li}$ spectrum in $0.70\text{Li}_2\text{S} + 0.30\text{B}_2\text{S}_3$ at 406 K and 77 K. The spectrum shows motional line narrowing at ~ 250 K. The rigid lattice spectrum is composed of dipolar broaden central line and broad wing of 1st order quadrupolar splitted satellites with possible distribution of the quadrupole frequencies and asymmetry parameters.

4.2.4. Analysis of the Data with a Distribution of Activation Energies and the Percolation model

We notice that the structure (SRO) of thio borate has both of 3 - coordinated boron's (BS₃) especially for high alkali glasses, and 4 - coordinated boron's (BS₄) a situation which is noticeably different from the (thio)silicate and (thio) germanates. Therefore ⁷Li hopping motion may probe distinct distributions of activation energies.

One may assume that there are two different kind of couplings of the ⁷Li nucleus to the "lattice". One coupling which we will denote with the constant A in equation (4.2) which is modulated by the motion in the vicinity of the BS₃ trigonal groups and is characterized by the distribution of activation energies Z₁ NMR. A second coupling which we will denote by the Li ion motion in the vicinity of the BS₄ tetrahedral group and is characterized by a different distribution of activation energies Z₂ NMR:

$$R_1(\omega, \tau) = A^2 \int_0^\infty \left[\frac{\frac{\tau}{z}}{1 + \omega^2 \left(\frac{\tau}{z}\right)^2} + \frac{\frac{4\tau}{z}}{1 + 4\omega^2 \left(\frac{\tau}{z}\right)^2} \right] Z_{1,NMR} dEa + B^2 \int_0^\infty \left[\frac{\frac{\tau}{z}}{1 + \omega^2 \left(\frac{\tau}{z}\right)^2} + \frac{\frac{4\tau}{z}}{1 + 4\omega^2 \left(\frac{\tau}{z}\right)^2} \right] Z_{2,NMR} dEa \quad (4.7)$$

Alternatively one can interpret equation (4.7) as the average relaxation rate of two kind of ⁷Li nuclei which have the same coupling but is modulated by different dynamics. In this case one would observe a single relaxation rate in presence of common spin temperature or a non exponential decay of the nuclear magnetization in absence of a common spin temperature. In the case of two kind of ⁷Li nuclei relaxing with different rate, the coupling constants in equation (4.7) can be written as $A^2 = A_0^2 \times f$ and $B^2 = A_0^2 \times (1-f)$ where

A_0 is the coupling constant common to both kind of nuclei and f is the fraction of ${}^7\text{Li}$ nuclei relaxed by the correlation function corresponding to Z_1 NMR. The correlation time in the equation (4.7) is given as usually by:

$$\tau = \tau_0 \exp\left(-\frac{E_a}{k_B T}\right) \quad (4.8)$$

where k_B is the Boltzman constant and T is expressed in Kelvin. Then the total rate on the ionic hopping is z times the f_{osc} of equation (3.23), where z is assumed to be 6 for the simple harmonic oscillator's in a one dimensional sinusoidal potential barrier of amplitude E_a and spacial period d as was explained in section 2.3.2.

As was mentioned in the previous section, the site distance d should not change much (therefore in the range of $2\text{Å} \sim 6\text{Å}$) to affect appreciably the calculation of the NSLR. Here we used $d = 3.7\text{Å}$ to be the site distance, which is estimated from the crystal structure of the di thio borate [138].

The results of the fit of the NSLR are shown in the Fig. 4.26 and 4.27 for $x = 0.65$ and $x = 0.70$. Each Gaussian Z_1 NMR and Z_2 NMR are shown in Fig. 4.28 for $x = 0.7$ with MHz data. By using the parameters from the fitting, the distribution of the activation energies are plotted for $x = 0.65$ and 0.70 in the Fig. 4.29 together with the ones for lithium thio germante. The Fig. 4.30 shows comparison of the distribution of activation energies obtained from the fit of the NMR data in different samples. The values of the average E_m correlates very well with the activation energies obtained from the dc conductivity. We calculate now the dc conductivity from our simple hopping model (see section 3.3.2) and by using the distribution of barriers in Fig. 4.29:

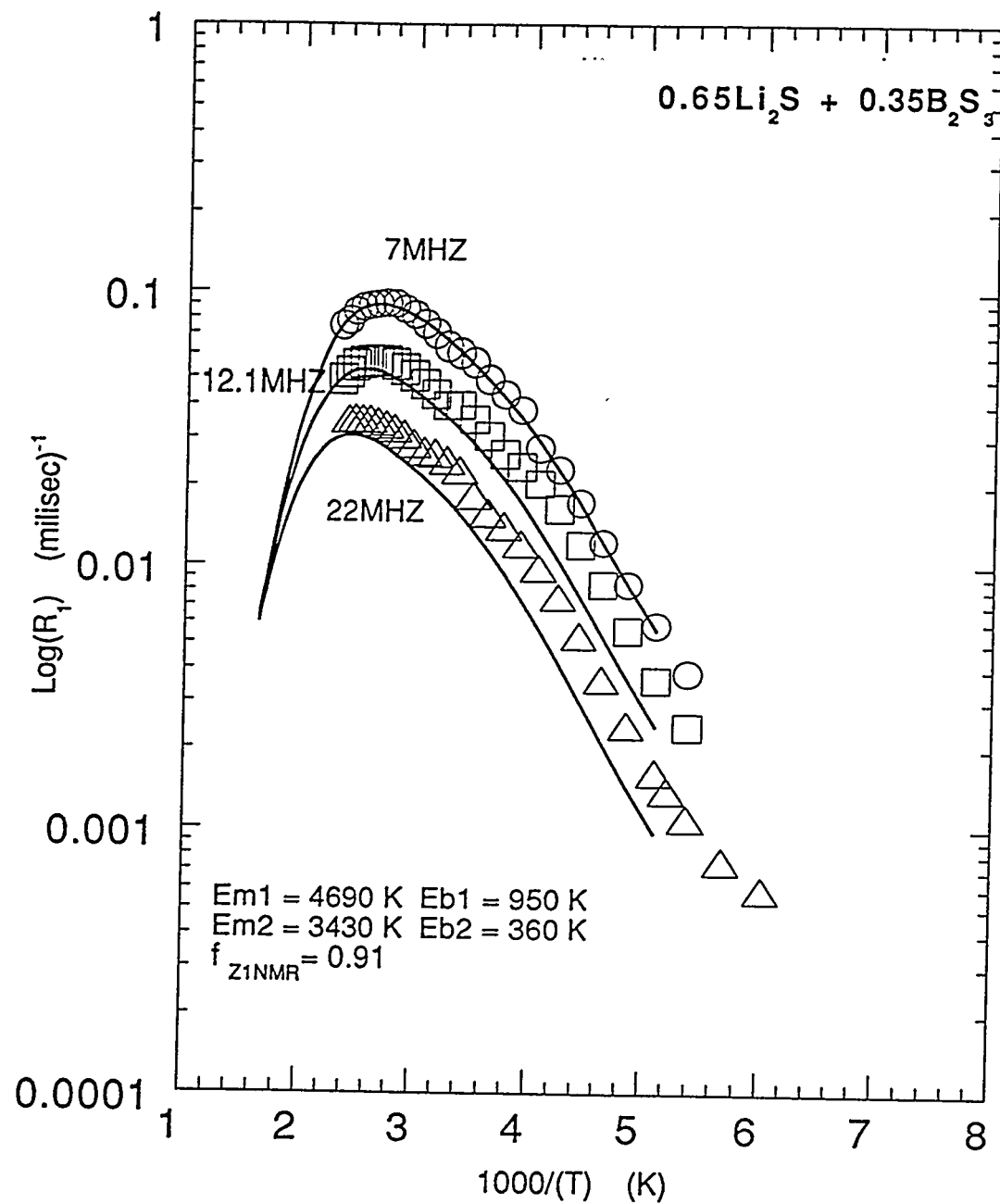


Fig. 4.26 ^7Li spin lattice relaxation rate in $0.65\text{Li}_2\text{S} + 0.35\text{B}_2\text{S}_3$. The solid line represent theoretical fit of equation (4.7) with the parameters shown inside graph. The fitting shows that $f_{z1\text{NMR}} = 0.91$ (see equation 4.7)

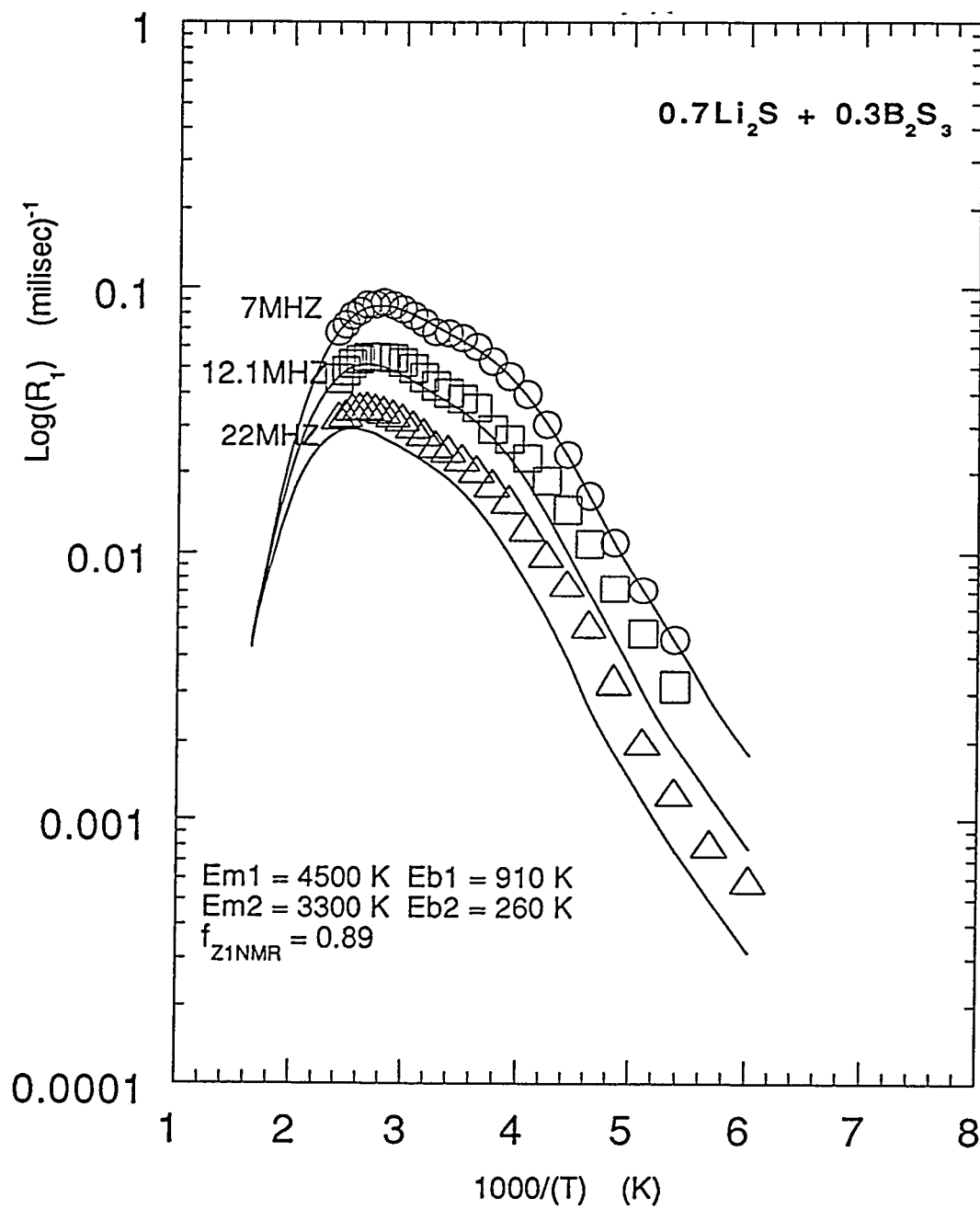


Fig. 4.27 ^7Li spin lattice relaxation rate in $0.70\text{Li}_2\text{S} + 0.30\text{B}_2\text{S}_3$. The solid line represent theoretical fit of equation (4.7) with the parameters shown inside graph. The fitting shows that $f_{z1\text{NMR}} = 0.91$ (see equation 4.7)

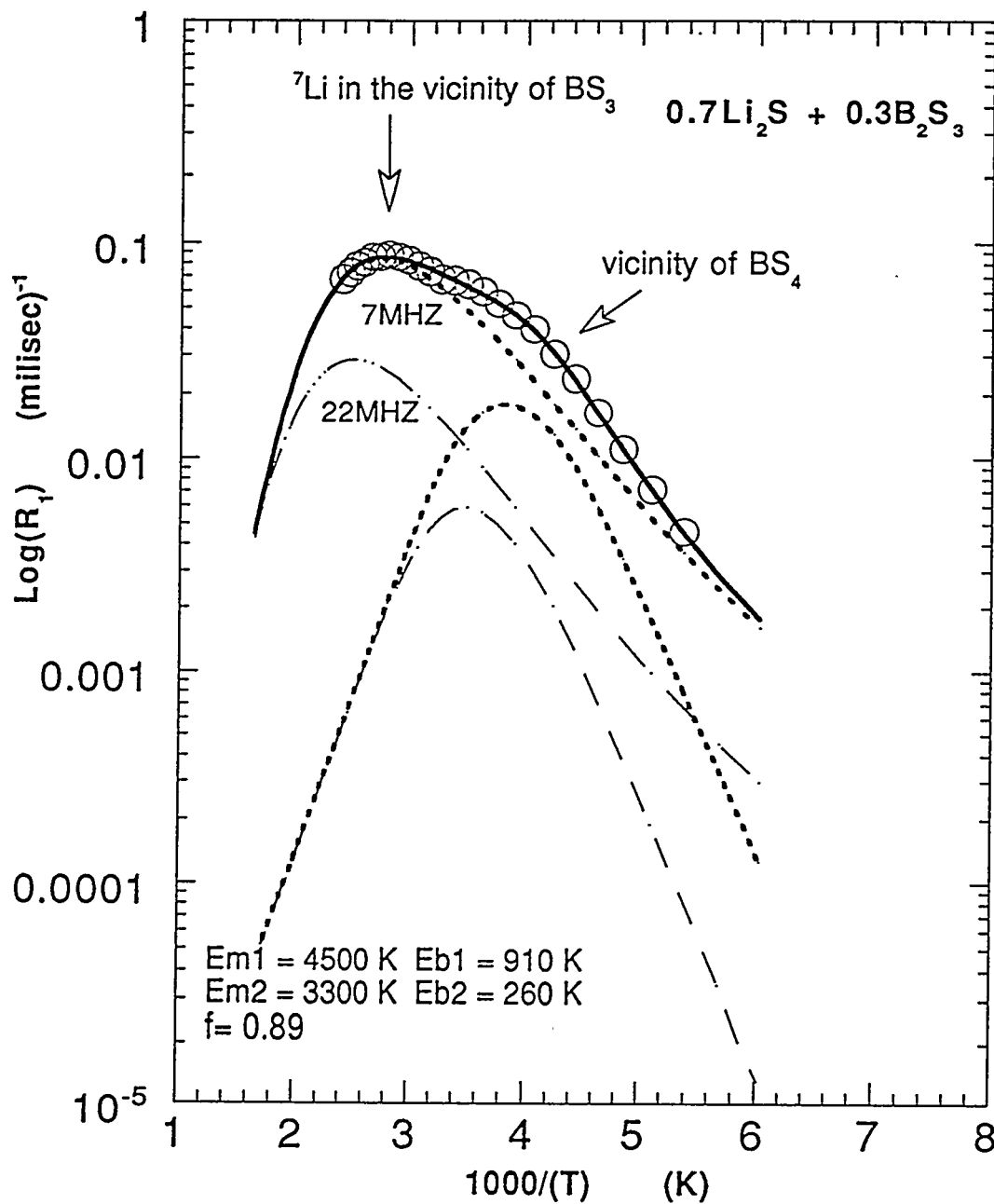


Fig. 4.28 Fitting curves of Fig. 4.27 (solid line) are decomposed into two contributions of NSLR due to each Gaussian distributions of activation energies, for 7 Mhz (thick broken line) and 22 Mhz (thin broken line) data. The main NSLR is assigned to be due to ${}^7\text{Li}$ motion in the vicinity of BS_3 groups.

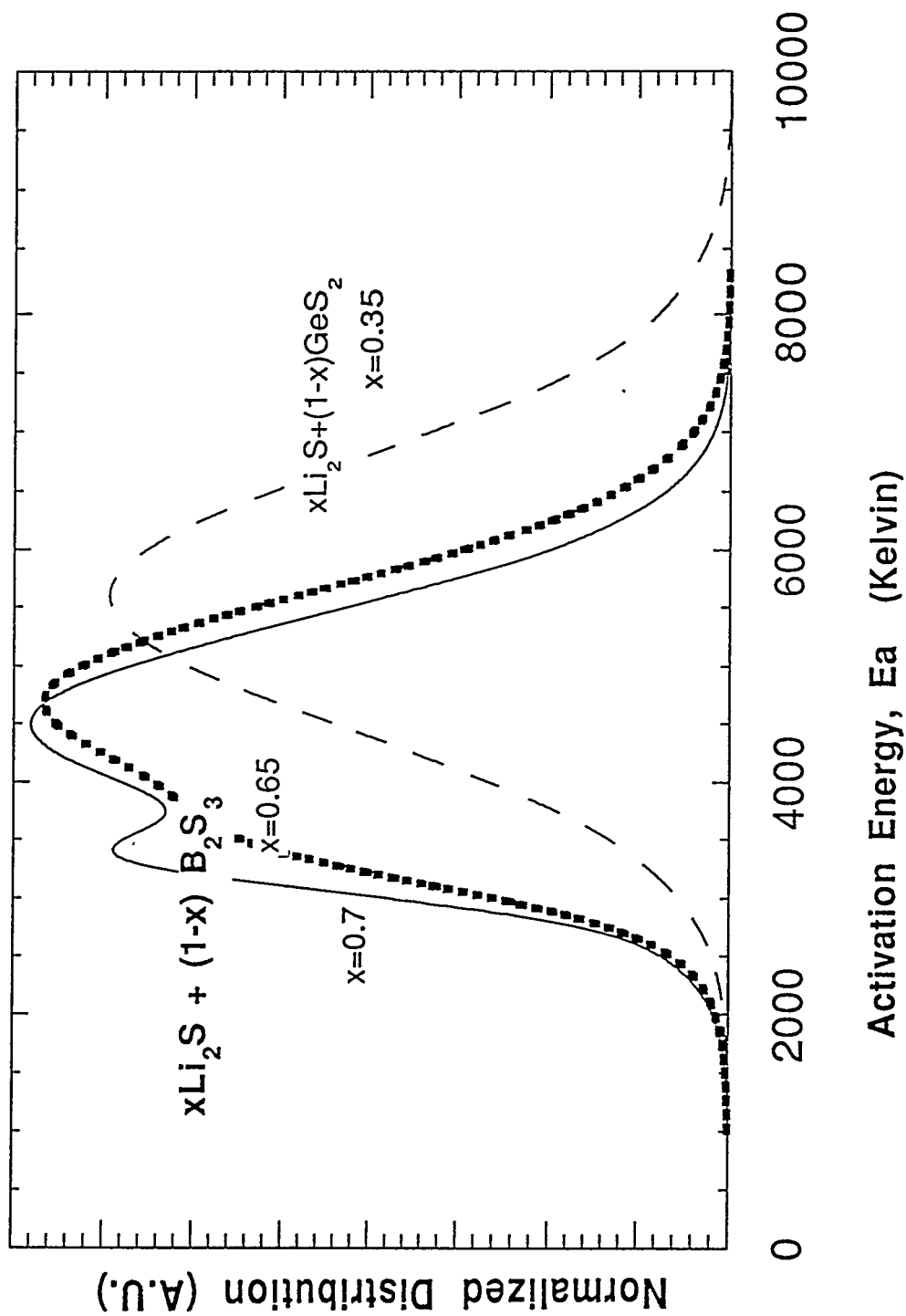


Fig. 4.29 Distribution of activation energies in the motion of Li^+ in $x\text{Li}_2\text{S} + (1-x)\text{B}_2\text{S}_3$. ($x=0.65$ and 0.70) derived from NMR relaxation is compared to $0.35\text{Li}_2\text{S} + 0.65\text{GeS}_2$.

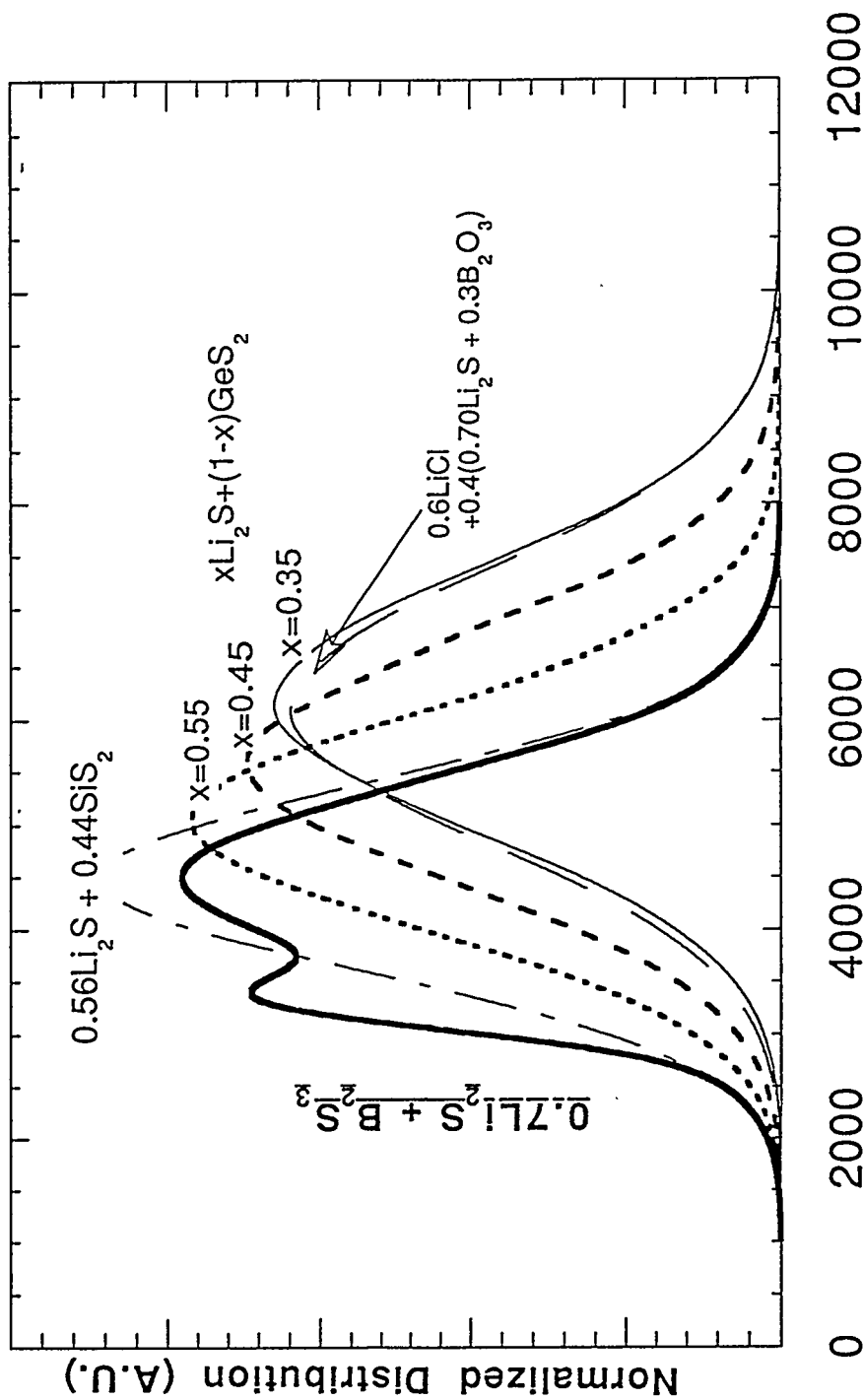


Fig. 4.30 . Distribution of activation energies in the motion of Li⁺ in xLi₂S + (1-x)B₂S₃.

(x=0.65 and 0.70) derived from NMR relaxation is compared to xLi₂S + (1-x)GeS₂,

0.56Li₂S + 0.44SiS₂ [54,56] and 0.6LiCl + 0.4(0.7Li₂O + 0.3B₂O₃) [55,57].

$$\sigma_{dc} = \frac{nPe^2d^2}{zk_B T \langle \tau \rangle} \quad (4.9)$$

here n is the concentration of the ionic charge carriers, $e = 1.6 \times 10^{-19}$ coulomb, $\langle \tau \rangle$ is the average correlation time by the Gaussian distribution up to the percolation threshold E_c .

$$\langle \tau \rangle = \left(\frac{1}{P} \right) \int_0^{E_c} \tau_0 \exp\left(-\frac{E_a}{k_B T} \right) \cdot Z_{NMR} dE_a \quad (4.10)$$

$$P = \int_0^{E_c} E_a \cdot Z_{NMR} dE_a$$

where P is the percolation fraction. As was done in the thio germanate, the parameter P is obtained from the fit. The fitted dc conductivity are plotted in Fig. 4.31 for $x = 0.70$ and shows again very good agreement.

4.2.5 Measurements of ^{11}B NSLR

The analysis of the ^7Li NSLR in terms of two “relaxation channels” suggests that one of the channel may be the hopping motion in the vicinity of the BS_3 groups and the other is due to Li nuclei moving in the vicinity of the BS_4 groups. From the analysis in terms of a double Gaussian distribution function one finds that the fraction of nuclei in the two relaxation channels is 90% and 10% respectively, which corresponds indeed to the relative fraction of BS_3 and BS_4 groups respectively as determined from ^{11}B NMR (see Fig 4.32). Furthermore this hypothesis agrees with the argument based on chemical bonding strength between Li - ion and non bridging sulfur in BS_3 and BS_4 structural units. The one extra sulfur bond to the boron (balance 3) in BS_4 results

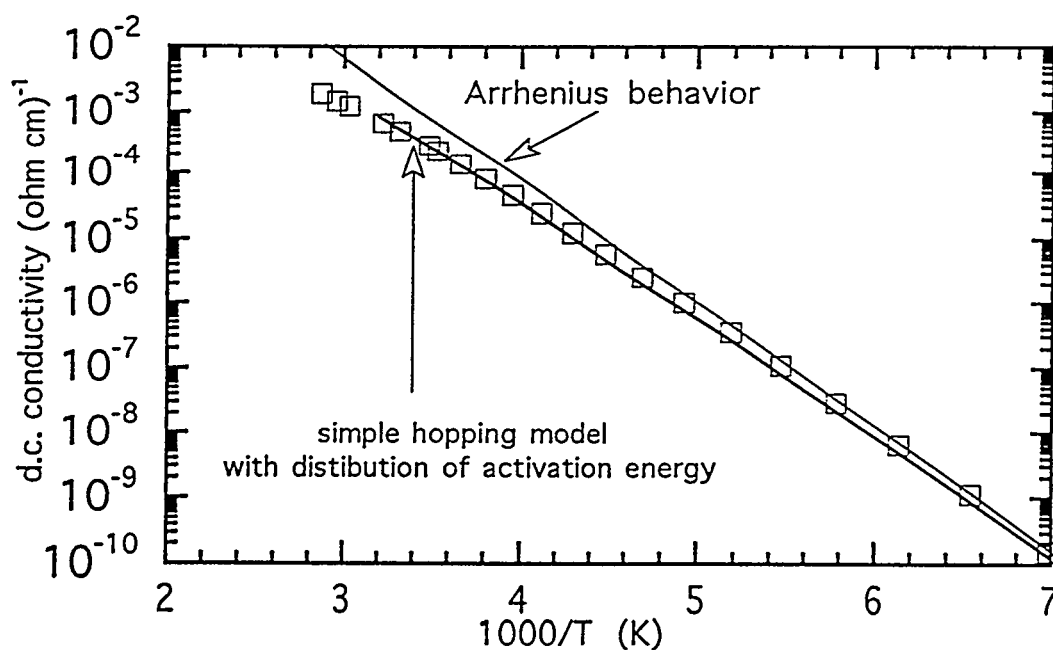
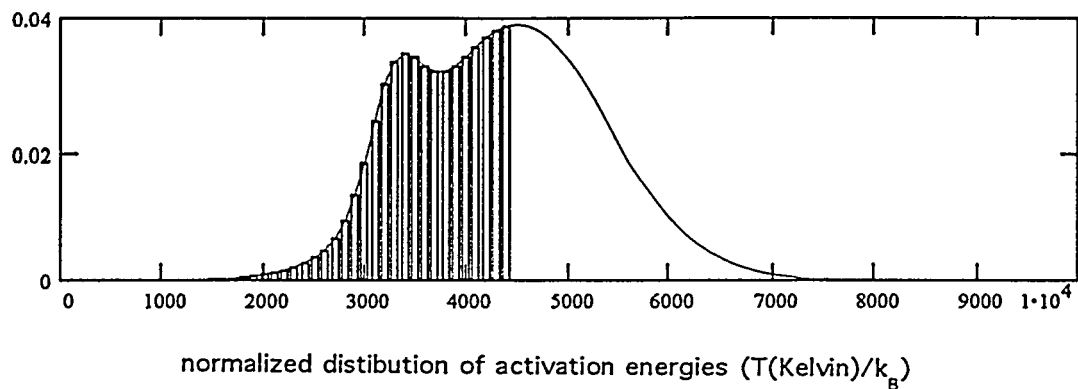


Fig. 4.31 Double - Gaussian distribution, Z_{NMR} , obtained from the fit of NSLR in Fig. 4.29 and 4.30. $E_{m1} = 4500$ K, width $E_{b1} = 910$ K, $E_{m2} = 3300$ K width $E_{b2} = 260$ K (Top graph), in $0.70\text{Li}_2\text{S} + 0.30\text{B}_2\text{S}_3$. Truncation at $E_c = 4400$ K gives the d.c. conductivity from the striped fraction $p = 0.54$ which is shown in the second graph (curve), as a function of inverse temperature, T . The squares represents experimental data.

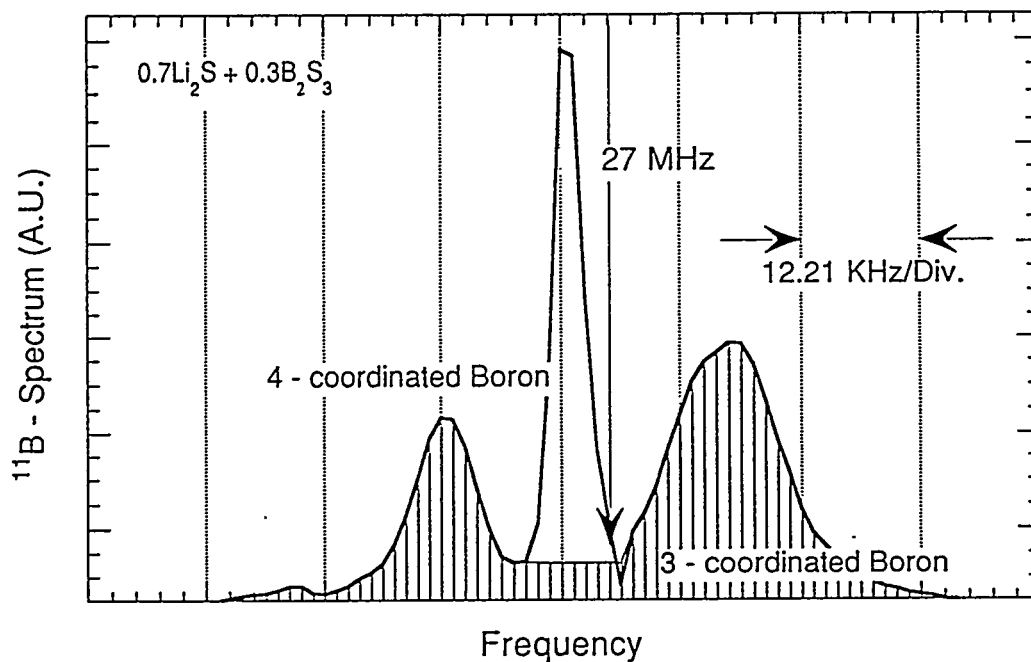


Fig. 4.32 ^{11}B powder spectrum at 27 MHz taken at room temperature in $0.70\text{Li}_2\text{S} + 0.30\text{B}_2\text{S}_3$. 3 - and 4 - coordinated Borons experiences $\nu_Q \sim 700$ and 200 kHz [119,120] respectively. 3 - coordinated Borons results in the 2nd order quadrupole split central transition in hatched area of spectrum thus represents 3 - coordinated boron fraction. The fraction of the 3 - coordinated Borons determined from the hatched area of the spectrum is about 90%.

in weaker bonding to Li - ion, thus corresponding to the lower activation energy. The result also agrees with the observed IR absorption line at 400 cm^{-1} and 450 cm^{-1} which were claimed to be the vibrational mode due to Li - ion motion in the potential well due to the non bridging sulfur sites in BS_4 units and BS_3 units respectively [195].

The circumstances listed above suggest an elegant and direct way to check the validity of our assumption. In fact as seen from Fig. 4.32 the ^{11}B NMR from the two SRO groups BS_3 and BS_4 are separated sufficiently in frequency that the NSLR can be measured separately in the two ^{11}B sites.

The measured NSLR of ^{11}B is shown in Fig. 4.33, where one can see clear dependence on external magnetic field and the existence of the motional maximum. The relaxation rate in Fig. 4.33 is only indicative since it represents a mixture of the relaxation of the two ^{11}B sites.

The next step is to make a separate measurements of ^{11}B - NSLR for each structural group. The measurements could be accomplished by using a narrow window in frequency domain to irradiate only the central line (corresponding to the BS_4 groups) or only one of the 2nd order quadrupolar split central line singularities (corresponding to the BS_3 groups) in the spectrum shown in Fig. 4.32. The experimental conditions were carefully set so that $H_1 > H_d$, where H_1 is rf field strength and H_d is dipolar field among nuclei.

The NSLR of ^{11}B for each structural group is shown in Fig. 4.34. One can see clearly two distinct relaxation maxima centered at different temperatures for the two ^{11}B sites corresponding to the BS_3 and BS_4 groups respectively. Due to extremely poor signal to noise ratio, we have concentrated the effort to measure the NSLR around the two maxima and their relative magnitude and position while the investigation over the whole temperature range was not performed. Contrary to what one might expect at first, the

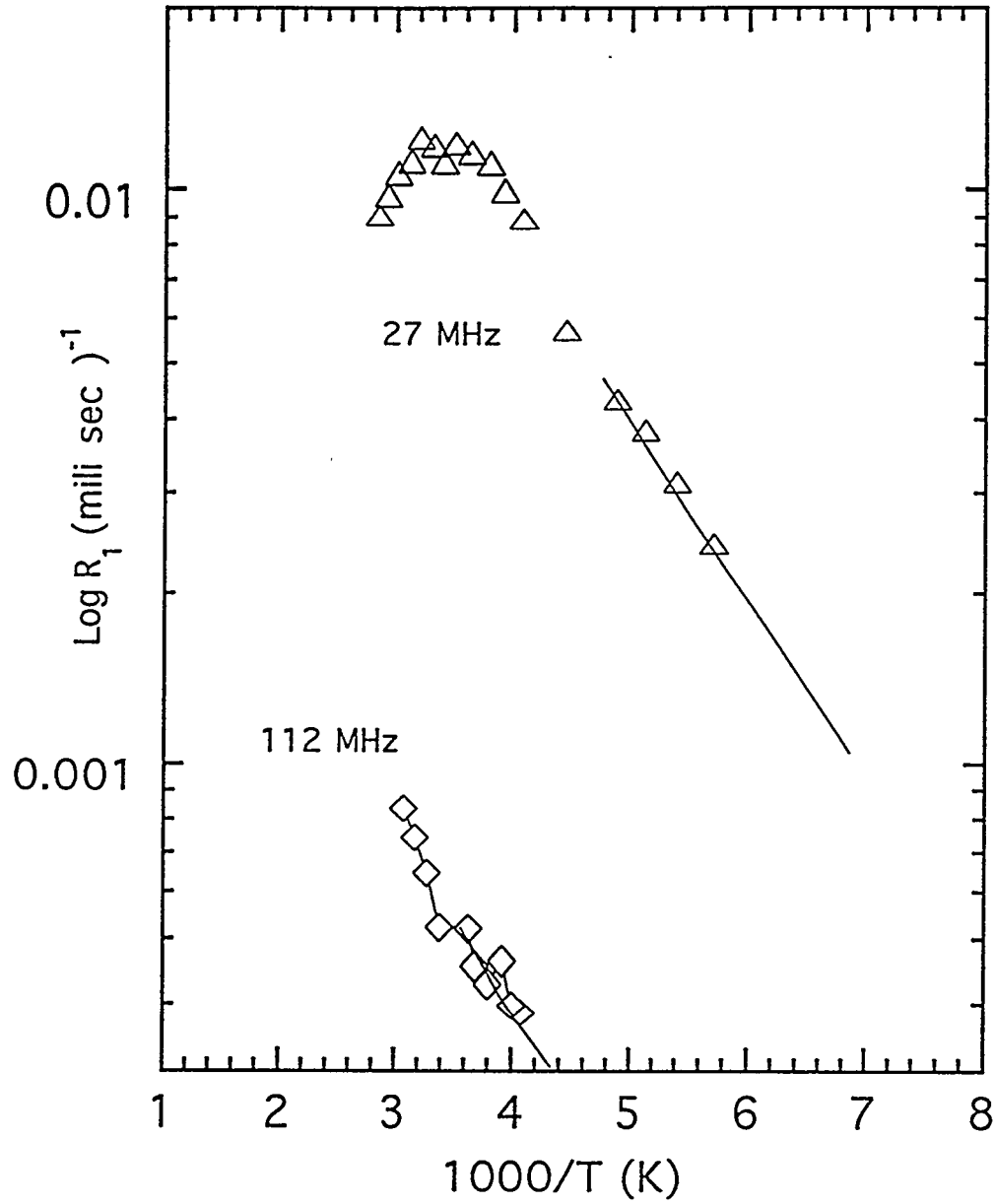


Fig. 4.33 ^{11}B NSLR in $0.70\text{Li}_2\text{S} + 0.30\text{B}_2\text{S}_3$ at 27 MHz and 112 MHz vs. reciprocal temperature; shows motional maximum and clear frequency dependence as described in section 2.2.4.

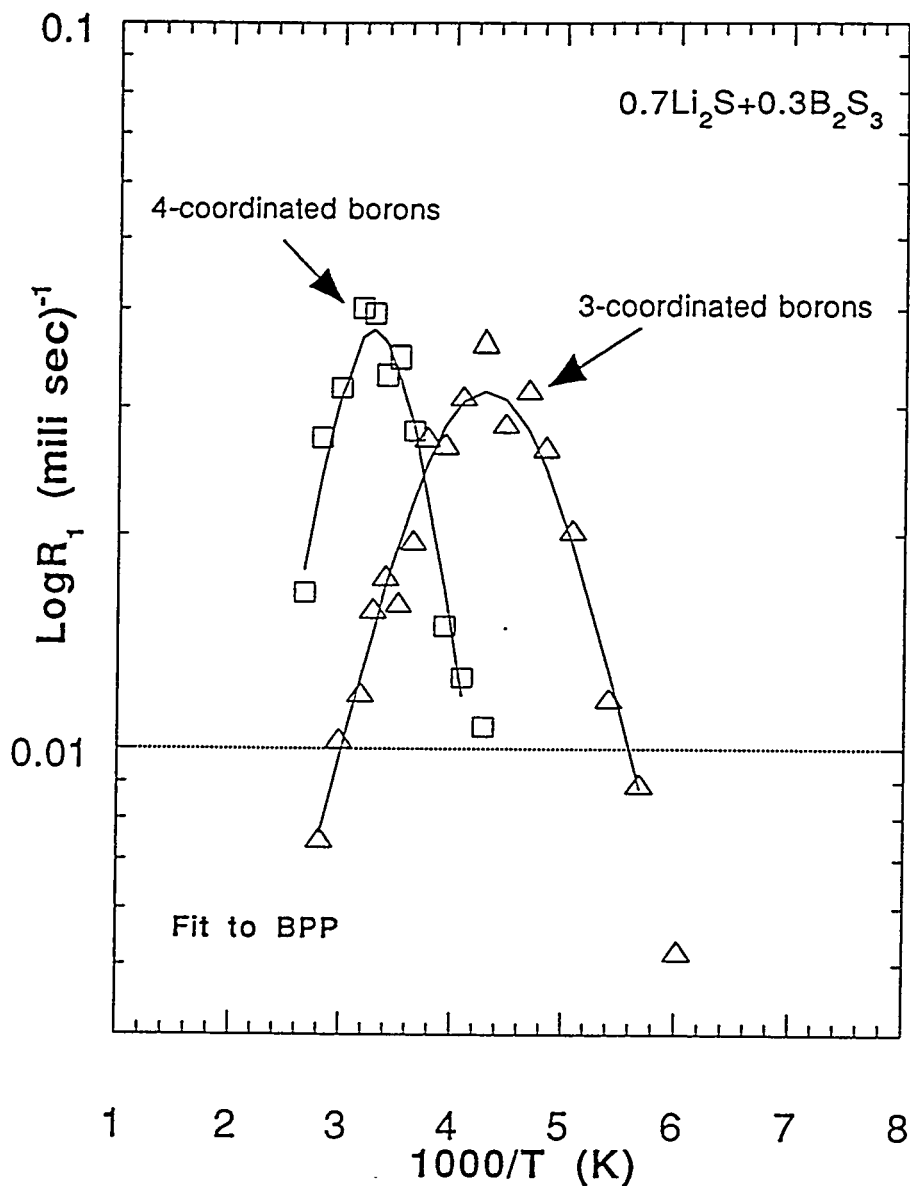


Fig. 4.34 ^{11}B NSLR in $0.70\text{Li}_2\text{S} + 0.30\text{B}_2\text{S}_3$ at 22 MHz vs. reciprocal temperature; shows two distinguishable motional maxima each corresponding to 4 - and 3 - coordinated Borons in the same sample. The assignment of each NSLR to the BS_3 and BS_4 group respectively is made possible by irradiation of different regions of the ^{11}B NMR spectrum (see Fig. 4.32). Table 4.3 Parameters from the fit of equation (4.11) to the ^{11}B NSLR data relaxation of ^{11}B is not directly driven by the interaction with the Li hopping ion. This

can be seen from the comparison of the position of the NSLR maximum for ^7Li and ^{11}B . The maximum of NSLR for ^{11}B in BS_4 occurs at higher temperature (see Fig. 4.34). Instead, the maximum of ^7Li NSLR associated with the motion in the vicinity of the BS_4 group occurs at lower temperature (see Fig. 4.28). In fact if the relaxation of both ^7Li and ^{11}B nuclei were due to the same dynamics (i.e., Li ion hopping), one should have the maxima in the same temperature range for the same Larmor frequency since at the maximum of the NSLR one has $\omega_L \tau = 1$ independent of the nucleus and/or of the coupling parameters. Furthermore the ^{11}B NSLR maxima can be fitted with a simple BPP expression:

$$\frac{1}{T_1} = c \left[\frac{\tau}{1 + \omega_L^2 \tau^2} + \frac{4\tau}{1 + 4\omega_L^2 \tau^2} \right] \quad (4.11)$$

with a single activation energy for τ . The parameters of the fit are given in the Table 4.3. It can be seen that the activation energy obtained from ^{11}B relaxation and the prefactor τ_0 are completely different than the average one obtained from ^7Li relaxation (see Table 4.3) besides being a single activation energy and not a distribution. It is interesting to point out that the values of the relaxation parameters obtained for ^{11}B NSLR in our sample are very similar to the one obtained for silver borates (see Table 4.3).

Thus we conclude that the ^{11}B NSLR must be driven by a local and thermally activated motion over a small barrier which can be microscopically envisioned as a structural reorientation of the $\text{BS}_4(\text{BS}_3)$ group following the interaction with hopping Li ion. The above qualitative picture supports the diffusion controlled model of Elliot [171] and the jump relaxation model of Funke [172].

Table 4.3 Parameters from the fit of equation (4.11) to the ^{11}B NSLR data (see Fig. 4.34) are compared to the result of A. Avogadro et al [164] for silver borate glass which is composed mainly of BS_4 units.

	^{11}B in BS_4 units	^{11}B in BS_3 units	$(\text{AgI})_{0.5}(\text{Ag}_2\text{O}\cdot 2\text{B}_2\text{O}_3)_{0.5}$ [164]
c (rad/sec) 2	3.6×10^9	3.1×10^9	1.5×10^9
τ_0 (sec)	1.8×10^{-12}	7.7×10^{-12}	2.0×10^{-12}
E_a (Kelvin)	2390	1490	2500

It is noted that for some temperatures the recovery of the ^7Li nuclear magnetization shows a departure from a single exponential recovery (see Fig. 4.23). This is probably due to a break down of the common spin temperature assumption whereby the ^7Li nuclei in the two "relaxation channels" relax independently.

CHAPTER V. CONCLUSIONS

The microscopic ion - dynamics in glassy fast ionic conductors, especially sulfide glasses has been investigated by both NMR techniques and IS (Impedance Spectroscopy) techniques below the glass transition temperature range , T_g . For lithium thio germanate glasses, the data were analyzed in terms of two schemes: i) a stretched exponential correlation function (KWW) and ii) a distribution of activation energies.

The approach by the phenomenological stretched exponential correlation function describes well the NMR data and from the fit one can derive reasonable values for parameters such as the correlation time, the effective activation energy and the β - exponent of the stretched exponential correlation function. The problem with the KWW - scheme is that it is not clear what the microscopic meaning of the parameters is. The coupling model ascribes a microscopic meaning for the parameters whereby $(\beta \cdot E_a^*)_{\text{NMR}}$ $(\beta \cdot E_a^*)$ conductivity is claimed to be the true microscopic single particle activation energy and the stretched exponential is explained as due to the time dependence of the single particle hopping rate. It is shown in the present work that while the first prediction is approximately borne out in the experiments, the second one is not.

Furthermore the KWW approach predicts a single Arrhenius behavior for the dc conductivity while it is shown that a small but detectable deviation from Arrhenius behavior can be observed in some glasses. The scheme based on a distribution of activation energies fits very well the NMR data. The value of the dc conductivity and its temperature dependence can be reproduced remarkably well by a simple hopping model with percolation factor which is obtained from the fit of the data and it represent an important parameters

for the characterization of the FIC. Furthermore the deviation from Arrhenius behavior is a natural consequence of the presence of a distribution of barriers.

Thus we conclude that the simple model of distribution of barriers which includes mostly disorder effects is best suited to describe the NMR and conductivity. Within the framework of this model one can interpret the difference in correlation times observed by the two techniques whereby the shorter time observed in the conductivity is due to the percolation of ions around the higher barriers.

By using a double Gaussian distribution of barriers we could interpret satisfactorily the anomalous NSLR of ^7Li in lithium thio borate glasses, and related it to the ^{11}B NSLR can be microscopically envisioned as a structural reorientation of the BS_4 (BS_3) group following the interaction with hopping Li ion in the same sample. It is concluded that the two different distributions correspond to the different structural environment around the two major structural groups i.e., BS_3 and BS_4 . Although the NSLR of the immobile ion is not a direct consequence of the mobile ion motion, it is shown that the NSLR of immobile ions are indirectly related to the mobile ion motion. It can be microscopically envisioned as a structural reorientation of the BS_4 (BS_3) group following the interaction with hopping Li ion. Therefore one should consider structure (SRO) carefully when one study the NSLR of immobile ion and correlate it to the NSLR of the mobile ion.

Therefore the effect of disorder on the motion of mobile ions in glassy fast ionic conductors have been modeled by the distribution of activation energy which indeed explain both the microscopic and macroscopic observations.

REFERENCES

1. H.L. Tuller and M. Balkanski, "Science and Technology of Fast Ion Conductors", NATO ASI series B: Physics, Vol.199, Plenum Press, NewYork (1989)
2. I. Riess, "Materials Systems in Science and Technology of Fast Ion Conductors", NATO ASI series B: Physics, Vol.199, Plenum Press, NewYork (1989) 23
3. A.K. Jonsher, Nature Vol.267, No.23, June (1977) 673
4. K.L. Ngai, A.K. Jonsher, C.T. White, Nature Vol.277, No.23 (1979) 185
5. P. Maass, J Peterson, A. Bunde, W. Dieterich and H.E. Roman, Phys. Rev. Lett. Vol.66, No.1 (1991) 52
6. M. Meyer, P. Maass, and A. Bunde, Phys. Rev. Lett. Vol.71, No.4 (1993) 573
7. C. Julien, "Glass Solid Electrolyte thin films Science and Technology of Fast Ion Conductors", NATO ASI series B: Physics, Vol.199, Plenum Press, NewYork (1989) 335
8. H.L. Tuller, "Some future Trends in Solid State Ionics Science and Technology of Fast Ion Conductors", NATO ASI series B: Physics, Vol.199, Plenum Press, NewYork (1989) 303
9. S. Chandra, "Super ionic Solids principle and applications", North Holland Publishing Co. NewYork (1981)
10. G. Stix, "Scientific American", Oct. (1993) 109
11. H.F. Taylor, J. Soc. Glass Technology, Vol.41 (1957) 382
12. H. Tuller and M. Barsoum, J. Non-Cryst.Solids, Vol.73 (1985) 331
13. K. Otto, Phys. Chem. Glasses, Vol.7 (1966) 29

14. J.H. Kennedy et al., *J. Non-Cryst. Solids*, Vol.123 (1990) 328
15. N.F Mott and E.A. Davis, "Electronic Process in Non crystalline Materials", 2nd ed. Clarendon, Oxford (1979)
16. Sir N. Mott, "Conduction in Non-Crystalline Materials", Oxford Science Publications, Oxford (1987)
17. N.F. Uvarov and E.F. Hairetdinov, *J. of Solid State Chemistry*, Vol.62 (1986) 1
18. C.A. Angell, *Solid State Ionics*, Vol.18 (1986) 72
19. M.D. Ingram, *Phys. and Chem. of Glasses*, Vol.28, No.6 (1987)
20. A. Pradel and M. Ribes, "Materials Science and Engineering", Vol.133 (1989) 45
21. L.P. Boesh and C.T. Moynihan, *J. of Non-Cryst Solids*, Vol.17 (1975) 44
22. S.W. Martin, *Materials Chemistry and Physics*, Vol.23 (1989) 225
23. H.E. Taylor, *J. Soc. Glass Technology*, Vol.41, (1957) 350
24. J.C. Dyre, *J. Appl. Phys.*, Vol.64(5), No.1 (1988) 2456
25. M. Pollak and T.H. Geballe, *Phys. Rev.* Vol.122. (1961) 1742
26. S. Brawer, "Relaxation in Viscous Liquid and Glasses", The American Ceramic Society Inc., Columbus, Ohio (1985)
27. J. Zarzycki, "Glasses and the vitreous State", Cambridge Univ. Press, Cambridge (1982)
28. E. Helfand, *J. Chem. Phys.*, Vol.78(4), No.15 (1983) 1931
29. G.Williams and P.J. Hains, *Faraday Symp. Chem. Soc.*, Vol.6 (1972)14
30. A.K. Rajugopal and K.L. Ngai, "Models of Temporal stretched Exponential Relaxation in Condensed Matter System" in "Relaxation in complex systems", edited by K.L. Ngai and G.B. Wright, Office of Naval Research, Arlington, VA. 22217 (1981)
31. R. Kohlausch, *Progg. Ann. Phys.*, Vol.92 (1854) 56

32. G. Williams and D.C. Watts, *Trans. Faraday Soc.* Vol.66 (1970) 80
34. C.T. Moynihan, L.P. Boesch and N.L. Laberge, *Physics and Chem. of Glasses*, Vol.14, No.6 (1973) 122
35. E.L. Pollock and B.J. Adler, *Phys. Rev. Lett.*, Vol.46, No.14 (1981) 950
36. C.T. Moynihan, L.P. Boesch and N.L. Laberge, *Phys. and Chem of Glasses*, Vol.14, No.6 (1973) 122
37. V. Provenzano, L.P. Boesch, V. Volterra, C.T. Moynihan and P.B. Macedo, *J. of The American Ceramic Soc.*, Vol.55, No.10 (1972) 492
38. P.B. Macedo, C.T. Moynihan and R. Bose, *Phys. and chem. of Glasses*, Vol.13, No.6, (1972) 171
39. T.J. Higgins, P.B. Macedo, and V. Volterra, *J. of The American Ceramic Soc.*, Vol.55, No.10 (1970) 488
40. C.T. Moynihan, N. Balitactac, L.Boone, and T.A.Litoritz, *The J. of Chemical Phys.*, Vol.55, No.6 (1971) 3013
41. J.M. Stevels, "Encyclopedia of Physics", Vol.xx Edited by S. Flugge, Springer Verlag, Berlin (1957) 372
42. J.O. Isard, "Study of Migration loss in Glass and Generalization Method of Calculating the Rise of Dielectric loss with temperature", *Proc. Inst. Elec Eng.*, Part B, Suppl., 22 (1962) 440
43. A.K. Rajagopal and K.L. Ngai, "Models of Temporal stretched Exponential in Relaxation" in "Condensed Matter System in Relaxation in complex systems", edited by K.L.Ngai and G.B.Wright, Office of Naval Research, Arlington, VA. 22217 (1981)
44. S.R. Elliot, *J. Non-Cryst. Solids*, Vol.170 (1944) 97
45. J.C. Dyre, *J. Non-Cryst. Solids*, Vol.135 (1991) 219

46. H.K. Patel, Ph.D. Thesis, Iowa State University, Ames (1993) Chapter 7.
47. L. Börjesson, L.M. Torell, S.W. Martin, C. Liu and C.A. Angell, Phys Lett. A., Vol.125, No.6&7 (1987) 330
48. J.O. Isard, J. Non-Cryst. Solids, Vol.4 (1970) 357
49. H. Namikawa, J. Non-Cryst. Solids, Vol.18 (1975) 173
50. U. Storm, "Elementary Excitations in Glass in Relaxation in Condensed Matter System", in "Relaxation in complex systems", edited by K.L.Ngai and G.B. Wright, Office of Naval Research, Arlington, VA. 22217 (1981)
51. K.L. Ngai, Comments Solid State Phys, Vol.9, No.5 (1980) 141
52. K.L. Ngai, Comments Solid State Phys, Vol.9, No.4 (1979) 127
53. R.W. Douglas, J. Non-Cryst. Solids, Vol.14 (1974) 1
54. F. Borsa, D.R. Torgeson, and S.W. Martin, H.K. Patel, Phys. Rev. B, Vol.46 (1992) 795
55. M. Trunell, D.R. Torgeson, S.W. Martin and F. Borsa, J. Non-Cryst. Solids, (1991) 257
56. I. Svare, F. Borsa, D.R. Torgeson, S.W. Martin, Phys. Rev. B Vol.48. (1993) 9336
57. I. Svare, F. Borsa, D.R. Torgeson, S.W. Martin, J. Non-Cryst. Solids, Vol.172 (1994) 1300
58. Discussion Session, J. Non-Cryst. Solids (1991) 131
59. S. Brawer "Relaxation in Viscous Liquid and Glass", The American Ceramics Society, Inc., Columbus, Ohio (1985)
60. F.S. Howell, R.A. Bose, P.B. Macedo, and C.T. Moynihan, J. Phys. Chem., Vol. 78, No.6 (1974) 639
61. D. Button, Ph.D. thesis, M.I.T., Cambridge (1988)

62. K.L. Ngai, *Solid State Ionics*, Vol.5 (1981) 27
63. K.L. Ngai and U. Storm, *Phys. Rev. B*, Vol.38 (1988) 10350
64. V. Ambegaolcar and B.I. Halperin and J.S. Langer, *Phys. Rev. B*, Vol.4, No.8 (1971) 2612
65. N.F. Mott, *J. Non-Cryst. Solids*, Vol.8 (1972) 1-8
66. H. Selbach and O.Kanert, D.Wolf, *Phys. Rev. B*, Vol.19, No.9 (1979) 4435
67. E.B. Ivkin and B.T Kolomiets, *Izv. Akad. Nank SSSR, Ser. Fiz.*28 (1964) 1288
68. R.M. Hill and A.K. Jonsher, *J. Non-Cryst. Solids*, Vol.32 (1979) 53
69. A.R. Long and N. Balkan, *J. Non-Cryst. Solids*, Vol.35 (1980) 415
70. L. Murawski, *J. Non-Cryst. Solids*, Vol.90 (1987) 629
71. M.F. Manning, *Rev. Modern. Phys.*, Vol.12 (1940) 215
72. S.H. Glarum, *J.Chem.Phys.*, Vol.33, No.5 (1960) 1371
73. R.H. Cole, *J. Chem. Phys.*, Vol.42, No.2 (1965) 637
74. B.U. Felderhof, *Physica*, Vol.101A (1980),275
75. K.L. Ngai and C.T. White, *Phys. Rev. B*, Vol.20, No.6 (1979) 2475
76. E.L. Police and B.J. Alder, *Phys. Rev. Lett.*, Vol.46, No.14 (1981) 950
78. G.P. Johari and K. Pathmanathan, *J. Phys. Chem. of Glasses*, Vol.29, No.6 (1988) 219
79. W. Dieterich, *Solid State Ionics*, Vol.40 (1990) 509
80. B. Bogchi and A. Chandra, *Phys. Rev. Lett.*, Vol.64, No.4 (1990) 455
81. W. Beier and G.H. Frischat, *J. Non-Cryst. Solids*, Vol.73 (1985) 113
82. I. Heinemann and G.H. Frischat, *J. Phys. chem.*, Vol.34, No.6 (1993) 255
83. E. Göbel, W. Müller-Warmuth, H.Olyschläger and H.Dutz, *J. Magn. Res.*, Vol.36 (1979) 371
82. I. Heinemann and G.H Frischat, *J. Phys. Chem.*, Vol.34, No.6 (1993) 255

84. T. Atake and C.A. Angell, *J. Non-Cryst. Solids*, Vol.38 (1980) 439
85. G. Carini, M. Cutroni, M. Federico, G. Galli and G. Tripodo, *Phys. Rev. B*, Vol.30 (1984) 7219
86. D.P. Almond and A.R. West, *J. Non-Cryst. Solid*, Vol.88 (1986) 222
87. C. Liu and C.A. Angell, *J. Chem. Phys.*, Vol. 93, No.10 (1990) 15
88. A. Burns, H.P. Brack and W.M. Risen Jr., *J. Non-Cryst. Solids* , Vol.131 (1991) 994
89. J.P. Cho, S.W. Martin, *J. Non-Cryst Solids*, Vol.170 (1994) 182
90. L. Börjessen and L.M. Torell, *Solid State Ionics*, Vol.25 (1987) 85
91. L.M. Torell and S. Schantz, *J. Non-Cryst. Solids*, Vol.131(1991) 981
92. C.A. Angell and S.W. Martin, *Solid State Ionics*, MRS Symposia Proceedings No.135, Materials Research Society, Pittsburgh (edited by G. Nazri, R.A. Huggins, and D.F. Shriver) (1989) 73
93. W.K. Lee, J.F. Lin and A.S. Nowick, *Phys. Rev. Lett.*, Vol.67, No.12 (1991) 1559
94. N. Bloembergen, E.M. Purcell, and R.V. Pound, *Physical Rev.*, Vol.73. No.7 (1948) 679
95. R. Kubo, *J. Jpn. Phys. Society*, Vol.12, No.6 (1957) 570
96. S.G. Bishop and P.J. Bray, *J. Chem. Phys*, Vol.48, No.4 (1968) 1709
97. S.W. Martin, *Materials Chemistry and Physics*, Vol.23 (1989) 225
98. C.A. Angel, *Solid State Ionics*, Vol.9 (1983) 3
99. A. Hunt, *J. Non-Cryst. Solids*, Vol.168 (1994) 258
100. M. Tatsumisago and C.A. Angell, S.W. Martin, *J. Chem. Phys.* Vol.97, No.9 (1992) 6968
101. K.L. Ngai, J.N. Mundy, H. Jain, O. Kanert, and G. B. Jollenbeck, *Phys. Rev.B.*, Vol.39, No.9 (1989) 6169

102. G. B. Jollenbeck and O. Kanert, H. Jain , K.L. Ngai, Phys. Rev. B., Vol.39, No.9 (1989) 6071
103. D. Ravaine and J.L. Souquet, Phys. Chem. Glasses, Vol.18 (1977) 27
104. K.L. Ngai, R.W. Rendell, A.K. Rajagopal, and S. Teitler, Ann. N.Y. Acad. Sci., Vol.484, No.150 (1986) and Vol.484, No.321 (1986)
105. D.W. Davidson and R.H. Cole, The J. of Chem. Phys., Vol.19, N0.12 (1952)1484
106. C.P. Lindsey and G.D. Patterson, J. Chem. Phys., Vol.73 (1980) 3348
107. W. Cao and R. Gehardt, Solid State Ionics, Vol.42 (1990) 213
108. R. Zallen, "The Physics of Amorphous", A.Willey-Interscience publication, NewYork (1983)
109. A. Shastri, Ph.D thesis, Iowa State University, Ames (1994)
110. J. Malek, J.of Thermal Analysis, Vol.40 (1993)159
111. A. Pradel and M Ribes, Materials Science and Engineering, Vol.133 (1989) 45
112. J.H. Kennedy, Z. Zhang and H. Eckert, J. Non-Cryst. Solids, Vol.123 (1990) 328
113. V. Clement, Thesis, Grenoble University, Grenoble (1986)
114. H. Diercks and B.Krebs, Angew. Chem., Vol.16 (1997) 313
115. S.W. Martin, D.R. Bloyer, and T.Polewik, J. Am. Cerm. Soc., Vol.74 (1991) 1446
116. J. Krogh-Moe, J. Non-Cryst. Solids, Vol.1 (1969) 269
117. R.L. Mozzi and B.E.Warren, J. Appl. Cryst. (Varschneya), Vol.3 (1970) 2512
118. D.R.Bloyer,Tr., M.S. thesis, Iowa State Universtiy, Ames (1990)
119. J.A. Sills, D.R. Torgeson, S.W. Martin, J. Non-Cryst. Solids, 168 (1994)86
120. J.A. Sills, D.R. Torgeson, S.W. Martin, J. Non-Cryst. Solids, (1994) to be published

121. Y.H. Yun and P.J. Bray, *J. Non-Cryst. Solids*, Vol.27 (1978) 363
122. P.J. Bray and J.G. O'kefe, *Phys. Chem. Glasses*, Vol.4 (1963) 37
123. D.R. Bloyer, and S.W. Martin, *J. of Am. Ceramic Soc.*, Vol.73, No.11 (1990) 3481
124. G.J. Exarhos and W.M. Risen Jr., *Solid State Commun.*, Vol.11 (1972) 755
125. G.J. Exarhos, P.J. Miller and W.M Risen Jr., *J. Chem. Phys.*, Vol.60 (1974) 4145
126. S.W. Martin and T.Polewik, *J. Am. Ceram. Soc.*, Vol.74, No.6 (1991) 1466
127. J.P. Cho, M.S. thesis, Iowa State Universtiy, Ames (1992)
128. M. Tomozawa and R.H. Dpremus, eds., "Glass Science and Technology", Academic Press, NewYork (1990) 318
129. J.W. Allen, *J. Non-Cryst. Sol.*, Vol.4 (1980) 69
130. H. Maekawa, T. Maejawa, K. Kawamura and T. Yokokawa, *J. Non-Cryst. sol.*, Vol.127 (1991) 3
131. H. Eckert, J.H. Kennedy, A. Pradel and M. Ribes, *J. Non-Cryst. Solids*, Vol.113 (1989) 280
132. M. Tenhover, R.D. Boyer, R.S. Henderson, T.E. Hammond and G.A. Shreve, *Solid State Commun.*, Vol.65 (1988) 1517
133. C.A. Angell, *J. Non-Cryst. Solid*, Vol.73 (1985)1
134. H. Eckert, J.H Kennedy, A. Pradel and M. Ribes, Jr., *J. Non-Cryst. Solids*, Vol.113 (1989) 287
135. D. Ravaine, J.L. Souquet, *Physics and Chemistry of Glasses*, Vol.19 (1978) 115
136. M. Ribes, B. Barrau, J.L. Souquet, *J. Non-Cryst. Solids*, Vol.38 (1980) 271
137. B.C. Gerstein, "Encyclopedia of Physical Science and Technology", Vol. II Academic Press, Inc., NewYork (1992)

138. R.E. Noberg, Am. J. Phys, Vol. 33, No. 2, Feb. (1965) 1
139. C.P. Slichter, "Nuclear magnetic Resonance in Solids", Edited by L. V. Gerren, NATO ADV. Study Inst. Series C, Plenum Press, (1974)
140. A. Abragam, "Principles of Nuclear Magnetism", Clarendon Press, Oxford (1961)
141. C.P. Poole, Jr., H.A. Farach, "Theory of magnetic resonance", 2nd Ed. John Wiley and Sons, Inc., NewYork (1987)
142. C.P. Slichter, "Principle of Magnetic Resonance", 3rd Ed., Springer Series in Solid State Sciences Vol.1, Springer-Verlag, Berlin (1990)
143. D. Wolf, "Spin Temperature and Nuclear Spin Relaxation in Matter" Clarendon Press, Oxford (1979)
144. T.C. Farrar and E.D. Becker, "Pulse Fourier Transform NMR Introduction to theory and Methods" Academic Press, NewYork (1971)
145. E. Fukushima and S.B.W. Roeder, "Experimental Pulse NMR A nut and Bolts Approach", Addison-Wesley Pub. Co., NewYork (1981)
146. D. Zamir and R. G. Barnes et al., Phys. Rev. B, Vol.29, No.1 (1984) 61
147. Yu Insuk, Ph.D thesis, University of Michigan, Ann Arbor (1981)100 - 108
148. F. Bloch, W.W. Hansen, M. Packard, Phys. Rev., Vol.69 (1946) 127
149. I.J. Lowe and R.E. Norberg, "Free induction decays in solids", Phys. Rev., Vol.107 (1957) 46
151. J.H. VanVleck, Phys Rev., Vol.74 (1949) 1168
152. W.D. Knight "Electron Paramagnetism and Nuclear Magnetic Resonance in Metals" in Solid State Physics, Vol.2, edited by F. Seitz, D. Turnbeull Academic, NewYork (1956) 93-136
153. J. Jener, R.Du bois, P. Broekaert, Phys. Rev., Vol.139A (1965) 1959

154. E.R. Andrew and D.P. Tunstall, Proc. Phys. Soc., Vol. 78, No.499, Part I (1961)
155. F.J. Owens, C.P. Poole and H.A. Farach, "Magnetic Resonance of Phase Transitions", Academic Press Inc., NewYork(1979) 79
156. A. Narath, "Hyperfine Interaction" Edited by A.J. Freeman and R.B. Frankel, National Magnetic Laboratory M.I.T., Cambridge (1967) 287
157. J. Korrynga, Physica, Vol.16 (1950) 601
158. N. Bloembergen, Physica (Utrecht), Vol.25 (1949) 386
159. C.A. Sholl, J. Phys., Vol.C7 (1974) 3378
160. P.A. Beckmann, Phys Reports (Rev Section of Phys Letter), Vol.171, No. 3, North Holland, Amsterdam (1988) 85-128
161. P.M. Richards and J. Shinar, J. Phys., Vol.F17 (1987) 1659
162. G.B. Jollenbeck, O. Kanert, J. Steinert and H.Jain, Solid St. Comm., Vol. 65, No. 5 (1988) 303
163. M. Rubinstein, H.A. Resing, T.L. Reineeke, and K.L. Ngai, Phys. Rev. Lett., Vol. 34, No. 23 (1975) 1441
164. A. Avogadro, F. Tabak, M .Corti and F. Borsa, Phys. Rev. B., Vol. 41, No.10 (1990) 6137
165. O. Kanert, J. Steinert, H. Jain and K.L. Ngai, J. Non-Cryst. Solids, Vol.131 (1991) 1001
166. J. Szeftel and H. Alloul, Phys. Rev. Lett., Vol. 34, No.11 (1975)657
167. J. Szeftel and H. Alloul, J. Non-Cryst Solids, Vol.29 (1978) 253
168. M. Villa and G.C. Farrington, Philosophical magazine B, Vol. 56, No.2 (1987) 14

169. Aschcroft and Mermin, "Solid State Physics", Holt, Rinehart and Winston, NewYork (1976)
170. Geiger, G.H. and Poirier, D.R., "Transport Phenomena in Metallurgy", Addison-Wesley Publishing Co., Reading, MA. (1973)
171. S.R. Elliot, A.P. Owens, Phys. Rev. B, Vol. 44, No. 1 (1991) 44
172. K. Funke, R. Hoppe, Solid State Ionics, Vol.40 (1990) 200
173. S. Kirkpatrick, Rev. of Modern Phys., Vol. 45, No. 4 (1973) 574
174. C.H. Seager and G.E. Pike, Phys Rev B., Vol. 10, No. 4 (1974) 1435
175. J.C. Dyre, Phys. Rev B., Vol 47, No 14 (1993) 9128
176. J.C. Dyre Phys Rev. B, Vol. 49, No. 17 (1994-I) 11709
177. W. Schirmacher, Solid State Ionics, Vol.28 (1988)129
178. S. Summerfield, Solid State. Comm., Vol. 39 (1981)40
179. T. Odagaki, M. Lax, Phys. Rev. B, Vol. 24, No.9 (1981) 5284
180. B. Movaghar and W. Schirmacher, J. Phys. C.: Solid State Phys., Vol.14 (1981) 859
181. H. Scher, M. Lax, Phys. Rev. B, Vol.7, No.10 (1973) 4491
182. S. Summerfield and P.N. Butcher, J. Phys. C: Condens. Matters (1991) 7003
183. A. Hunt, J. Phys C: Condens. Matters (1991)7831
184. O. L. Anderson and D. A. Stuart, J. of the Am. Ceramic Soc., Vol.37 (1954) 573
185. S. R. Elliot, Solid State Ionics, Vol.27 (1988) 131
186. R. D. Williams and S. R. Elliot J. of Non - Cryst. Solids, Vol.146 (1992) 43
187. S. R. Elliot, J. of Non - Cryst. Solids, (1994) to be published
188. K. L. Ngai Phys. Rev. B, Vol. 48, No.18 (1993) 13481
189. D.J. Adduci, P. A. Hornung, D. R. Torgeson, Rev. Sci. Instr. Vol.47 (1976) 1503

190. E. L. Hahn Phys. Rev., Vol.30, No.4 (1950) 580
191. H. Y. Carr, E. M. Purcell Phys. Rev., Vol.94, No.3 (1954) 630
192. S. Meiboom and D. Gill, The Rev. Sci. Instr., Vol.29, No.8 (1958) 688
193. M. Dishon, G. H. Weiss and J.T. Bendler, J. of Research of the N.B.S., Vol.90,
No.9 (1985) 27
194. P.W. Anderson, "Physics Today", Am. Phys. Soc., Collingwood, Feb. (1990)
195. E.I. Kamitsos, J. De Physique IV C2. supplement au J. de Physique
III, Vol.2, Oct. (1992)
196. J. Kincs, M.S. thesis, Iowa State University, Ames (1993)

ACKNOWLEDGMENTS

This work was completed with the help of many individuals.

I thank my advisor, Dr. F. Borsa, and D.R. Torgeson, for help with the theoretical and practical aspects of NMR. I learned a great deal about scientific reasoning and writing from Dr. F. Borsa. Thanks go also to Dr. S.W. Martin for his continuing encouragement and knowledge, and to his graduate student Jephil Cho, H.P. Patel, J. Kincks and J. Sills for supplying various samples and the measurement of the conductivity. I appreciate Dr. R.A. Leacock and Dr. DC Johnstone for their warm encouragement. In the process, I learned a great deal in the discussions with BungJin. Suh and Dr. Ananda Shastri. Dr. Ivar Svare at University of Trondheim gave useful help for the analysis.

Special thanks to my wife Jongyeon, my son Huijun, my daughter sywoon and my parents in Korea for their lovely support, care and encouragement.

This work was performed at Ames Laboratory under Contract No. W - 7405 - Eng - 82 with the U.S. Department of Energy. The United States government has assigned the DOE Report number IS - T 1744 to this thesis.

APPENDIX

FORTTRAN programs to optimize the models to the measured data of NSLR and conductivity are presented in this appendix. The optimization package "DBCLSF" in IMSL MATH/LIBRARY, Version 1.1 of Problem-Solving Software Systems is used in the main program as a subroutine. The other sub routines are to evaluate the functional form of the model (e.g., KWW and distribution of activation energies) used in the analysis. Therefore each program has similar structures in the main program except the assignment of the fitting parameters and data structure, however each subroutines are programmed according to the model. The functional form of each model is described in the section 3.4. The usage of each program is appear on the first line of the comment statements.

Program i

```

c*****
c FIT KWW TO NMR T1 DATA
c PREPARED BY K.H.KIM MAY '94 FOR FIC-PROJECT
c   IN NMR/PHYSICS DEP'T ISU
c*****
      IMPLICIT REAL*8 (A-H,O-Z)
      DIMENSION XGUESS(4),X(4),XLB(4),XUB(4),XSCALE(4),
&      FSCALE(50),FVEC(50),IPAR(6),RPAR(7),FJAC(50,4)
      COMMON TEMP(50),T1(50),OHMEGA
      COMMON /PI/ PI,TIP
      COMMON /GAM/ A1,A3,A5,A7
      common /pre/ ALPHA,Ea
      common frequency
      DATA XSCALE/4*1.D0/,FSCALE/50*1.D0/
      EXTERNAL fcn
      A1=1.D0/1.2D1
      A3=-1.D0/3.6D2
      A5=1.D0/1.26D3
      A7=-1.D0/1.68D3
      PI=DATAN(1.D0)*4.D0
      TIP=DLOG(6.2831853D0)/2.D0

```

```

print*,'enter NMR-frequency in MHz'
read*,frequency
OHMEGA=2.D0*PI*frequency/10.
PRINT*,'ENTER A=E10 TAU0=E-14 BETA Ea=T/1000 iexcess.'
READ*,XGUESS,iexc
xguess(1)=2.*xGuess(1)
print*,xguess(1),xguess(2),xguess(3),xguess(4)
T1MIN=1.D3
I=1
1 READ(7,*,END=2) TEMP(I),T1(I)
TEMP(I)=TEMP(I)/1.D3
IF (T1(I).Le.T1MIN) THEN
  ISP=I
  T1MIN=T1(I)
END IF
I=I+1
GO TO 1
2 NDAT=I-1
print*,'iexcess=',iexc
print*,'ndat=',ndat
C*****
C VARIABLE ASSIGNMENT
C X(1)=A
C X(2)=TAU0
C X(3)=ALPHA
C X(4)=Ea
C*****
CALL DU4LSF(IPAR,RPAR)
IPAR(3)=5000
IPAR(4)=4*IPAR(3)
CALL
DBCLSF(FCN,isp+iexc,4,XGUESS,1,XLB,XUB,XSCALE,FSCALE,IPAR,RPAR,
& X,FVEC,FJAC,isp+iexc)
sum=0.d0
do i=1,isp+iexc
  sum=sum+fvec(i)
end do
print*,ipar(3),ipar(4)
PRINT*,'A=',X(1)*1.D10/2
PRINT*,'TAU0=',X(2)/1.d14
PRINT*,'Alpha=',X(3)
PRINT*,'Ea=',X(4)*1.d3
print*,'Error=',sum
STOP
END

```

```

C*****
C   SUBROUTINE FOR EVALUATING FUNCTION
C*****
      SUBROUTINE FCN(M,N,X,F)
      IMPLICIT REAL*8 (A-H,O-Z)
      INTEGER N
      DIMENSION X(N),F(M)
      COMMON TEMP(50),T1(50),OHMEGA
      common frequency
      A=OHMEGA/X(1)
      ALPHA=X(3)
      PRE=OHMEGA*x(2)/1.d7
      print*, 'A=',x(1)*1.D10/2., '      TAUO=',x(2)/1.d14
      print*, 'beta=',x(3), '      Ea=',x(4)*1.d3
      print*, '=====  
NMR T1 fit using KWW====='  
      print*, 'temperature(k)      T1-data(mili sec)      KWW-fit'  
      fsum=0.d0
      DO I=1,M
        Z=PRE*DEXP(x(4)/TEMP(I))
5      CALL QEVAL(ALPHA,Z,Q1,Q2)
        F(I)=A/Z/(Q1+4*Q2)-T1(I)
      PRINT*,TEMP(I)*1.D3,T1(I),F(I)+T1(I)
      END DO
      PRINT*, '=====  
(Frequency=',frequency,'MHz', '=====  
      RETURN
      END
C*****
C   SUBROUTINE FOR EVALUATING Q
C*****
      SUBROUTINE QEVAL(ALPHA,Z,Q1,Q2)
      IMPLICIT REAL*8 (A-H,O-Z)
      INTEGER N
      COMMON /PI/ PI,TIP
      COMMON /GAM/ A1,A3,A5,A7
      Q1=0.0D+00
      Q2=0.0D+00
      FACT=0.0D+00
      ZLOG=DLOG(Z)
      ZLOG2=DLOG(Z*2.D0)
      ARG=PI/2.D0*ALPHA
      DO 10 N=1,1000
        D=N
        ONA=1.D0+D*ALPHA
        ONASQ=ONA**2

```

```

      GAMMA=(ONA-0.5D0)*DLOG(ONA)-
ONA+TIP+(A1+(A3+(A5+A7/ONASQ)/
&      ONASQ)/ONASQ)/ONA
      FACT=FACT+DLOG(D)
      DSD=DSIN(D*ARG)
      Q1=Q1+(-1)**(N-1)*DEXP(GAMMA-FACT-ONA*ZLOG)*DSD
      Q2=Q2+(-1)**(N-1)*DEXP(GAMMA-FACT-ONA*ZLOG2)*DSD
10  CONTINUE
      RETURN
      END

```

Program ii

```

C*****
C FIT KWW TO FIXED TEMPERATURE CONDUCTIVITY DATA
C PREPARED BY K.H.KIM MAY '94 FOR FIC-PROJECT IN NMR/PHYSICS DEP'T
C..ISU
C*****
      IMPLICIT REAL*8 (A-H,O-Z)
      DIMENSION XGUESS(4),X(4),XLB(4),XUB(4),XSCALE(4),
&      FSCALE(100),FVEC(100),IPAR(6),RPAR(7),FJAC(100,4)
      COMMON FREQ(100),S(100),OHMEGA(100),A(100),PRE(100),V(100)
      COMMON /ALPHA/ ALPHA,TEMP
      COMMON /PI/ PI,TIP
      COMMON /GAM/ A1,A3,A5,A7
      DATA XSCALE/4*1.D0/,FSCALE/100*1.D0/
      EXTERNAL fcn
      A1=1.D0/1.2D1
      A3=-1.D0/3.6D2
      A5=1.D0/1.26D3
      A7=-1.D0/1.68D3
      PI=DATAN(1.D0)*4.D0
      TIP=DLOG(6.2831853D0)/2.D0
      print*,'enter TEMPERATURE=K/1000'
      read*,TEMP
      PRINT*,'TEMPERATURE=',TEMP,'E3K'
      PRINT*,'ENTER A=E0E00 TAU0=TAU0*1E14 BETA Ea=T/1000'
      READ*,XGUESS
      print*,xguess(1),xguess(2),xguess(3),xguess(4)
      PRINT*,'ENTER #PT TO EXCLUDE FROM END OF DATA'
      READ*,STP
      I=1
1  READ(7,*,END=2) FREQ(I),S(I),V(I)

```

```

      FREQ(I)=FREQ(I)/1.D7
      I=I+1
      GO TO 1
2     NDAT=I-1
      print*, 'ndat=', ndat
      ndat=NDAT-STP
      print*, 'ANAdat=', ndat
C*****
C     VARIABLE ASSIGNMENT
C     X(1)=A
C     X(2)=TAU0
C     X(3)=ALPHA(=BETA)
C     X(4)=Ea
C*****
      CALL DU4LSF(IPAR, RPAR)
      IPAR(3)=5000
      IPAR(4)=4*IPAR(3)
      CALL
DBCLS F(FCN, NDAT, 4, XGUESS, 1, XLB, XUB, XSCALE, FSCALE, IPAR, RPAR,
&      X, FVEC, FJAC, NDAT)
      sum=0.d0
      do i=1, NDAT
        sum=sum+fvec(i)
      end do
      print*, 'MAX# ITERATIONS=', ipar(3), ' ', 'MAX# FUNC EVAL=', ipar(4)
      PRINT*, 'A=', X(1)
      PRINT*, 'TAU0=', X(2)/1.d14
      PRINT*, 'Alpha=', X(3)
      PRINT*, 'Ea=', X(4)*1.d3
      print*, 'Error=', sum
      STOP
      END
C*****
C     SUBROUTINE FOR EVALUATING FUNCTION
C*****
      SUBROUTINE FCN(M, N, X, F)
      IMPLICIT REAL*8 (A-H, O-Z)
      INTEGER N
      DIMENSION X(N), F(M)
      COMMON FREQ(100), S(100), OHMEGA(100), A(100), PRE(100)
      COMMON /ALPHA/ ALPHA, TEMP
      COMMON /PI/ PI, TIP
      ALPHA=X(3)
      print*, 'A=', x(1), '   TAU0=', x(2)/1.D14
      PRINT*, 'BETA=', X(3), '   Ea=', x(4)*1.d3

```

```

print*, '====Conductivity relaxation fit using KWW correlation===='
print*, '===== at constant temperature ====='
print*, 'FREQUENCY(HZ)      Real Conductivity      KWW - Fit'
fsum=0.d0
DO I=1,M
  OHMEGA(I)=2.D0*PI*FREQ(I)
END DO
DO I=1,M
  A(I)=OHMEGA(I)*X(1)
  PRE(I)=OHMEGA(I)*X(2)/1.d7
  Z=PRE(I)*DEXP(x(4)/TEMP)
5  CALL QEVAL(ALPHA,Z,QC,QS)
  PRINT*, 'qc=', qc, 'qs=', qs
  F(I)=1.D7*(A(I)/Z)*(QS/(QS**2+QC**2))-S(I)
  print*, 'F(I)=', F(I)
  print*, 'FREQ(I)*1.D7, S(I), S(I)+F(I)'
END DO
print*, '====KyungHan, Kim/NMR/Physics===='
RETURN
END
C*****
C  SUBROUTINE FOR EVALUATING Q
C*****
SUBROUTINE QEVAL(ALPHA,Z,QC,QS)
IMPLICIT REAL*8 (A-H,O-Z)
INTEGER N
COMMON /PI/ PI,TIP
COMMON /GAM/ A1,A3,A5,A7
Qc=1/Z
Qs=0.0D+00
FACT=0.0D+00
ZLOG=DLOG(Z)
ZLOG2=DLOG(Z*2.D0)
ARG=PI/2.D0*ALPHA
DO 10 N=1,1000
  D=N
  ONA=1.D0+D*ALPHA
  ONASQ=ONA**2
  GAMMA=(ONA-0.5D0)*DLOG(ONA)-ONA+TIP+(A1+(A3+(A5+A7/ONASQ)/
&      ONASQ)/ONASQ)/ONA
  FACT=FACT+DLOG(D)
  DSD=DSIN(D*ARG)
  DCD=DCOS(D*ARG)
  QS=QS+(-1)**(N-1)*DEXP(GAMMA-FACT-ONA*ZLOG)*DSD
  QC=QC+(-1)**N*DEXP(GAMMA-FACT-ONA*ZLOG)*DCD

```

```

10 CONTINUE
   RETURN
   END

```

Program iii

```

C*****
C FIT KWW TO FIXED FREQUENCY CONDUCTIVITY DATA (ARRHENIUS
C PLOT)
C PREPARED BY K.H.KIM MAY '94 FOR FIC-PROJECT IN NMR/PHYSICS
  DEP'T ISU
C*****
  IMPLICIT REAL*8 (A-H,O-Z)
  DIMENSION XGUESS(4),X(4),XLB(4),XUB(4),XSCALE(4),
&           FSCALE(50),FVEC(50),IPAR(6),RPAR(7),FJAC(50,4)
  COMMON TEMP(50),S(50),OHMEGA
  COMMON /PI/ PI,TIP
  COMMON /GAM/ A1,A3,A5,A7
  common /pre/ ALPHA,Ea
  DATA XSCALE/4*1.D0/,FSCALE/50*1.D0/
  EXTERNAL fcn
  A1=1.D0/1.2D1
  A3=-1.D0/3.6D2
  A5=1.D0/1.26D3
  A7=-1.D0/1.68D3
  PI=DATAN(1.D0)*4.D0
  TIP=DLOG(6.2831853D0)/2.D0
  print*,'enter CONDUCTIVITY-frequency in MHz'
  read*,frequency
  PRINT*,'FREQUENCY=',FREQUENCY,'MHZ'
  OHMEGA=2.D0*PI*frequency/10.
  PRINT*,'ENTER A=E0E00 TAU0=TAU0*1E14 BETA Ea=T/1000 #dat for
Ana'
  READ*,XGUESS,nodt
  print*,xguess(1),xguess(2),xguess(3),xguess(4)
  I=1
1  READ(7,*,END=2) TEMP(I),S(I)
   TEMP(I)=TEMP(I)/1.D3
   I=I+1
   GO TO 1
2  NDAT=I-1
   print*,'ndat=',ndat

```

```

      ndat=nodt
      print*,'# of data to be analyzed=',nodt
C*****
C   VARIABLE ASSIGNMENT
C   X(1)=A
C   X(2)=TAU0
C   X(3)=ALPHA(=BETA)
C   X(4)=Ea
C*****
      CALL DU4LSF(IPAR,RPAR)
      IPAR(3)=5000
      IPAR(4)=4*IPAR(3)
      CALL
DBCLSF(FCN,NDAT,4,XGUESS,1,XLB,XUB,XSCALE,FSCALE,IPAR,RPAR,
&      X,FVEC,FJAC,NDAT)
      sum=0.d0
      do i=1,NDAT
        sum=sum+fvec(i)
      end do
      print*,'MAX# ITERATIONS=',ipar(3),'   ','MAX# FUNC EVAL=',ipar(4)
      PRINT*,'A=',X(1)
      PRINT*,'TAU0=',X(2)/1.d14
      PRINT*,'Alpha=',X(3)
      PRINT*,'Ea=',X(4)*1.d3
      print*,'Error=',sum
      STOP
      END
C*****
C   SUBROUTINE FOR EVALUATING FUNCTION
C*****
      SUBROUTINE FCN(M,N,X,F)
      IMPLICIT REAL*8 (A-H,O-Z)
      INTEGER N
      DIMENSION X(N),F(M)
      COMMON TEMP(50),S(50),OHMEGA .
      A=OHMEGA*X(1)
      ALPHA=X(3)
      PRE=OHMEGA*x(2)/1.d7
      print*,'A=',x(1),'   TAU0=',x(2)/1.D14
      PRINT*,'BETA=',X(3),'   Ea=',x(4)*1.d3
      print*,'====Conductivity relaxation fit using KWW correlation===='
      print*,'===== at constant frequeney ====='
      print*,'Temperature(Kelvin)      Real Conductivity      KWW - Fit'
      fsum=0.d0
      DO I=1,M

```

```

      Z=PRE*DEXP(x(4)/TEMP(I))
5      CALL QEVAL(ALPHA,Z,QC,QS)
      F(I)=1.D7*(A/Z)*(QS/(QS**2+QC**2))-S(I)
      print*,temp(i)*1.d3,S(I),S(I)+F(I)
      END DO
      print*,'=====KyungHan, Kim/NMR/Physics=====!'
      RETURN
      END
C*****
C  SUBROUTINE FOR EVALUATING Q
C*****
      SUBROUTINE QEVAL(ALPHA,Z,QC,QS)
      IMPLICIT REAL*8 (A-H,O-Z)
      INTEGER N
      COMMON /PI/ PI,TIP
      COMMON /GAM/ A1,A3,A5,A7
      Qc=1/Z
      Qs=0.0D+00
      FACT=0.0D+00
      ZLOG=DLOG(Z)
      ZLOG2=DLOG(Z*2.D0)
      ARG=PI/2.D0*ALPHA
      DO 10 N=1,1000
          D=N
          ONA=1.D0+D*ALPHA
          ONASQ=ONA**2
          GAMMA=(ONA-0.5D0)*DLOG(ONA)-
ONASQ+TIP+(A1+(A3+(A5+A7/ONASQ)/
&      ONASQ)/ONASQ)/ONA
          FACT=FACT+DLOG(D)
          DSD=DSIN(D*ARG)
          DCD=DCOS(D*ARG)
          QS=QS+(-1)**(N-1)*DEXP(GAMMA-FACT-ONA*ZLOG)*DSD
          QC=QC+(-1)**N*DEXP(GAMMA-FACT-ONA*ZLOG)*DCD
10      CONTINUE
      RETURN
      END

```

Program iv

```

c*****
c FIT (Gaussian distribution of Ea) TO NMR T1 DATA version 1.1
c PREPARED BY K.H.KIM SEPT '94 FOR FIC-PROJECT IN NMR/PHYSICS DEP'T
ISU
c*****
      IMPLICIT REAL*8 (A-H,O-Z)
      DIMENSION XGUESS(3),X(3),XLB(3),XUB(3),XSCALE(3),
&           FSCALE(50),FVEC(50),IPAR(6),RPAR(7),FJAC(50,3)
      COMMON TEMP(50),T1(50),OHMEGA
      COMMON PI,FREQUENCY,Eai,Eaf,D
      DATA XSCALE/3*1.D0/,FSCALE/50*1.D0/
      EXTERNAL fcn
      PI=DATAN(1.D0)*4.D0
      print*,'ENTER FREQ(MHZ)'
      read*,frequency
      OHMEGA=2.D0*PI*frequency
      PRINT*,'ENTER A[e9] Eb[K] Em[K] WELL-DISTANCE[ANGSTROM]
iexcess.'
      READ*,XGUESS,D,iexc
      print*,xguess(1),xguess(2),xguess(3),D,IEXC
      T1MIN=1.D3
      I=1
1     READ(7,*,END=2) TEMP(I),T1(I)
      IF (T1(I).Le.T1MIN) THEN
          ISP=I
          T1MIN=T1(I)
      END IF
      I=I+1
      GO TO 1
2     NDAT=I-1
      print*,'iexcess=',iexc
      print*,'ndat=',ndat
      print*,'enter summation range Ea,init(K) Ea,final(K)'
      read*,Eai,Eaf

C*****
C     VARIABLE ASSIGNMENT
C     X(1)=A
C     X(2)=Eb
C     X(3)=Em
C
C*****
      CALL DU4LSF(IPAR,RPAR)

```

```

IPAR(3)=5000
IPAR(4)=4*IPAR(3)
CALL
DBCLSF(FCN,isp+iexc,3,XGUESS,1,XLB,XUB,XSCALE,FSCALE,IPAR,RPAR,
&      X,FVEC,FJAC,isp+iexc)
  hap=0.d0
  do i=1,isp+iexc
    hap=hap+fvec(i)
  end do
  print*,ipar(3),ipar(4)
  PRINT*,'A=',X(1)
  PRINT*,'Eb',X(2)
  PRINT*,'Em=',X(3)
  PRINT*,'interwell distance',d
  print*,'Error=',hap
  STOP
  END
C*****
C  SUBROUTINE FOR EVALUATING FUNCTION
C*****
SUBROUTINE FCN(M,N,X,F)
IMPLICIT REAL*8 (A-H,O-Z)
INTEGER N
DIMENSION X(N),F(M)
COMMON TEMP(50),T1(50),OHMEGA
common pi,FREQUENCY,Eai,Eaf,D
A=X(1)
print*,'A=',x(1),' Eb=',x(2)
print*,'Em=',x(3),' interwell distance=',d
print*,'=====NMR T1 fit using ditribution of Ea=====
print*,'temperature(k) T1-data(milisec) fit'
fsum=0.d0
DO I=1,M
sum=0.D0
do 33 j=Eai,Eaf
R0=6.d0*24.3366178d0*(J**0.5)*1.D4/d
RT=Dexp(-j/temp(I))*R0
rho=(1./SQRT(2.*PI)/X(2))*exp(-(J-X(3))**2/2./x(2)**2)
R1=a*rho*(1./RT/(1.+(ohmega/RT)**2)+4./RT/(1.+(2.*ohmega/RT)**2))
r1=r1*1.d3
sum=sum+R1
33 continue
f(I)=(1./sum)*1.d3-T1(I)
PRINT*,TEMP(I),T1(I),F(I)+T1(I)
END DO

```

```

PRINT*,'===== Frequency=',frequency,'MHz','=====
RETURN
END

```

Program vi

```

c*****
c FIT DOUBLE-Gaussian distribution of Ea TO NMR T1 DATA version 0.1
c PREPARED BY K.H.KIM OCT '94 FOR FIC-PROJECT IN NMR/PHYSICS DEP'T
c ISU
C*****
  IMPLICIT REAL*8 (A-H,O-Z)
  DIMENSION XGUESS(6),X(6),XLB(6),XUB(6),XSCALE(6), .
&          FSCALE(50),FVEC(50),IPAR(6),RPAR(7),FJAC(50,6)
  COMMON TEMP(50),T1(50),OHMEGA
  COMMON PI,FREQUENCY,Eai,Eaf,D
  DATA XSCALE/6*1.D0/,FSCALE/50*1.D0/
  EXTERNAL fcn
  PI=DATAN(1.D0)*4.D0
  print*,'ENTER FREQ(MHZ)'
  read*,frequency
  OHMEGA=2.D0*PI*frequency
  PRINT*,'ENTER A[e9] Eb[K] Em[K] Eb1 Em1 x(ratio of two Gaussian)'
  PRINT*,'ENTER interwell distance iexcess'
  READ*,XGUESS,D,iexc
  print*,xguess(1),xguess(2),xguess(3),xguess(4),xguess(5),xguess(6),D
  T1MIN=1.D3
  I=1
1  READ(7,*,END=2) TEMP(I),T1(I)
   IF (T1(I).Le.T1MIN) THEN
     ISP=I
     T1MIN=T1(I)
   END IF
   I=I+1
   GO TO 1
2  NDAT=I-1
   print*,'iexcess=',iexc
   print*,'ndat=',ndat
   print*,'enter summation range Ea,init(K) Ea,final(K)'
   read*,Eai,Eaf
C*****
C  VARIABLE ASSIGNMENT
C  X(1)=A

```

```

C      X(2)=Eb  x(4)=Eb1
C      X(3)=Em  x(5)=Em1
C      x(6)=x
C*****
      CALL DU4LSF(IPAR,RPAR)
      IPAR(3)=5000
      IPAR(4)=4*IPAR(3)
      CALL
DBCLS F(FCN,isp+iexc,6,XGUESS,1,XLB,XUB,XSCALE,FSCALE,IPAR,RPAR,
&      X,FVEC,FJAC,isp+iexc)
      hap=0.d0
      do i=1,isp+iexc
        hap=hap+fvec(i)
      end do
      print*,ipar(3),ipar(4)
      PRINT*,'A=',X(1),'Eb=',x(2),'Em=',x(3)
      print*,'Eb1=',x(4),'Em1=',x(5)
      PRINT*,'x=',X(6)
      PRINT*,'interwell distance',d
      print*,'Error=',hap
      STOP
      END
C*****
C      SUBROUTINE FOR EVALUATING FUNCTION
C*****
      SUBROUTINE FCN(M,N,X,F)
      IMPLICIT REAL*8 (A-H,O-Z)
      INTEGER N
      DIMENSION X(N),F(M)
      COMMON TEMP(50),T1(50),OHMEGA
      common pi,FREQUENCY,Eai,Eaf,D
      A=X(1)
      print*,'A=',x(1),' Eb=',x(2) 'Em=',x(3), ' interwell distance=',d
      print*,' print*,'Eb1=',x(4), 'Em1=',x(5), 'x=',x(6)
      print*,'=====NMR T1 fit using ditribution of Ea=====
      print*,'temperature(k) T1-data(milisc) fit'
      fsum=0.d0
      DO I=1,M
      sum=0.D0
      do 33 j=Eai,Eaf
        R0=6.d0*24.3366178d0*(J**0.5)*1.D4/d
        RT=Dexp(-j/temp(I))*R0
        rho=(1./SQRT(2.*PI)/X(2))*exp(-(J-X(3))**2/2./x(2)**2)
        rhoo=(1./sqrt(2.*pi)/x(4))*exp(-(j-x(5))**2/2./x(4)**2)
        rhotot=x(6)*rho+(1-x(6))*rhoo

```

```
R1=a*rhotot*(1./RT/(1.+(ohmega/RT)**2)+4./RT/(1.+(2.*ohmega/RT)**2))
r1=r1*1.d3
sum=sum+R1
33 continue
f(I)=(1./sum)*1.d3-T1(I)
PRINT*,TEMP(I),T1(I),F(I)+T1(I)
END DO
PRINT*,'===== (Frequency=',frequency,'MHz', '=====
RETURN
END
```